Earth-Science Reviews 190 (2019) 190–223

Contents lists available at ScienceDirect

Earth-Science Reviews

journal homepage: www.elsevier.com/locate/earscirev

Cyclostratigraphy and the problem of astrochronologic testing

Stephen R. Meyers

Department of Geoscience, University of Wisconsin-Madison, 1215 W. Dayton Street, Madison, WI 53706, United States

ARTICLE INFO

Keywords:
Cyclostratigraphy
Milankovitch cycles
Astrochronology
Geologic time scale
Transfer functions
Optimization

ABSTRACT

When Milankovitch cycles are preserved in the geologic record they provide a direct link between chronometer and climate change, and thus a remarkable opportunity to constrain the evolution of the surficial Earth System. The identification of such cycles has allowed exploration of the geologic record with unprecedented temporal resolution, and has spurred the development of a rich theoretical framework for climatic change. Accompanying these successes, however, has been a persistent skepticism: how does one reliably test for astronomical forcing/pacing in stratigraphic and paleoclimate data, especially when time is poorly constrained? From this perspective, it would seem that the merits and promise of astrochronology – a Phanerozoic time scale measured in 20,000 to 400,000 year increments – also serves as its Achilles heel, if the confirmation of such geologically short temporal rhythms defies rigorous hypothesis testing. The implications are substantial, since much of our understanding of paleoclimate change throughout the Cenozoic (and beyond) is firmly rooted in astrochronologic interpretation.

In this study, a conceptual framework for assessing Earth System response to astronomical-insolation changes, and the propagation of that signal into the geologic record, is used as a guide to understand the nature of the problem of astrochronologic testing. This framework emphasizes three challenges – *contamination, stratigraphic distortion*, and *temporal calibration*. A statistical optimization method (TimeOpt; Meyers, 2015) is formulated as a solution to these three challenges, providing an approach for astrochronologic testing that objectively evaluates time scale uncertainty while simultaneously identifying an optimal model for climate and depositional system response to astronomical forcing. New extensions to the technique are presented, allowing explicit reconstruction of distortions to the primary forcing that are known to be omnipresent in the stratigraphic record. To illustrate the utility of this approach, it is applied to five well-studied stratigraphic series throughout the Phanerozoic, supporting their astronomical origin, and yielding constraints on the evolution of the Earth System and the astronomical solutions themselves. Future directions that build on this foundation are discussed, including the utility of process-based null models, approaches for Earth System transfer function reconstruction, and mapping out ancient Solar System behavior and Earth-Moon history using the geologic archive of Milankovitch cycles. The TimeOpt approach recognizes astronomy, geochronology, paleoclimatology and depositional system reconstruction as a unified geoscientific inverse problem.

1. Introduction

The geologic record is the only available documentation of long-term environmental change and the factors that influence it, such as atmospheric carbon dioxide, solar radiation, and plate tectonics (Zachos et al., 2001). The field of astrochronology (Box 1; Strasser et al., 2006; Hinnov, 2013) utilizes the geologic record of climate oscillations – those ascribed to quasiperiodic changes in the Earth's orbit and rotation – to measure the passage of time from rhythmic layers in strata. These climate rhythms, or "Milankovitch cycles", are related to changes in the ellipticity of Earth's orbit (eccentricity; ~405 ka, 123 ka, 95 ka), as well as changes in the tilt (obliquity; ~41 ka today) and the precession (climatic precession; ~20 ka today) of Earth's rotational axis; note that the periods of precession and obliquity were shorter in the geologic past (Berger et al., 1989; Waltham, 2015). A powerful aspect of astrochronology is the direct link between chronometer and various aspects of climate change, providing an unprecedented opportunity to constrain rates and mechanisms of biologic, chemical, and physical change in Earth's distant past.

The impact of astrochronology on the quantification of deep time, and the evaluation of past perturbations to the Earth system including extinctions and climatic changes, has been substantial (e.g., Hays et al., 1976; Hilgen et al., 1995; Shackleton, 2000; Lisiecki and Raymo, 2005; van Dam et al., 2006; Gradstein et al., 2012; Crampton et al., 2018). Much of this work is motivated by the prospect of a high-precision, high-resolution, in situ chronometer that overcomes the limitations of

E-mail address: smeyers@geology.wisc.edu.

https://doi.org/10.1016/j.earscirev.2018.11.015
Received 3 June 2018; Received in revised form 23 November 2018; Accepted 23 November 2018
Available online 26 November 2018
0012-8252/ © 2018 Elsevier B.V. All rights reserved.

Box 1
Definitions of terms as used in the present study.

Cyclostratigraphy-related terms:

Anchored astrochronology: an astrochronology that specifies numerical ages for stratigraphic horizons (e.g., in millions of years before present). Astrochronologies may be anchored to the theoretical astronomical solutions, and/or independent geochronologic information, such as that derived from radioisotopic dating.
Astrochronology: the subdiscipline of cyclostratigraphy that uses the geologic record of astronomical cycles (or Milankovitch cycles) to develop geological timescales. Also, an "astronomical time scale" or "orbital time scale" constructed using this approach.
Astronomical cycles: quasi-periodic variations in Earth's orbital eccentricity, and the orientation of Earth's rotational axis (due to axial precession, and changes in axial obliquity). Astronomical cycles can influence climate through their impact on the seasonal and latitudinal redistribution of incoming solar radiation. Synonymous with "Milankovitch cycles", "orbital cycles", "astronomical signals", "orbital signals".
Astronomical solutions: theoretical computational solutions for the orbital motion of the Earth, Earth's rotational parameters (precession and obliquity), and their impact on Earth's incoming solar radiation (e.g., Laskar et al., 2004).
Astronomical parameters: the parameters of eccentricity, obliquity and precession, which define the shape of the Earth's orbit (eccentricity) and the orientation of Earth's rotational axis (obliquity and precession) (after Strasser et al., 2006). Synonymous with "orbital parameters".
Cyclostratigraphy: the branch of stratigraphy that is concerned with the identification, characterization, correlation, and interpretation of cyclic variations in the stratigraphic record, and their application in geochronology to improve the accuracy and resolution of time- stratigraphic frameworks (after Hilgen et al., 2004; Strasser et al., 2006).
Earth System transfer functions (ESTF): mathematical descriptions of the processes that sequentially modify (e.g., filter) the astronomical signal during its transit through the Earth System. ESTF are analogous to model components.
Floating astrochronology: an astrochronology that specifies time elapsed (duration) between a series of stratigraphic horizons, but does not specify numerical ages.

Statistical terms:

Duplication: An approach for verification of results, which depends upon the replication of results of a prior study. Astrochron is a computational tool for facilitating duplication. Reproduction of mutually consistent astrochronologies at multiple sites is another critical aspect of duplication.
False negative^{+}: An incorrect *acceptance* of the null hypothesis (stochastic variability), and rejection of the alternative hypothesis (an astronomical signal is present). Synonymous with "Type II Error".
False positive^{+}: An incorrect *rejection* of the null hypothesis (stochastic variability), and acceptance of the alternative hypothesis (an astronomical signal is present). Synonymous with "Type I Error"
Noise model: A model of stochastic variability, commonly used as a null hypothesis (or null model) in astrochronologic testing. Typical examples include autoregressive models, and power-law models.
Spectral power: data variance as a function of frequency (e.g., cycles/ka or cycles/m), typically expressed using a power spectrum.
Statistical power^{+}: the probability that an astrochronologic testing method will correctly reject the null hypothesis (stochastic variability) at a given significance level, when an astronomical signal is indeed present.
Triangulation: An approach for verification of results, which utilizes disparate lines of evidence to test a hypothesis. Triangulation combines information from multiple methodologies and/or disciplines (Wasserstein and Lazar, 2016; Munafò and Smith, 2018). The TimeOpt method, as discussed in this study, uses triangulation in astrochronologic testing.
+ Note that these are general concepts that apply to statistical hypothesis testing methods; the concepts are specifically adapted here with reference to astrochronologic testing.

conventional approaches, allowing reliable quantification of rates, a time derivative. Traditional radioisotopic, biostratigraphic and magnetostratigraphic methods are commonly insufficient to provide rate information over short timescales (10^4 years), due to limitations of their precision and/or the paucity of datable horizons in strata; this highlights a major advantage of astrochronologic approaches to time. Because of its high temporal resolution, and the predictive framework it provides, astrochronology is now a central component of integrated stratigraphy (e.g., Aswasereelert et al., 2013; Hilgen et al., 2014; Sageman et al., 2014), and has also been employed to calibrate radioisotopic dating methods and test their veracity (e.g., Kuiper et al., 2008; Rivera et al., 2011; Meyers et al., 2012a; Zeeden et al., 2014a), and to refine our understanding of the Solar System and Earth-Moon history (Pälike and Shackleton, 2000; Lourens et al., 2001; Pälike et al., 2004;Hinnov, 2013; Zeeden et al., 2014b; Ma et al., 2017; Meyers and Malinverno, 2018).

Notwithstanding these major achievements, reading the astronomical rhythm from the stratigraphic record is often challenging, as climate change is influenced by other factors, including stochastic climate variability (Hasselmann, 1976); these processes can be considered as a type of *contamination* of the astronomical signal (Fig. 1). Further, climate is only one of numerous controls on the formation of the sedimentary rock record, providing additional sources of *contamination* of the preserved astronomical signal, including autogenic variability within the depositional system (Hallam, 1986; Miall, 1995; Miall and Miall, 2004; Westphal et al., 2004; Westphal et al., 2015; Hajek and Straub, 2017). Perhaps most troubling, the rate of formation of the rock record can be highly variable, and strata are often riddled with long and short pauses and omissions – gaps in the recording that can be difficult to quantify, or even identify (Miall and Miall, 2004). Some of these *stratigraphic distortions* (Fig. 1) are stochastic, while others may be driven by astronomical responses of the sedimentary environment (e.g., astronomically-forced sedimentation rates; "missing beats" of Goldhammer et al., 1990). Allied to this issue is the challenge of assigning observed spatial rhythms to temporal cycles (*temporal calibration;*Fig. 1) – a critical step in the development of an astrochronology – which is often poorly constrained by independent time control, confounding tests of the null hypothesis of no astronomical

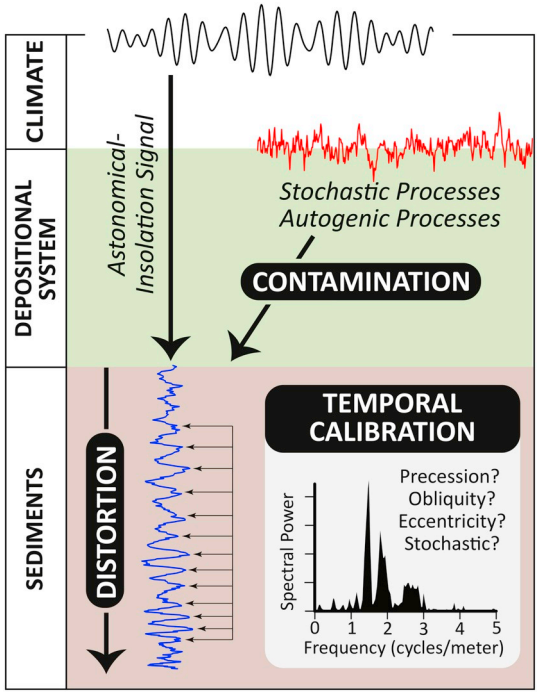

Fig. 1. The three fundamental challenges that complicate an evaluation of astronomical influence on paleoclimate and stratigraphic data: contamination, stratigraphic distortion, and temporal calibration. Stochastic/autocyclic variability within the climate and depositional systems (including diagenesis; e.g., "diagenetic unmixing"; Westphal et al., 2008) can serve to *contaminate* the astronomical signal. *Stratigraphic distortions* that emerge from sedimentation rate changes, variable compaction, and hiatus, can further obfuscate an astronomical signal. These stratigraphic distortions may be stochastic, may be associated with longer-term basin evolution, or may be driven by astronomical responses of the sedimentary environment ("missing beats" of Goldhammer et al. (1990)). *Temporal calibration* is the problem of assigning observed spatial wavelengths to temporal periods, which is often poorly constrained by independent time control, confounding tests of the null hypothesis of no astronomical forcing.

influence (Miall and Miall, 2004). Taken together, the problems of *contamination*, *stratigraphic distortion* and *temporal calibration* result in a stratigraphic record that is a patchy amalgam of astronomical signal and noise, subject to interpretation that has oftentimes been challenging to verify statistically.

Due to this complexity, astrochronologic evaluation requires careful consideration of the many geological, astronomical and statistical aspects that underpin cyclostratigraphy. In this study, a conceptual framework for assessing Earth System response to astronomical-insolation changes, and the propagation of that signal into the geologic record through a series of *Earth System transfer functions* (ESTF; Box 1, Fig. 2), is used as a guide to understand the nature of the problem of astrochronologic testing. This framework considers the three challenges of *contamination*, *stratigraphic distortion* and *temporal calibration*, and three "fundamental propositions" that provide a foundation for astrochronologic testing (Box 2). A quantitative solution is then articulated using this framework, by posing astrochronologic testing and ESTF reconstruction (e.g., the climate-deposition transfer function) as a unified optimization problem that can leverage the geological and astronomical information. We discuss variants of the optimization approach, known as TimeOpt (Meyers, 2015), and apply it to numerous synthetic models and five Phanerozoic stratigraphic records. The results demonstrate the flexibility and broad applicability of TimeOpt, support the astronomical origin of the stratigraphic signals, and yield new constraints on the Earth System and the theoretical astronomical solutions. The TimeOpt methodology underscores that time is a central component of paleoenvironmental reconstruction; a simultaneous

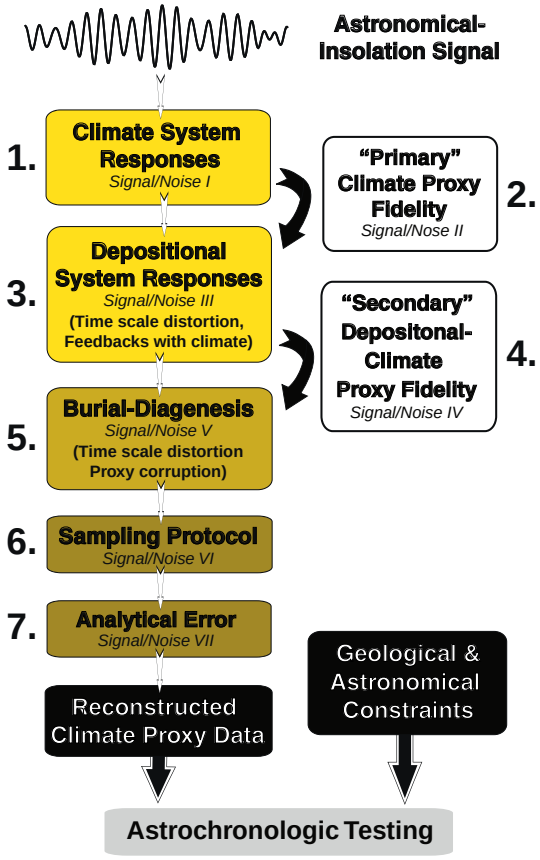

Fig. 2. The pathway of the astronomical signal (after Meyers et al., 2008 and Meyers, 2017). These steps, or *Earth System transfer functions* (ESTF), include: 1) the responses of the climate system to insolation changes, 2) the fidelity of "primary" climate proxies, which are directly linked to the climate variable of interest (e.g., $\delta^{18}O$ of ice as a proxy for atmospheric temperature), 3) the responses of the depositional system to the climate forcing, which can include climate feedbacks (e.g., ice-albedo feedback) and sedimentary distortions from variable sedimentation rates, 4) the fidelity of "secondary" climate proxies, which record a depositional system response to climate (e.g., clay accumulation along a continental margin, reflecting river discharge which responds to precipitation), 5) alteration of the proxy record during burial and diagenesis, which can corrupt the proxies and serve to distort the time scale, 6) sampling of the record by paleoclimate scientists (ocean drilling site selection, selection of samples for analysis, etc.), and 7) analytical measurement error of the climate proxy variable (e.g., 2σ uncertainties). Astrochronologic testing of the reconstructed climate proxy record is informed by geological (e.g., radioisotopic geochronology, biostratigraphy, paleoceanographic/paleoclimatic constraints) and astronomical constraints, and generally employs statistical evaluation via spectral analysis. Note that, within the context of this framework, autocyclic variability is considered a type of noise that can be introduced at various points along the pathway, particularly during steps 1 and 3. Note that steps 2, 4 and 7 include proxy calibration uncertainties, and that proxies can be a combination of multiple "primary" (climate) and/or "secondary" (depositional-climate) responses. For more information, see Meyers et al. (2008).

optimization on the time scale and ESTF, using relatively simple models that embody the behavior of climate and deposition, enhances the power of statistical astrochronologic testing, and also provides a means for more accurate reconstruction of the ancient Earth System.

This study also seeks to address the problem of reproducibility in cyclostratigraphy. The challenge of reproducing published cyclostratigraphic results and verifying conclusions can be exacerbated by the fact that complex procedures are often utilized during data processing and analysis – with computational algorithms that are not always transparent (i.e., 'open source') or appropriate – the statistical consequences of which are not necessarily obvious (Meyers, 2012; Vaughan et al.,

Box 2
The three fundamental propositions that serve as the basis for astrochronologic testing and astronomical time scale development.

Proposition 1. (Existence): An astronomical signal is preserved within a given stratigraphic succession or climate proxy record, to some measurable degree.

Proposition 2. (Calibration): The stratigraphic succession or climate proxy record preserves specified astronomical parameters that can be clearly discerned (observed sedimentary oscillations can be unambiguously attributed to precession, obliquity and/or eccentricity).

Proposition 3. (Tuning): A reliable astrochronology can be developed from the stratigraphic succession or climate proxy record, with well-constrained uncertainties.

2014). More broadly, the issue of how to improve reproducibility and accuracy in science has received much attention as of late (Nature, "Five ways to fix statistics", Leek et al., 2017, v. 551, p. 557–559). To aid in the broad dissemination of the statistical methods, enhance transparency, and improve reproducibility, software associated with this study is developed and implemented in the *Astrochron* (Meyers, 2014) package for R (R Core Team, 2017). The freely-available software includes detailed descriptions of the methods, and examples of their application. Key analyses presented in this study are also accompanied by the relevant Astrochron R-code (see supplement), to facilitate their reproduction.

2. The nature of the problem

When preserved within the stratigraphic archive, Milankovitch cycles can be viewed as encrypted astronomical signals (Meyers, 2017). A useful way to understand the problem of astrochronologic testing is through consideration of the pathway of the astronomical signal (Fig. 2), which constitutes an encryption algorithm (Meyers et al., 2008; Meyers, 2017). This conceptual framework recognizes that the preserved climate signal has been sequentially filtered through an array of processes, each of which can serve to distort – and may even render unrecognizable – the climate response that we seek to quantify. These *Earth System transfer functions* (Box 1) are analogous to model components that sequentially modify the astronomical signal during its transit (see Fig. 2. caption for a complete description, and Meyers et al., 2008; Meyers, 2017).

Within the context of this framework, skepticism about the veracity of astrochronology has emerged from concerns regarding the astronomical-climate transfer function (step 1 in Fig. 2), the climate-deposition transfer function (step 3 in Fig. 2), the burial-diagenesis transfer function (step 5 in Fig. 2), and the suitability of the approaches used for astrochronologic testing. For example, studies have argued that (1) the magnitude of astronomical climate forcing relative to stochastic climate variability is small (e.g., Wunsch, 2003, 2004), (2) the sensitivity of sedimentation to astronomical-climate forcing is minor within a given depositional environment (e.g., Peper and Cloetingh, 1995; Wilkinson et al., 1998; Wilkinson and Drummond, 2006), (3) stratigraphic distortion related to variable depositional rates and diagenesis prohibit a reliable assessment of the astronomical hypothesis (e.g., Hallam, 1986; Westphal et al., 2004; Westphal et al., 2015) and (4) insufficient independent time control makes temporal calibration of spatial periods to astronomical cycles ambiguous (e.g., Miall and Miall, 2004; Waltham, 2015). It should be emphasized that while these concerns require careful consideration, none apply uniformly to all cyclostratigraphic studies.

At the nexus of this debate, however, is the issue of astrochronologic testing. If indeed a strong astronomical signal can be confirmed, and its tempo established (note that confirmation of astronomical influence, and its accurate temporal calibration, are separate but related issues; see Section 3.1 and Box 2), then the other sources of skepticism are necessarily diminished in their strength. Two primary avenues of astrochronologic testing have been routinely employed for this purpose, oftentimes in a complimentary manner: (1) arguments that rely on a detailed "expert" knowledge of the integrated stratigraphy of a basin (including available biostratigraphic, magnetostratigraphic, chemostratigraphic, and radioisotopic constraints), comparative sedimentology, and paleoceanographic/paleoclimatologic constraints (sometimes from model output), and (2) arguments based on the statistical analysis of proxy or lithologic data. For simplicity, these will be referred to as the "integrated stratigraphy" and "statistical" approaches for astrochronologic testing. The pioneering work of Hays et al. (1976) provides a historical foundation for both classes of approaches.

To gain further insight into these challenges and better appreciate some of the skepticism, it is illustrative to examine one of the most commonly used statistical approaches for evaluating astronomical influence on sedimentation, the method of power spectral analysis. This technique quantifies data variance as a function of frequency (cycles/ka or cycles/m; Weedon, 2003), allowing the identification of frequency bands that disproportionately contribute to data variance ("spectral power"; Box 1), which can potentially be linked to an astronomical source. The approach is demonstrated in Fig. 3, which displays results from the power spectral analysis (Fig. 3b) of a simulated wt% $CaCO_3$

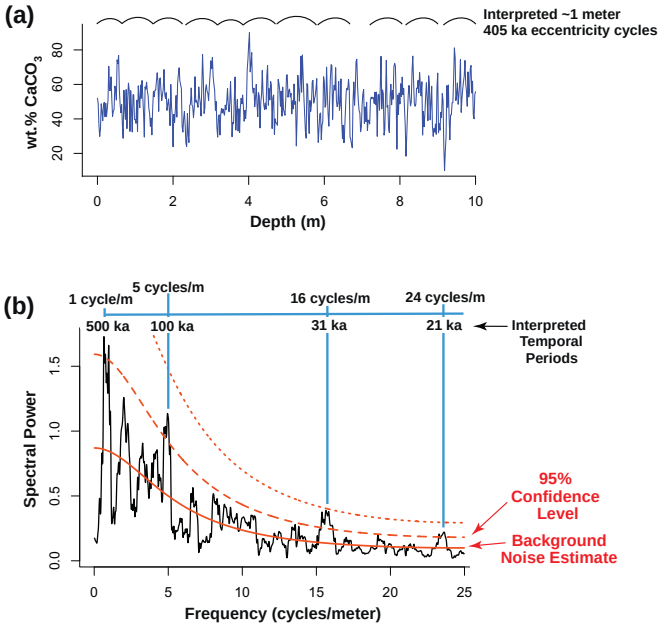

Fig. 3. An example of the use of power spectral analysis as an astrochronologic testing tool. (a) a simulated wt% $CaCO_3$ series that is 10 meters long, with a sampling interval of 0.02 m. (b) The power spectrum of the series in "a" using the multitaper method of Thomson (1982). The spectral background, which represents the AR1 red noise null hypothesis, is identified with a solid red line, and the dashed red line is the standard 95% confidence level for rejecting the null AR1 model. The dotted line indicates the 95% confidence level corrected for multiple testing (using the Bonferroni correction). The 3π multi-taper power spectrum was calculated using the Astrochron function 'mtm'.

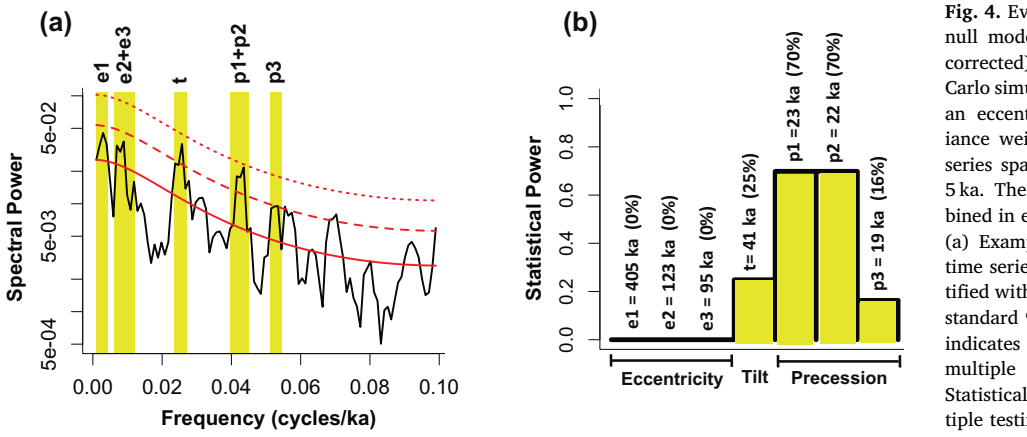

Fig. 4. Evaluation of the statistical power of an AR1 null model using the multiple testing (Bonferroni corrected) 95% Confidence Level. The 5000 Monte Carlo simulations combine AR1 noise ($\rho = 0.5$), with an eccentricity-tilt-precession model (with a variance weighting of 1:0.5:0.5). The simulated time series span 0–1000 ka with a sampling interval of 5 ka. The astronomical signal and noise are combined in equal measure (variance weighting of 1:1). (a) Example spectrum from one of the simulated time series. The AR1 red noise background is identified with a solid red line, the dashed red line is the standard 95% confidence level, and the dotted line indicates the 95% confidence level corrected for multiple testing (Bonferroni corrected). (b) Statistical power of the AR1 null model at the multiple testing (Bonferroni corrected) 95% confidence level, for the detection of the main eccentricity, obliquity and precession terms. All spectra in the simulations utilize the multitaper method (Thomson, 1982) with three 2π prolate tapers.

series that is 10 meters long, sampled every 2 cm (Fig. 3a). As is common in cyclostratigraphy, the statistical significance of each spectral peak is evaluated using a "red noise" null model (solid red line in Fig. 3b; "red" refers to the observation that spectral power increases as the frequency decreases, an analogy to light; in contrast, "blue noise" would demonstrate an increase in spectral power with frequency). Application of the "red noise" approach recognizes that *stochastic* oscillatory variability is a common feature of climate, and that memory within climate system components – and their interactions – can serve to generate strong low frequency oscillations, even in the absence of changes in climate forcing parameters (e.g., insolation; see Hasslemann, 1976 for a good discussion). In the context of cyclostratigraphy, the goal of significance testing is to guard against the erroneous attribution of such stochastic oscillations to astronomical forcing.

Confidence levels for rejecting the null model ("red noise") are determined using an estimate of the spectral background, which is taken to represent the stochastic variability. The autoregressive lag-1 (AR1) stochastic noise model (Gilman et al., 1963) is among the most common approaches for evaluating the significance of cycles in astrochronologic studies, and it is a straightforward model to estimate from the data (Weedon, 2003). Application of this approach in Fig. 3 suggests the presence of four significant cycles at the 95% confidence level. Independent time control is absent in this example, but as is common practice in cyclostratigraphy, we can prospect for cycle hierarchies ("bundling") that match the theoretical astronomical cycles, revealing a potential interpretation of long eccentricity (~400 ka), short eccentricity (~100 ka) and precession (~21 ka). Taken at face value, the mismatch between the expected long eccentricity cycle of ~400 ka, and observed cycle of 500 ka could be interpreted as due to *stratigraphic distortions*, or *contamination* of the eccentricity signal from stochastic climate processes.

What should cause concern, however, is the fact that the record analyzed in Fig. 3 is a noise simulation; it is AR1 noise with a lag-1 autocorrelation coefficient of ~0.5, generated using the Astrochron function 'ar1'. There are several key points that this example emphasizes. First, relatively simple stochastic models consistent with our understanding of climate and deposition (Gilman et al., 1963; Wunsch, 1972; Hassleman, 1976; Jerolmack and Paola, 2010; Hajek and Straub, 2017) are capable of generating strong oscillatory changes, which appear as prominent peaks in power spectra. In many cyclostratigraphic studies, these stochastic oscillations are strongest within the Milankovitch band, or some portion of it. In the parlance of this article, these represent *contamination* of the astronomical signal. Second, this example illustrates a limitation of standard power spectrum significance testing as an astrochronologic testing tool (Weedon, 2003). The goal of power spectral analysis is to decompose the data variance into many individual contributing frequencies, but this necessarily means that a single power spectral analysis conducts many independent null hypothesis tests. A confidence level of 95% implies that we are comfortable being wrong 5% of the time (the null hypothesis was correct, but we rejected it in favor of the astronomical hypothesis). If a power spectrum contains 100 independent frequencies, on average 5 of them should achieve the 95% confidence level when analyzing pure noise (Fig. 3). Typical paleoclimate spectral analyses evaluate hundreds to thousands of independent frequencies. Other fundamental issues regarding appropriate spectral background estimation and significance testing with power spectral analysis have been discussed in the literature (see Mann and Lees, 1996; Meyers, 2012; Vaughan et al., 2014; Kemp, 2016; Crampton et al., 2018), and indeed, concerns about appropriate spectrum confidence level estimation have been voiced numerous times in the history of astrochronology, going back to the seminal work of Hays et al. (1976); see the comment on that paper by Evans and Freeland (1977).

Some studies have argued for increasing the confidence levels depicted in Fig. 3 to address the problem of multiple-testing (the dotted line in Fig. 3; Vaughan et al., 2014; Kemp, 2016), the consequence of which is a dramatic decrease in the reliability (statistical power; Box 1) of the method; that is, even when astronomical cycles are known to be present – for example in astronomically forced simulations – they are difficult to detect. This is illustrated in Fig. 4, which summarizes the results of 5000 Monte Carlo simulations that are generated by combining an eccentricity-tilt-precession model with AR1 noise, in equal measure. The eccentricity terms are not detectable at the 95% multiple testing level, the dominant obliquity term is detected in 25% of the simulations, and the precession terms are detected in < 70% of the simulations (Fig. 4b).

The problem illustrated in Fig. 4 is compounded by the fact that the geologic record contains *stratigraphic distortions* that serve to defocus narrow spectral peaks, further reducing their estimated significance (Herbert, 1994; Meyers et al., 2001; Weedon, 2003). For this reason, many cyclostratigraphic studies still adopt the standard confidence levels, as depicted in Fig. 3. Detailed reviews on this issue can be found Kemp (2016) and in Crampton et al. (2018). While the statistical issues discussed above are indeed problematic, it should also be noted that there are many instances where multiple-testing procedures identify "significant" spectral peaks in records that are putatively astronomically-influenced (Section 4). However, even under such circumstances, the development of a reliable astrochronology requires accurate characterization of the tempo of the cycles, and careful reconstruction of their distortion by sedimentary processes (Section 3.1;

Box 2). How do we objectively address these concerns?

The pathway of the astronomical signal (Fig. 2), hints at a potential solution. The recognition that this pathway constitutes a framework of linked Earth System components suggests that it may be possible to leverage proxy data, geological knowledge, and astronomical knowledge to simultaneously conduct astrochronologic testing and transfer function reconstruction (such as *stratigraphic distortion*). If the key steps in the pathway of Fig. 2 can be quantitatively constrained through a statistical optimization, the resulting transfer functions yield information about a wide range of Earth surface processes, including paleoenvironmental change, but also the dynamics within depositional systems (ice sheets, continental margins, etc.) and their feedbacks with climate change. Thus, while Fig. 2 emphasizes the complexity that underlies astrochronological analysis, it also suggests that much of what is commonly regarded as noise in the stratigraphic record may be untapped signal, if approaches can be developed to harness the encrypted rhythms (Meyers, 2017). As discussed further below, achievement of this goal motivates a new statistical framework for evaluating astronomical cycles, one that explicitly considers time scale uncertainty, allows for the incorporation of geologic/radioisotopic constraints, and fully exploits the multiple attributes of the astronomical hypothesis (cycle hierarchies, amplitude modulations, etc.) to provide a reliable means for *statistical* astrochronologic testing. The proposed methodology, termed TimeOpt, builds upon the concept of triangulation (Box 1), where disparate lines of evidence are combined to improve the reliability of hypothesis testing (Lawlor et al., 2016; Munafò and Smith, 2018).

Before proceeding, several items are prudent to address. First, is it not the intention of this study to dismiss or understate the remarkable advancements in spectral analysis technique – as embodied by the multi-taper method of Thomson (1982) – which allow a reliable probabilistic assessment of the magnitude of band-limited variance within short and complex data series. Power spectrum evaluation is a crucial step in statistical cyclostratigraphic evaluation, and can provide strong evidence in support of astronomical influence. The central issue of relevance to cyclostratigraphy is that these spectral methods do not, in themselves, provide a test of the source of the observed cycles. This latter issue of attribution requires additional hypothesis testing against a null model (see discussion of the analysis in Fig. 3, and Section 5.2), and judgment about appropriate temporal calibration of observed cycles (Section 3.1; Box 2). The goal of the present work is to articulate a statistical framework that is well suited for the unique challenges of astrochronologic testing, and flexible enough to be broadly applied.

Second, a number of other statistical astrochronologic testing approaches have been advanced (e.g., Huybers and Wunsch, 2005; Huybers, 2007; Meyers and Sageman, 2007; Meyers, 2008; Lisiecki, 2010; Huybers, 2011; Proistosescu et al., 2012; Meyers et al., 2012b; Zeeden et al., 2015; Li et al., 2018). Each of these methods provides an explicit null hypothesis test, and some consider time scale uncertainty. In addition, a range of other useful astrochronologic methods have been developed (e.g., Hinnov and Park, 1998; Lisiecki and Raymo, 2005; Malinverno et al., 2010) that do not explicitly test the null hypothesis beyond standard spectral analysis approaches. While this article does not provide a comprehensive review of these published techniques, each has its merits; we refer the reader to those studies for details on the individual approaches.

Finally, there has been considerable debate among academic statisticians about the utility of *p*-values or confidence levels as a governing criterion for determining the significance of results, and more generally, about how to improve reproducibility in science (Wasserstein and Lazar, 2016; Nature, “Five ways to fix statistics”, 2017, v. 551, p. 557–559). Here we adopt the philosophy that p-values and their associated confidence levels provide one useful measure of the statistical evidence for a hypothesis – which should be considered in combination with other statistical and non-statistical criteria (e.g., geological and astronomical constraints; see Appendix A.5). The present work seeks to explicitly leverage the geological and astronomical constraints (“triangulation”, Box 1) to provide a more reliable cyclostratigraphic reconstruction, and more appropriate p-values/confidence levels. Yet ultimately, the confidence level threshold selected for designation of ‘significant’ results in cyclostratigraphic research (e.g., 99%, 95%, 90%) is a subjective one (e.g., see Thomson, 1990; Kemp, 2016). What is especially important, however, is the ability of other investigators to reproduce the results and evaluate other parameterizations for themselves; the latter objective is facilitated by incorporation of these procedures in the freely-available software Astrochron (Meyers, 2014).

3. Astrochronologic testing and Earth System reconstruction as an optimization problem

3.1. An evaluation of three propositions

It is useful to consider astrochronologic testing and astronomical time scale development as evaluating three distinct but related propositions, each of which embodies increasing specificity (Box 2). The ultimate ambition of astrochronology is to develop a reliable astronomical time scale with well-constrained uncertainties (Proposition 3). Achievement of this objective requires that a given stratigraphic succession or proxy series preserve astronomical variability that can be discerned from noise/autocyclic variability (Proposition 1), and that such variability be unambiguously attributed to specific astronomical parameters (Proposition 2). The existence of multiple astronomical interpretations for a given stratigraphic succession (e.g., Meyers and Sageman, 2007; Preto et al., 2001; Kent et al., 2004) illustrates the distinction between Propositions 1 and 2. However, even when Propositions 1 and 2 are accepted, the development of a reliable astrochronology (Proposition 3) can be complicated by the presence of hiatus, uncertainty in the tuning target, lack of radioisotopic data for anchoring, and other such factors. It is also important to note that confirmation of Propositions 1 and 2 may be of merit in their own right, as they can provide valuable information about the behavior of both climate and depositional system (e.g., the role of allocyclic forcing), even when it is not possible to develop a floating or anchored astrochronology (Box 1) with well-constrained uncertainties.

Section 2 highlights the challenges of using power spectra (with noise modeling) to evaluate Propositions 1 and 2, especially under scenarios where time is poorly constrained by independent means (e.g., radioisotopic data with sufficiently small uncertainties). A fundamental limitation of this approach – and other techniques such as lithofacies thickness-based methods (Wilkinson et al., 1996; Hinnov and Park, 1998; Bailey and Smith, 2008) – is that they do not explicitly evaluate time scale uncertainty, nor do they consider the multiple attributes of the astronomical hypothesis that can be employed for astrochronologic testing. TimeOpt is designed to specifically address these challenges. It starts from a theoretical statistical foundation – reframing astrochronologic testing using a probabilistic regression model framework – and explicitly leverages multiple attributes of the astronomical signal (concentration of spectral power at the predicted astronomical frequencies, the presence of expected amplitude modulations of precession, etc.), and available independent time control. The original formulation (Section 3.2; Meyers, 2015) addresses Propositions 1 and 2, while the introduction of sedimentation templates in the present paper (Section 3.3), and the recently published Bayesian extension of the method (TimeOptMCMC; Meyers and Malinverno, 2018), are designed to further improve its reliability and address Proposition 3.

3.2. The TimeOpt approach

The discussion in Sections 1 & 2 outlines the key problems of *contamination*, *stratigraphic distortion* and *temporal calibration*, and also illuminates the related problem of significance testing (spectral background estimation and multiple testing). The TimeOpt method (Meyers,

2015) is an astrochronologic testing approach that is designed to quantitatively address these problems, while also providing a flexible analytical framework for reconstruction of Earth System transfer functions. In terms of historical precedents, it shares the philosophical perspective of Brüggemann (1992), which sought to simultaneously optimize on a sedimentation model and a model for ice-sheet response to astronomical forcing, during the late Pleistocene.

The TimeOpt methodology recognizes that there are multiple attributes of the astronomical hypothesis that can be employed to increase the reliability of astrochronologic testing, and in doing so, utilizes the concept of "triangulation" (Box 1). The full TimeOpt methodology is described in Meyers (2015), and is briefly summarized here, with some further extensions of the method in Meyers and Malinverno (2018) and in Section 3.3.

TimeOpt is an abbreviation for "Time Scale Optimization", emphasizing that the evaluation of time scale uncertainty should be a central component of astrochronologic testing. At the core of the method is an assessment of two attributes that are diagnostic of an astronomical signal: (1) the concentration of spectral power at predicted astronomical frequencies (e.g., precession and eccentricity; Hays et al., 1976), and (2) the amplitude modulation of astronomical periods (e.g., eccentricity-related amplitude modulation of the precession band; Shackleton et al., 1995). These two astronomical attributes are evaluated using a probabilistic regression model framework. The discussion below is developed for the hypothesis of eccentricity and precession forcing, but as will be shown in Section 4.2, the method can also be applied to obliquity-forced records.

For a given proposed sedimentation rate (temporal calibration), the precession-band amplitude envelope is extracted from the proxy data using bandpass filtering and the Hilbert transform (Taner et al., 1979). The fit of the extracted precession-band envelope to the predicted eccentricity target periods is assessed with a probabilistic linear regression model (Eq. (1)):

$$\boldsymbol{y}_{envelope} = \boldsymbol{X}_{e}\boldsymbol{\beta}_{e} + \varepsilon \quad (1)$$

where: $\mathbf{y_{envelope}}$ is the precession-band amplitude envelope for the temporally calibrated data series; $\mathbf{X_e}$ is a matrix of sine and cosine predictor terms representing the eccentricity periods; $\boldsymbol{\beta}_e$ is a vector of regression coefficients for each predictor; ε is a vector of error terms.

This probabilistic regression model (Eq. (1)) is evaluated across a range of sedimentation rates (typically a grid) constrained by radioisotopic and/or bio-chemo-magnetostratigraphic data. The quality of the "fit" at each sedimentation rate is quantified using the Pearson correlation coefficient ($r^2_{envelope}$) between the resultant eccentricity model, $f(X_e,\beta_e)$, and the observed precession band envelope ($y_{envelope}$).

In a second step, the concentration of spectral power at the predicted astronomical target periods (for each proposed sedimentation rate) is evaluated using another probabilistic linear regression model (Eq. (2)):

$$\boldsymbol{y}_{data} = \boldsymbol{X}_{ep}\boldsymbol{\beta}_{ep} + \varepsilon \quad (2)$$

where: $\mathbf{y_{data}}$ is the temporally calibrated data series; $\mathbf{X_{ep}}$ is a matrix of sine and cosine predictor terms representing the eccentricity and precession periods; $\boldsymbol{\beta}_{ep}$ is a vector of regression coefficients for each predictor; ε is a vector of error terms.The quality of the "fit" between the resultant astronomical model series, $f(X_{ep},\beta_{ep})$, and the temporally-calibrated series (y_{data}), is estimated using the Pearson correlation coefficient, yielding $r^2_{spectral}$. The final measure of fit (r^2_{opt}) combines information from the evaluation of both amplitude envelope and spectral power, and is determined as:

$$r^2_{opt} = r^2_{envelope}\, r^2_{spectral} \quad (3)$$

This optimization approach identifies the sedimentation rate at which spectral power is concentrated at the precession and eccentricity frequencies, while simultaneously the hypothesized precession envelope expresses expected eccentricity modulation. In both regressions (Eqs. (1) and (2)), the amplitudes and phases of the astronomical periods are determined during model optimization, allowing for nonlinear Earth System responses, and accommodating the fact that the phases and amplitudes of the theoretical astronomical cycles are unconstrained for strata older then ~50 Ma (Laskar et al., 2004, 2011a).

Monte Carlo simulation with a first-order autoregressive model is used to determine the statistical significance of the observed r^2_{opt} value (Gilman et al., 1963); any number of noise models could be evaluated (see Section 5.2). In the present study, we implement an improved significance-testing methodology (introduced in Meyers and Malinverno, 2018) that conducts surrogate simulations across all sedimentation rates in the TimeOpt grid, rather than exclusively at the optimal sedimentation rate. This updated approach explicitly accounts for multiple-testing (Fisher, 1929), and yields more conservative *p*-values then the original method (Meyers, 2015).

Example applications of the TimeOpt approach are shown for two synthetic models in Figs. 5 and 6. The first example evaluates a 1000 ka long synthetic series composed of eccentricity and precession (each normalized to unit variance; this is referred to as a standardized EP model), with a sampling interval of 5 ka and a sedimentation rate of 2 cm/ka (Fig. 5a). The TimeOpt technique correctly resolves an optimal sedimentation rate of 2.00 cm/ka (r^2_{opt} = 0.823; Fig. 5f) that is highly significant (p = 0.005; Fig. 5g). The reliability of this temporal calibration is underscored by the correspondence of the maxima in the envelope fit and spectral power fit (Fig. 5e), as well as the simplicity of the time calibrated spectrum (Fig. 5b) and the fidelity of the observed precession amplitude modulations (Fig. 5c,d).

Fig. 6 illustrates a TimeOpt analysis of the AR1 noise series presented in Fig. 3. As expected, the noise simulation does not yield a highly significant result (r^2_{opt} = 0.095; p-value = .3685; Fig. 6f,g), and the fit of the spectral power and envelope regression models (Fig. 6e) are far more complicated and inconsistent. We should expect that, if we were to repeat this exercise 100 times, approximately 5 cases should yield a p-value < .05. The analysis of an AR1 simulation can be reproduced using the script in the supplement; try your luck to see if you obtain a noise simulation with a p-value < .05.

3.3. Extensions of the TimeOpt approach for Earth System transfer function (ESTF) reconstruction

The original TimeOpt formulation (Meyers, 2015) utilizes a constant sedimentation rate model. This approach is often reasonable for relatively short segments of the stratigraphic record deposited in deep-sea environments, but it can be problematic over longer time scales, and is less likely to be valid in more proximal shelf and continental realms. While the constant sedimentation model is capable of providing a reliable astrochronologic test under conditions of moderate sedimentation rate instability, the *statistical power* of the method decreases and the reconstructed time scale is biased. The latter issue is not necessarily a problem, if the main goal of the TimeOpt application is to test the astronomical hypothesis and develop a nominal astronomical calibration (Propositions 1 and 2; Box 2) of the observed stratigraphic cycles, for astronomical tuning by other means (e.g., tuning to a target insolation series, frequency domain minimal tuning, etc.; Martinson et al., 1987; Meyers et al., 2001; Lisiecki and Raymo, 2005). In most cases, the constant sedimentation rate assumption is the best one to start with, as it is the simplest a priori model (depth as a proxy for time) adding only one degree of freedom to the statistical optimization.

Ultimately, however, sedimentation rate instability of a large enough magnitude will compromise the utility of the nominal TimeOpt approach. One way to overcome this problem, for gradual secular changes in sedimentation rate (e.g., associated with basin evolution, relative sea level change, etc.), is to apply TimeOpt in an evolutive manner (Astrochron function 'eTimeOpt'). In such an implementation, the TimeOpt analysis window is sequentially shifted through the

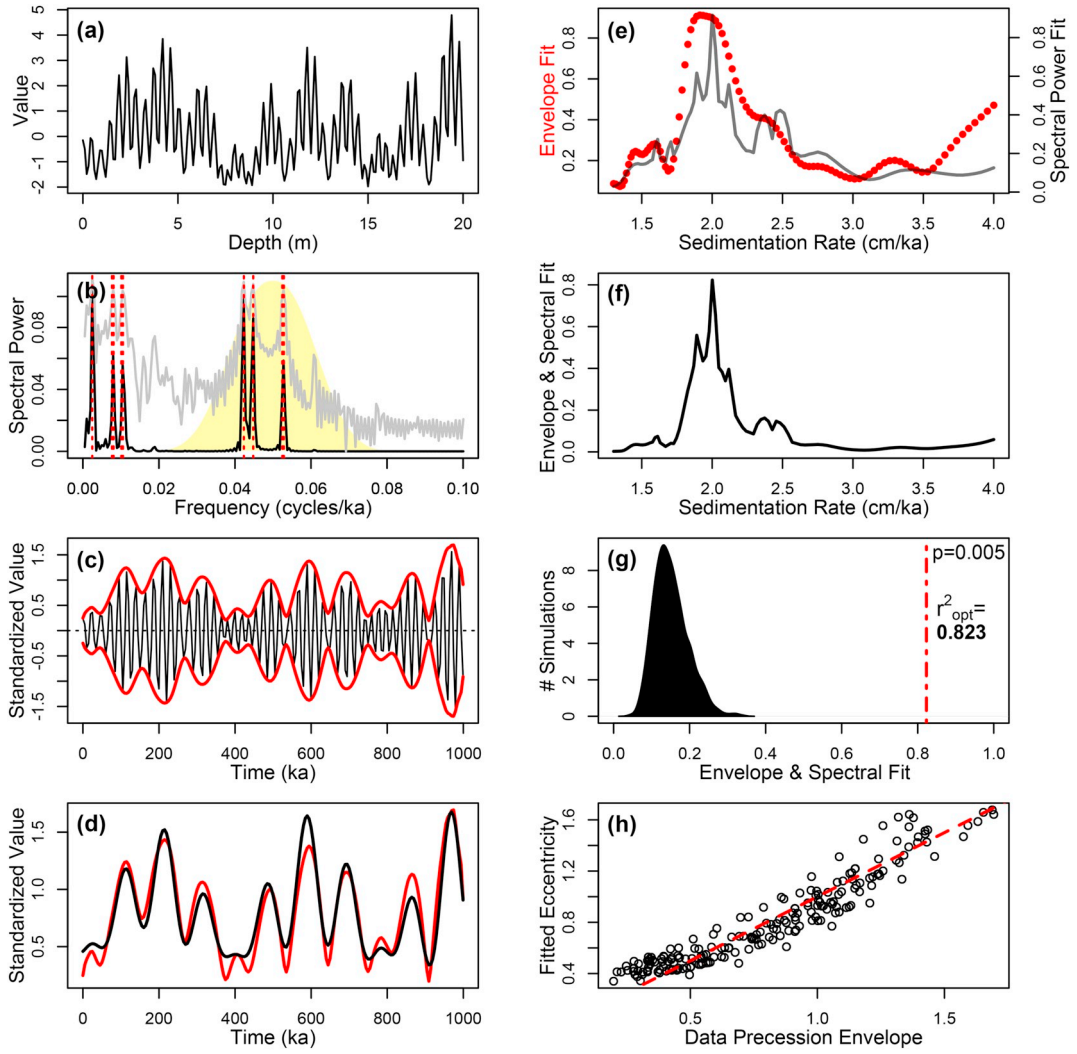

Fig. 5. Demonstration of TimeOpt using a standardized eccentricity + precession (EP) model (0–1000 ka, sampling interval of 5 ka), with a sedimentation rate of 2 cm/ka. (a) The standardized EP stratigraphic model. (b) Periodogram for the EP model, given the TimeOpt derived sedimentation rate of 2.00 cm/ka (black line = linear spectrum; gray line = log spectrum). Yellow shaded region illustrates the bandpass filter for evaluation of the precession amplitude envelope. Vertical dashed red lines indicate the eccentricity and precession target periods. (c) Comparison of the band-passed precession signal (black line), and the data amplitude envelope (red line) determined via Hilbert transform. (d) Comparison of the data amplitude envelope (red line) and the TimeOpt-reconstructed eccentricity model (black line; derived using Eq. (1)). (e) Squared Pearson correlation coefficient for the amplitude envelope fit ($r^2_{envelope}$; red dots) and the spectral power fit ($r^2_{spectral}$; dark gray line) at each evaluated sedimentation rate. (f) Combined envelope and spectral power fit (r^2_{opt}) at each evaluated sedimentation rate. (g) Summary of 2000 Monte Carlo simulations with AR1 surrogates (ρ_{AR1} = 0.551), used to evaluate the significance of the maximum observed r^2_{opt} of 0.823 (*p*-value = .005). (h) Cross plot of the data amplitude envelope and the TimeOpt-reconstructed eccentricity model in panel "d"; dashed red line is the 1:1 line.

stratigraphic record (see the example in Section 4.4). This approach is useful, but it is ultimately limited to situations where sedimentation rate does not vary strongly within the analysis window.

Alternatively, the regression model framework that is the foundation of TimeOpt can be adapted to accommodate complex sedimentation models, allowing a more versatile reconstruction of depositional system transfer functions, and enhancing the reliability of astrochronologic testing under such scenarios (Astrochron function 'timeOptTemplate'). To allow for the inclusion of complex sedimentation models, we introduce the concept of a *sedimentation template*: a unitless expression of the depositional system transfer function. The essential concept is a familiar one to stratigraphers, as embodied in relative sea level curves and interpretations of energy gradients in depositional systems (low energy to high energy environments). The form of the *sedimentation template* (Fig. 7) is defined by the analyst, and allows stratigraphic knowledge ("integrated stratigraphy") to be directly considered in the statistical assessment. Once the form of the template is proscribed, it dynamically interacts with the astronomical target and data during optimization; the units and magnitude of the depositional system transfer function are acquired during the optimization process.

The constant sedimentation rate model (Fig. 7a) of the nominal TimeOpt approach is the simplest form of *sedimentation template,* in that it utilizes minimal constraints from stratigraphic knowledge: only the minimum and maximum plausible sedimentation rates are specified. One useful *sedimentation template* that incorporates a greater degree of stratigraphic knowledge is based on a linear scaling of the observed lithologic parameter or proxy value (or any transformation of it) as a model for sedimentation rate (Fig. 7f). This formulation is founded upon the hypothesis that – if the depositional system is sensitive to climate – it is plausible that climate may influence the bulk accumulation rate of sediment and the observed proxy value or and/or lithology (e.g., wt% $CaCO_3$) (Schiffelbein and Dorman, 1986; Herbert, 1992; Meyers et al., 2001). The proxy/lithology-specific *sedimentation template* approach allows one to evaluate facies-specific sedimentation rates, and thus draws some similarities to the "gamma method" of Kominz and Bond (1990), and the "spectral simplicity" method of

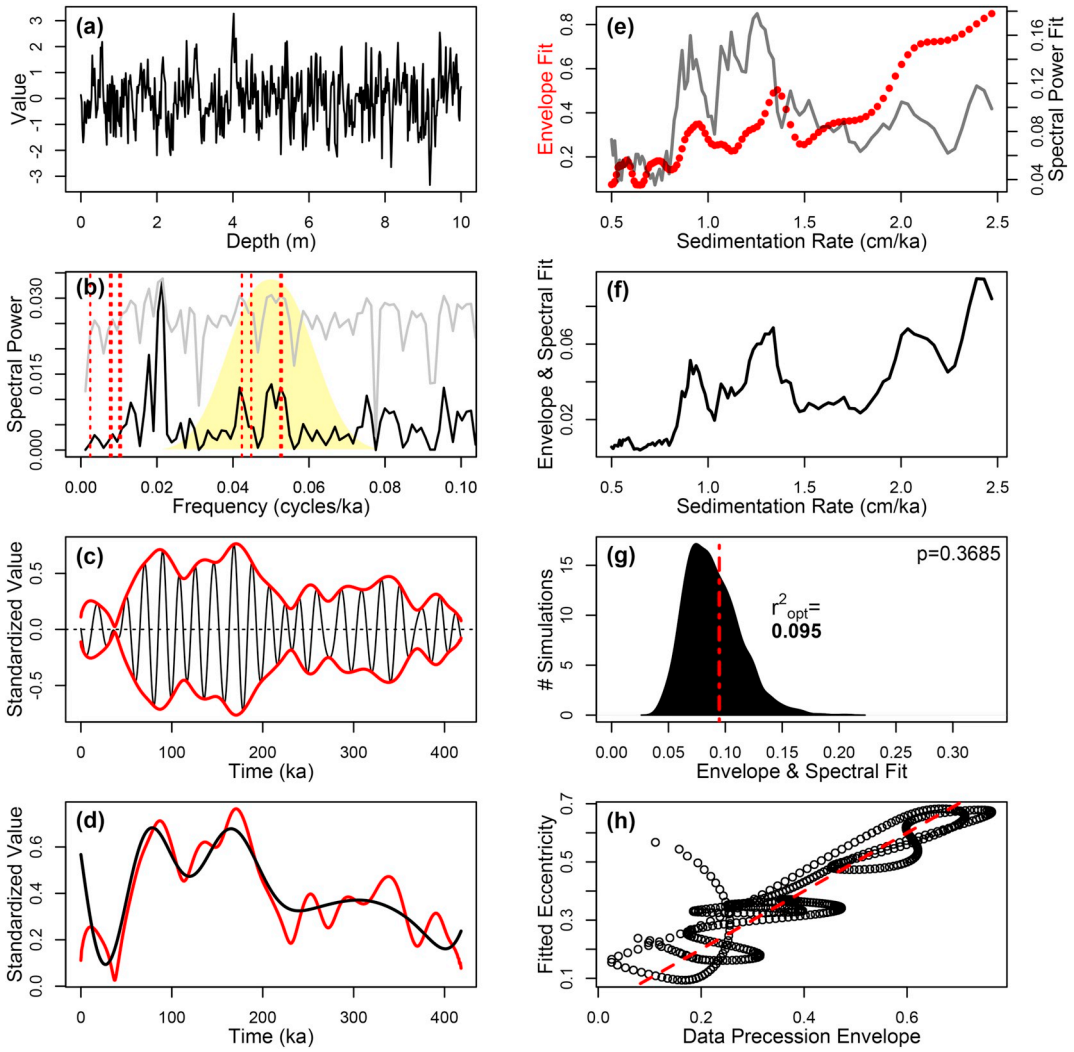

Fig. 6. .TimeOpt analysis of the AR1 noise model in Fig. 3. (a) The synthetic AR1 noise model analyzed in Fig. 3. (b) Periodogram for the noise model, given the TimeOpt derived sedimentation rate of 2.39 cm/ka (black line = linear spectrum; gray line = log spectrum). Yellow shaded region illustrates the bandpass filter for evaluation of the precession amplitude envelope. Vertical dashed red lines indicate the eccentricity and precession target periods. (c) Comparison of the band-passed precession region (black line), and the data amplitude envelope (red line) determined via Hilbert transform. (d) Comparison of the data amplitude envelope (red line) and the TimeOpt-reconstructed eccentricity model (black line; derived using Eq. (1)). (e) Squared Pearson correlation coefficient for the amplitude envelope fit ($r^2_{envelope}$; red dots) and the spectral power fit ($r^2_{spectral}$; dark gray line) at each evaluated sedimentation rate. (f) Combined envelope and spectral power fit (r^2_{opt}) at each evaluated sedimentation rate. (g) Summary of 2000 Monte Carlo simulations with AR1 surrogates (ρ_{AR1} = 0.495), used to evaluate the significance of the maximum observed r^2_{opt} of 0.095 (*p*-value = .3685). (h) Cross plot of the data amplitude envelope and the TimeOpt-reconstructed eccentricity model in panel "d"; dashed red line is the 1:1 line.

Schiffelbein and Dorman (1986). This *sedimentation template* provides two additional degrees of freedom for the statistical optimization, associated with estimation of the slope and y-intercept of the linear sedimentation rate scaling.

Figs. 8 and 9 illustrate the analysis of a synthetic record distorted by systematic changes in sedimentation rate across the lithologic cycles (Fig. 8a). This model is constructed using a standardized EP model, with a sedimentation rate that linearly scales from 1 cm/ka to 5 cm/ka across the observed proxy range. The nominal TimeOpt analysis, using a constant *sedimentation template*, reveals a highly distorted spectrum and does not yield a significant result (r^2_{opt} = 0.268, *p*-value = .3045; Fig. 8f,g). Application of the proxy-based *sedimentation template* (Fig. 7f), however, resolves the correct temporal calibration (r^2_{opt} = 0.787; p-value = .005; Fig. 9e,f), and provides a more reliable high-resolution sedimentation history throughout the study interval (Fig. 9b).

Another useful *sedimentation template* that incorporates stratigraphic knowledge is a linear sedimentation rate increase/decrease (ramp) throughout the stratigraphic interval (Fig. 7b,c), which adds one additional degree of freedom beyond the constant *sedimentation template*, for estimation of the slope of the ramp. Note that a constant sedimentation rate model is included in this assessment, which is the case when the slope is zero. Figs. 10 and 11 illustrate TimeOpt analyses of a standardized EP model with a linear sedimentation rate increase from 1 cm/ka to 5 cm/ka (Fig. 10a). Evaluation with a constant *sedimentation template* identifies an optimal average sedimentation rate of 4.23 cm/ka (r^2_{opt} = 0.202; Fig. 10f), although the spectrum peaks do not align well with the predicted astronomical targets (Fig. 10b), and the precession envelope suffers loss of amplitude in the interval < 200 ka (Fig. 10c); the latter is due to the spatial of drift (distortion) of the astronomical cycles, which places the precession cycles outside the bandpass region (Fig. 10b), and is also due to the undersampling of precession cycles by the 15 cm sampling resolution (Fig. 10a). The statistical significance of the result is relatively low (*p*-value = .1325).

Application of an increasing ramp *sedimentation template* (Fig. 7b) resolves a linear sedimentation rate increase from 1.59 to 5.23 cm/ka

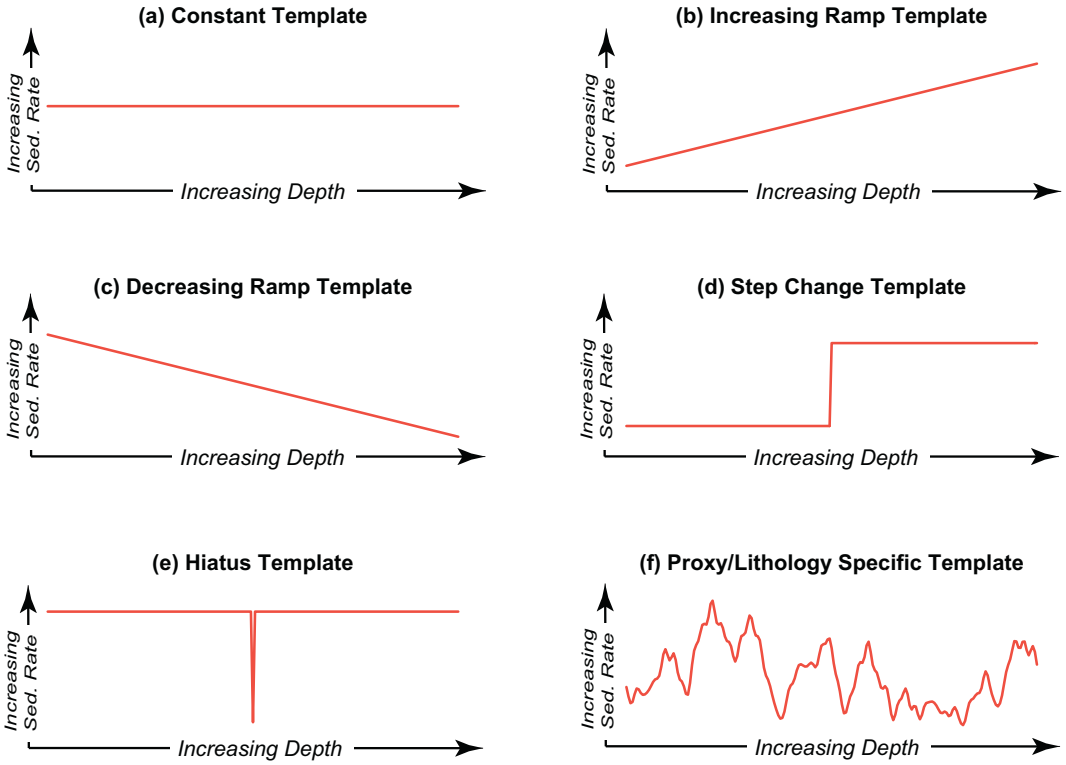

Fig. 7. Examples of TimeOpt sedimentation templates. (a) Constant sedimentation template, (b) Increasing ramp template (increasing with height or depth), (c) Decreasing ramp template (decreasing with height or depth), (d) Step change template, (e) Hiatus template, (f) Proxy/lithology specific template.

through the interval (Fig. 11b), improves the spectral peak alignment to the target periods (Fig. 11g), and increases the statistical significance of the result (Fig. 11f; $r^2_{opt} = 0.539$; *p*-value = .005). Several notable distortions are observed in the results, however, each of which is a consequence of an undersampling of the precession signal through the interval of lowest sedimentation rate (< 100 ka or < 1.5 m; Fig. 11a). These distortions are observed as (1) the presence of scattered spectral peaks within the precession band (Fig. 11g), (2) a weak precession signal for the interval < 100 ka (Fig. 11c,d), and (3) a mismatch between the TimeOpt-reconstructed eccentricity and the observed precession envelope for the interval < 100 ka (Fig. 11d). An increase in the sample resolution will help resolve these issues, or alternatively, a TimeOpt evaluation of the 15 cm resolution data series that excludes the envelope fit (allowing sharpening of the spectral fit). This example emphasizes how the multiple diagnostics provided by the TimeOpt approach provide a means to improve the cyclostratigraphic assessment through iterative analyses.

A final illustration considers segmented *sedimentation templates* that incorporate a stepwise change in sedimentation rate (Fig. 7d), or the presence of hiatus (Fig. 7e). In cases where geologic observation (radioisotopic data, biostratigraphy, sedimentology, etc.) reveals evidence for such stratigraphic distortions, they can be explicitly modeled within the TimeOpt framework. An example of hiatus reconstruction is shown in Figs. 12 and 13, which evaluate a synthetic cyclostratigraphic model identical to example 1 (Fig. 5), but with a 100 ka long hiatus at 10 m depth (Fig. 12a). The nominal TimeOpt approach identifies an optimal average sedimentation rate of 1.91 cm/ka that is highly significant ($r^2_{opt} = 0.291$, p-value = .039; Fig. 12f,g). The TimeOpt calibrated result includes many unexplained peaks in the precession band (Fig. 12b), splits the long eccentricity peak (Fig. 12b; Meyers and Sageman, 2007), and reveals a distortion of the precession envelope in the vicinity of the hiatus (Fig. 12c). As expected, we also observe a mismatch between the precession envelope and the TimeOpt-reconstructed eccentricity signal, near the location of the hiatus (Fig. 12d).

The incorporation of a hiatus *sedimentation template* in the TimeOpt analysis indicates an average background sedimentation rate of 1.87 cm/ka ($r^2_{opt} = 0.327$; Fig. 13e), but more importantly, the sedimentation rate outside the level of hiatus is 1.99 cm/ka (Fig. 13b), and a 70 ka hiatus is reconstructed at 10 meters height (at ~500 ka; Fig. 13c). Note that, in this case, the p-value of the TimeOpt result using the hiatus *sedimentation template* is substantially larger ($p = .199$) than when a constant *sedimentation template* is used ($p = .039$). This indicates that the hiatus *sedimentation template* can readily adjust noise to an astronomical signal when a hiatus of large duration is permitted in the optimization process (in this case, up to 1 million years). Reduction in the p-value is possible if we assign a shorter maximum possible hiatus duration. In the present case we can ascertain that the hiatus template does not improve the statistical power of the TimeOpt approach (related to Proposition 1), but it does reduce bias in the reconstructed astronomical time scale (related to Proposition 3).

In order to better understand the hiatus reconstruction process, and the discrepancy between the observed (70 ka) and expected hiatus duration (100 ka), it is illustrative to perform a finer grid search near the r^2_{opt} maximum (Fig. 13e), using only the spectral power fit. Such an analysis reveals the oscillatory nature of the spectral power fit, associated with the addition and deletion of precession cycles (Fig. 14a). This analysis also accurately reconstructs the duration of the hiatus (Fig. 14c), and improves the alignment of the spectral peaks to the target periods (Fig. 14b). Note that the TimeOpt eccentricity model in Fig. 14d (black line) correctly identifies the amplitude and phase of the long eccentricity cycle through the interval of hiatus, even though the precession signal is absent (blue line; Fig. 14d). This result emphasizes that, if hiatus is known to exist, application of the spectral power fit to estimate the optimal temporal calibration may be preferred, since the precession envelope is highly distorted through the interval of hiatus.

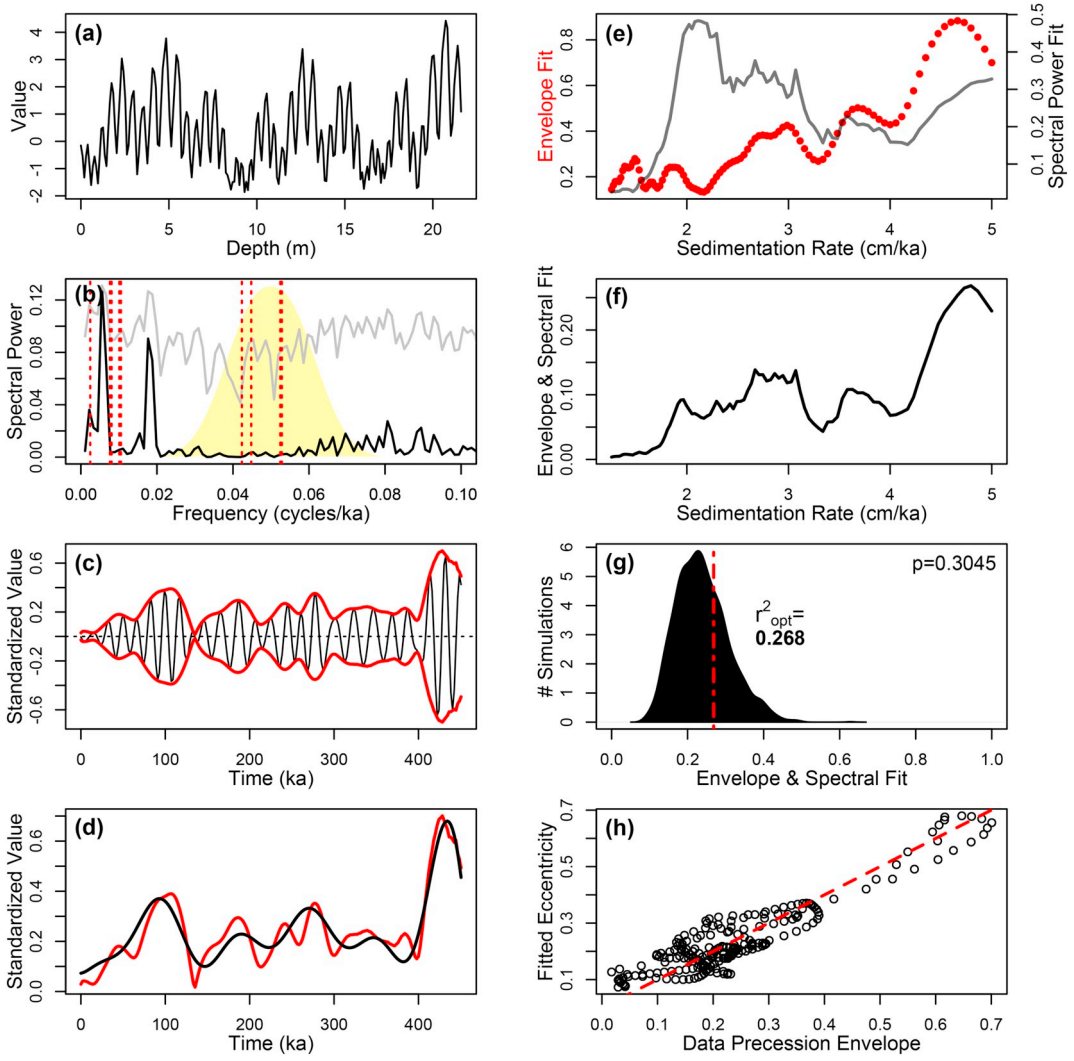

Fig. 8. TimeOpt analysis of an EP model distorted by systematic changes in sedimentation rate across the lithologic cycles, evaluated with a constant *sedimentation template*. (a) The synthetic EP series that is analyzed. (b) Periodogram for the EP model, given the TimeOpt derived average sedimentation rate of 4.80 cm/ka (black line = linear spectrum; gray line = log spectrum). Yellow shaded region illustrates the bandpass filter for evaluation of the precession amplitude envelope. Vertical dashed red lines indicate the eccentricity and precession target periods. (c) Comparison of the band-passed precession signal (black line), and the data amplitude envelope (red line) determined via Hilbert transform. (d) Comparison of the data amplitude envelope (red line) and the TimeOpt-reconstructed eccentricity model (black line; derived using Eq. (1)). (e) Squared Pearson correlation coefficient for the amplitude envelope fit ($r^2_{envelope}$; red dots) and the spectral power fit ($r^2_{spectral}$; dark gray line) at each evaluated sedimentation rate. (f) Combined envelope and spectral power fit (r^2_{opt}) at each evaluated sedimentation rate. (g) Summary of 2000 Monte Carlo simulations with AR1 surrogates (ρ_{AR1} = 0.755), used to evaluate the significance of the maximum observed r^2_{opt} of 0.268 (*p*-value = .3045). (h) Cross plot of the data amplitude envelope and the TimeOpt-reconstructed eccentricity model in panel "d"; dashed red line is the 1:1 line.

4. Applications of the TimeOpt approach

In this section, we demonstrate the application of TimeOpt to five classic cyclostratigraphic datasets (Fig. 15). These include examples from the Pleistocene of the North Atlantic (Site 607; Lisiecki and Raymo, 2005), the Miocene of Morocco (Ain el Beida section, van der Laan et al., 2012), the Eocene of Walvis Ridge (Zachos et al., 2004), the Triassic Newark Basin (Olsen, 1986) and the Triassic Latemar Platform (Preto et al., 2001). As is commonplace in cyclostratigraphy, each analysis consists of an initial power spectral analysis of the stratigraphic series (Fig. 16). In all cases considered here, an AR1 null model is found to provide a reasonable approximation to the spectral background, and a Bonferroni correction is applied to account for multiple-testing. It is not the intent this present work to provide a comprehensive assessment of the significance of spectral peaks; however, a range of multiple testing procedures for power spectra are presented in Crampton et al. (2018), and are available in the Astrochron package. The initial spectral assessments in the spatial domain (Fig. 16) are then followed by a more comprehensive astrochronologic evaluation using the TimeOpt approach, where the timescale uncertainty and the statistical significance of the results are more fully considered (using Monte Carlo simulation).

4.1. The Eocene: a return to Walvis Ridge

As a first case study, we consider one of the key archives of the early Eocene hyperthermal events (Kennett and Stott, 1991), ODP Site 1262 in the South Atlantic (Leg 208; Zachos et al., 2004; Fig. 15a). Red/green (a*) color reflectance data from this site, spanning the interval between the Paleocene-Eocene Thermal Maximum (PETM; Zachos et al., 2005) and Eocene Thermal Maximum 2 (ETM2; Lourens et al., 2005), was previously evaluated using the nominal TimeOpt approach by Meyers (2015). Sediments at this site are generally characterized by nannofossil ooze with some interbedded chert layers, while the PETM and ETM2 intervals are distinctive deep red clay layers (Zachos et al., 2004). The a* data has a strong positive correlation with XRF iron counts (Westerhold et al., 2007; Zachos et al., 2010), where large a* values

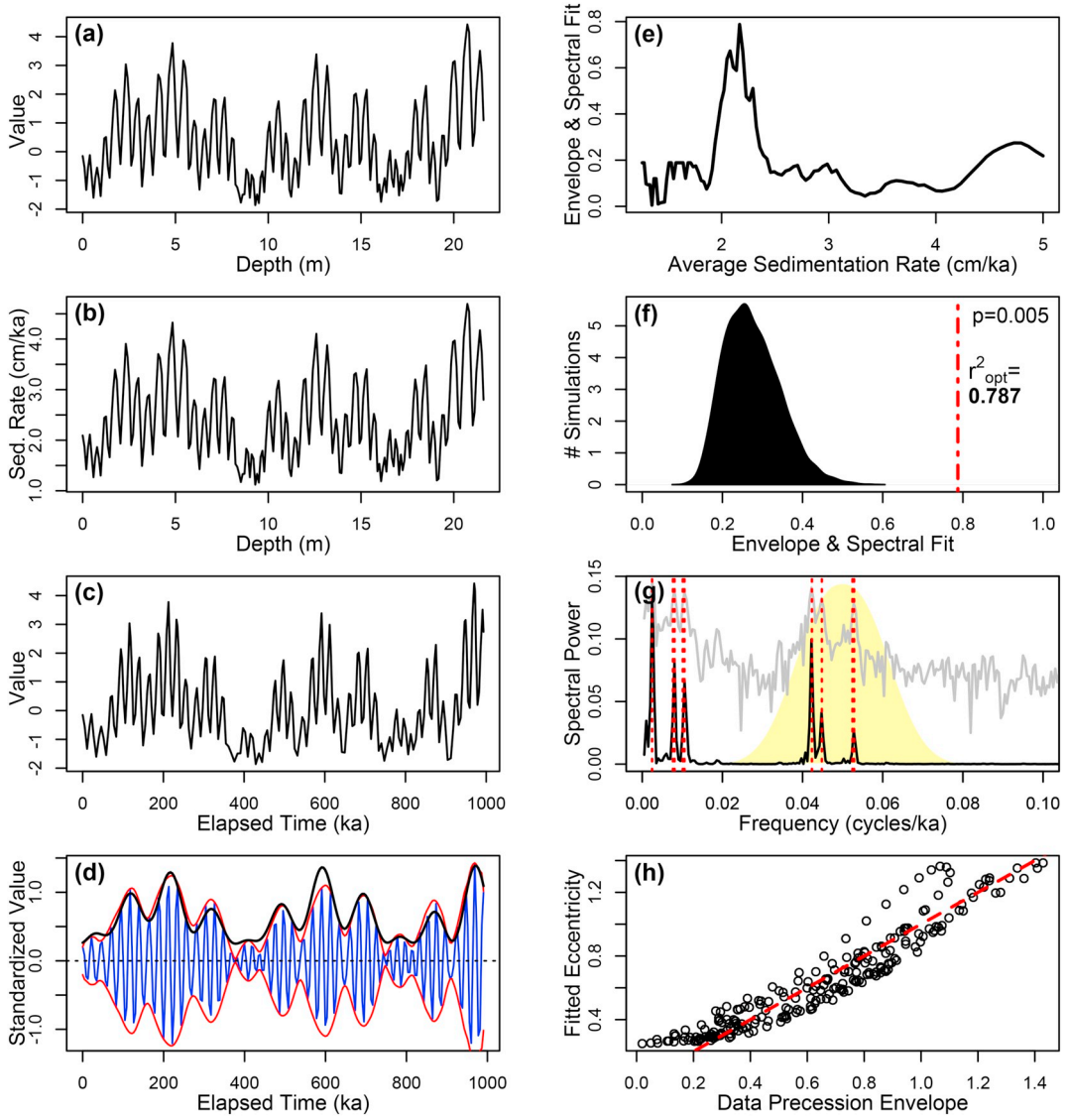

Fig. 9. TimeOpt analysis of an EP model distorted by systematic changes in sedimentation rate across lithologic cycles, evaluated with a proxy/lithology specific *sedimentation template*. (a) The synthetic EP series that is analyzed. (b) TimeOpt-reconstructed sedimentation rate history. (c) Astronomically-tuned stratigraphic series using the sedimentation rate history in (b). (d) Comparison of the band-passed precession signal (blue line), the data amplitude envelope (red line) determined via Hilbert transform, and the TimeOpt-reconstructed eccentricity model (black line; derived using Eq. (1)). (e) Combined envelope and spectral power fit (r^2_{opt}) at each evaluated average sedimentation rate. (f) Summary of 2000 Monte Carlo simulations with AR1 surrogates (ρ_{AR1} = 0.755), used to evaluate the significance of the maximum observed r^2_{opt} of 0.787 (*p*-value = .005). (g) Periodogram for the EP model, given the TimeOpt derived sedimentation history in (b) (black line = linear spectrum; gray line = log spectrum). Yellow shaded region illustrates the bandpass filter for evaluation of the precession amplitude envelope. Vertical dashed red lines indicate the eccentricity and precession target periods. (h) Cross plot of the data amplitude envelope and the TimeOpt-reconstructed eccentricity model in panel "d"; dashed red line is the 1:1 line.

reflect increased terrigenous Fe content and reduced carbonate content.

Power spectral analysis of the a* data reveals spatial bedding cycles that exceed the 95% multiple testing confidence level, relative to an AR1 null model (Fig. 16a). TimeOpt analysis with a constant *sedimentation template* identifies an optimal sedimentation rate of 1.33 cm/ka (r^2_{opt} = 0.214; Fig. 17f) that is highly significant (*p*-value = .005; Fig. 17g), confirming the astronomical interpretation of Lourens et al. (2005) (see a detailed discussion of this analysis in Meyers, 2015).

The oceanographic mechanism that has been invoked to generate the lithologic cycles at Site 1262 implicates a vertical migration of the lysocline, and consequent changes in carbonate preservation; the PETM and ETM2 intervals represent the most extreme of these interpreted lysocline shallowing events (Zachos et al., 2010; Kirtland Turner et al., 2014; Zeebe et al., 2017). Two additional mechanisms can also plausibly contribute to the generation of the lithologic cycles: changes in carbonate productivity due to nutrient availability, and changes in clay flux associated with weathering (Kelly et al., 2005).

If changes in carbonate production and/or preservation are the primary driving mechanism for these sedimentary rhythms (in contrast to clay flux), the accumulation rates associated with the carbonate-poor lithofacies should be substantially reduced as compared to the carbonate-rich lithofacies, across multiple scales of astronomical forcing. To test the above hypothesis, we utilize a proxy-specific *sedimentation template* to evaluate the Site 1262 a* data, where sedimentation rate is inversely scaled to a* (Fig. 18). The result is a millennial scale sedimentation history (Fig. 18b) that more effectively concentrates spectral power at the eccentricity and precession target periods (Fig. 18g), and improves the overall fit (r^2_{opt} = 0.284, *p*-value = .005; Fig. 18e,f), thus confirming the hypothesized reduced sedimentation rate for the carbonate-poor lithofacies, and quantifying the magnitude of the

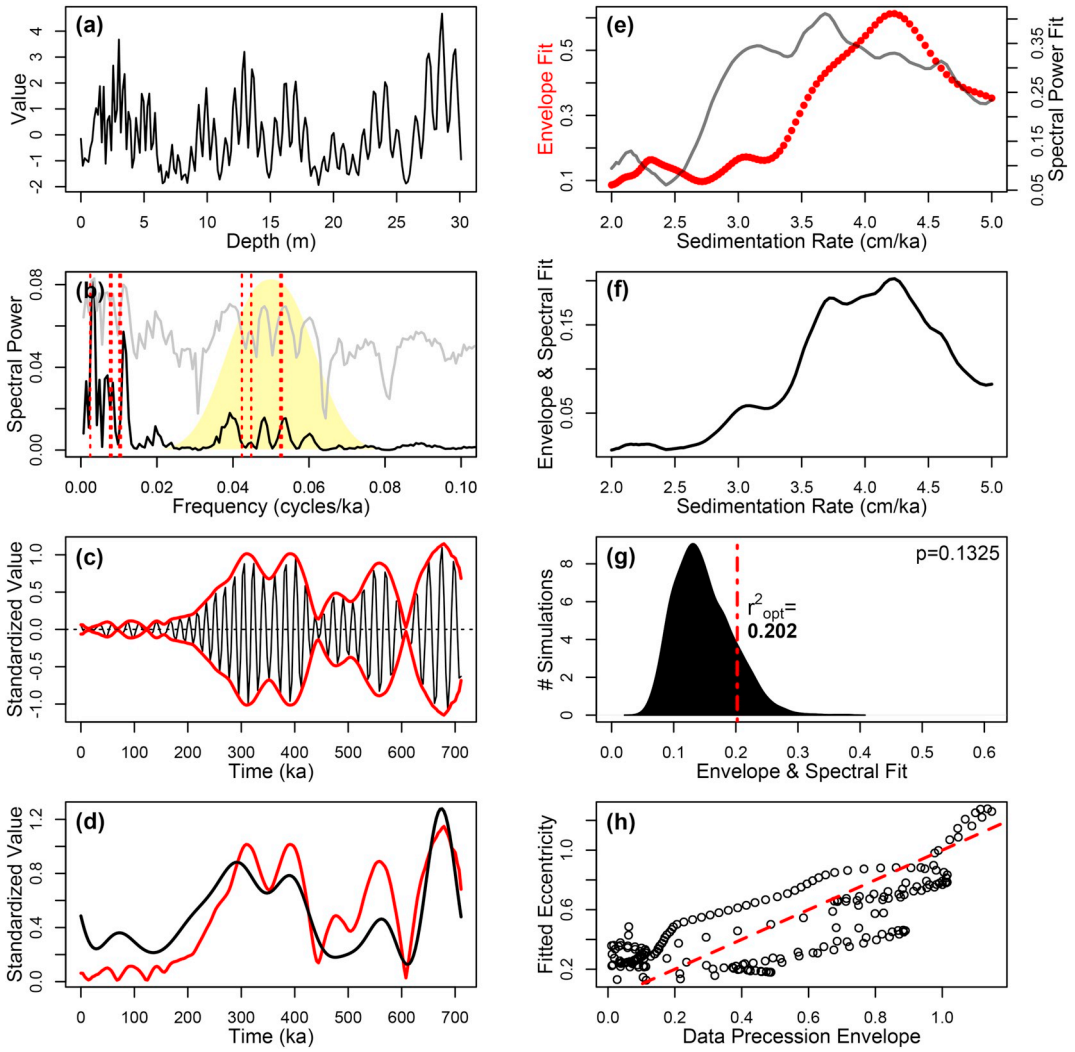

Fig. 10. TimeOpt analysis of an EP model distorted by a linear sedimentation rate increase across the stratigraphic interval, evaluated with a constant *sedimentation template*. (a) The synthetic EP series that is analyzed. (b) Periodogram for the EP model, given the TimeOpt derived average sedimentation rate of 4.23 cm/ka (black line = linear spectrum; gray line = log spectrum). Yellow shaded region illustrates the bandpass filter for evaluation of the precession amplitude envelope. Vertical dashed red lines indicate the eccentricity and precession target periods. (c) Comparison of the band-passed precession signal (black line), and the data amplitude envelope (red line) determined via Hilbert transform. (d) Comparison of the data amplitude envelope (red line) and the TimeOpt-reconstructed eccentricity model (black line; derived using Eq. (1)). (e) Squared Pearson correlation coefficient for the amplitude envelope fit ($r^2_{envelope}$; red dots) and the spectral power fit ($r^2_{spectral}$; dark gray line) at each evaluated sedimentation rate. (f) Combined envelope and spectral power fit (r^2_{opt}) at each evaluated sedimentation rate. (g) Summary of 2000 Monte Carlo simulations with AR1 surrogates (ρ_{AR1} = 0.670), used to evaluate the significance of the maximum observed r^2_{opt} of 0.202 (*p*-value = .1325). (h) Cross plot of the data amplitude envelope and the TimeOpt-reconstructed eccentricity model in panel "d"; dashed red line is the 1:1 line.

astronomically-forced reduction in carbonate due to lysocline movement and/or productivity. The TimeOpt approach also yields an improved time scale (Fig. 18c), with a temporal resolution that is an order of magnitude smaller than previous eccentricity-based tunings (e.g., Westerhold et al., 2015). Finally, the TimeOpt-reconstructed eccentricity model provides a means to validate proposed theoretical models for eccentricity, as discussed in Meyers, 2015; (see their Fig. 4; see also Meyers and Malinverno, 2018).

4.2. The early Pleistocene: obliquity influence at Site 607

One of the classic data sets that has informed our understanding of Plio-Pleistocene climate evolution comes from Site 607 in the North Atlantic (Ruddiman et al., 1989; Raymo et al., 1989; Raymo et al., 1992; Lisiecki and Raymo, 2005). The early Pleistocene benthic foraminiferal $\delta^{18}O$ data from Site 607 has been interpreted to preserve a strong obliquity signal, and has been used to develop numerous chronologies for the ice ages (Ruddiman et al., 1989; Lisiecki and Raymo, 2005; Huybers and Wunsch, 2004; Huybers, 2007). According to the LR04 (Lisiecki and Raymo, 2005) chronology, the 40 m thick interval investigated here spans 1.36 Ma–2.25 Ma (Fig. 15b). This data set provides an ideal case study to evaluate the suitability of the TimeOpt approach for assessing obliquity forcing in stratigraphic archives.

Power spectral analysis of the benthic foraminiferal $\delta^{18}O$ data reveals a single spatial bedding cycle that exceeds the 95% multiple testing confidence level, relative to an AR1 null model (Fig. 16b). The theoretical obliquity signal is characterized by a strong monochromatic signal at ~41 ka, with amplitude modulation periods near ~100 ka and ~170 ka, and a longer period modulation near ~1.2 Myr (Laskar et al., 2004). In contrast to climatic precession, the obliquity amplitude modulation periods are not commonly observed in the spectral signatures from proxy data. To adapt the TimeOpt approach for obliquity assessment, we evaluate spectral power ($r^2_{spectral}$) at the 41.08 ka period, and amplitude modulation ($r^2_{envelope}$) at periods of 174.8 ka, 106.6 ka, and 97.1 ka (as determined from an assessment of the Laskar et al.,

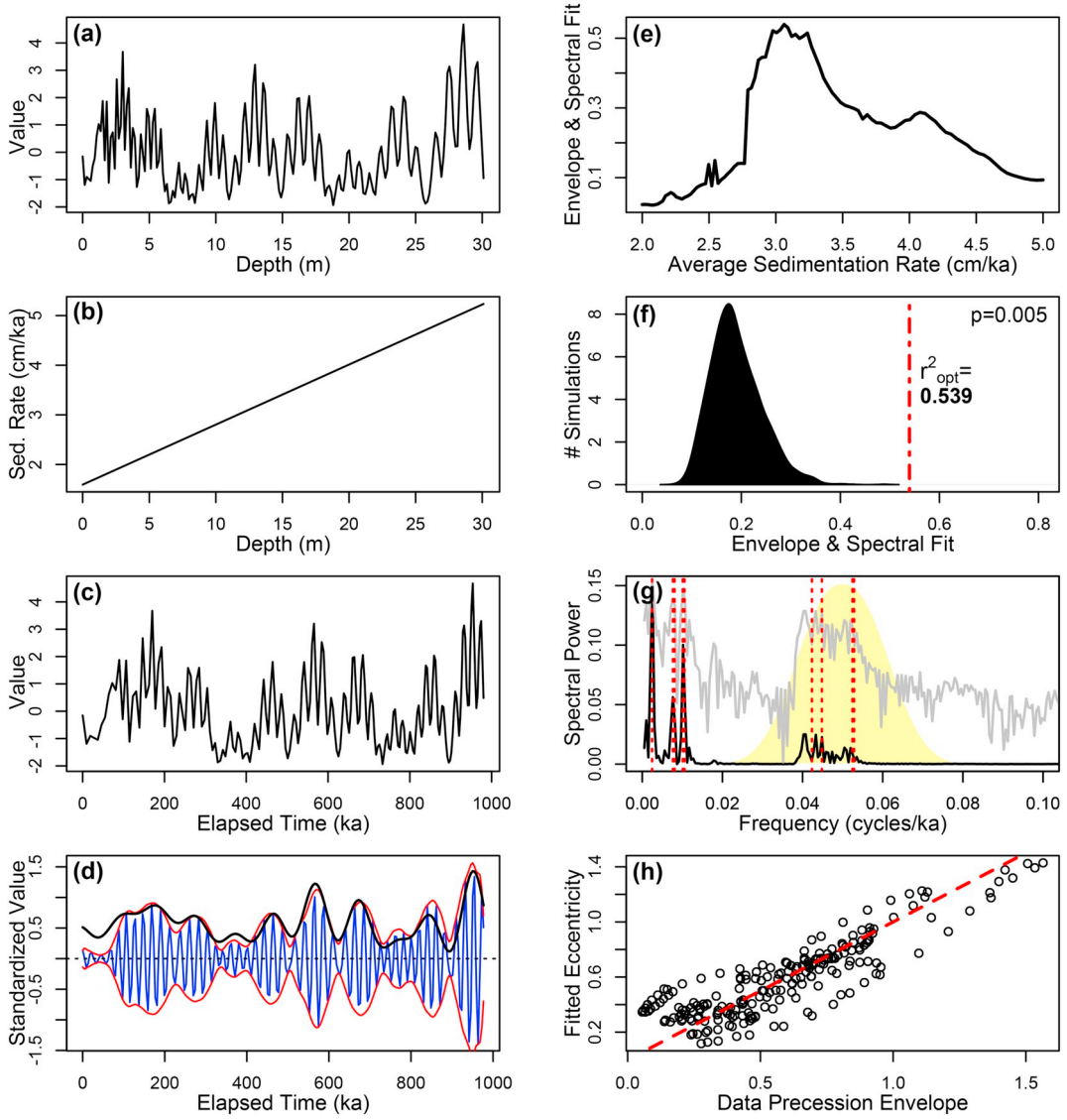

Fig. 11. TimeOpt analysis of an EP model distorted by a linear sedimentation rate increase across the stratigraphic interval, evaluated with an increasing ramp *sedimentation template*. (a) The synthetic EP series that is analyzed. (b) TimeOpt-reconstructed sedimentation rate history. (c) Astronomically-tuned stratigraphic series using the sedimentation rate history in (b). (d) Comparison of the band-passed precession signal (blue line), the data amplitude envelope (red line) determined via Hilbert transform, and the TimeOpt-reconstructed eccentricity model (black line; derived using Eq. (1)). (e) Combined envelope and spectral power fit (r^2_{opt}) at each evaluated average sedimentation rate. (f) Summary of 2000 Monte Carlo simulations with AR1 surrogates (ρ_{AR1} = 0.670), used to evaluate the significance of the maximum observed r^2_{opt} of 0.539 (p-value = .005). (g) Periodogram for the EP model, given the TimeOpt derived sedimentation history in (b) (black line = linear spectrum; gray line = log spectrum). Yellow shaded region illustrates the bandpass filter for evaluation of the precession amplitude envelope. Vertical dashed red lines indicate the eccentricity and precession target periods. (h) Cross plot of the data amplitude envelope and the TimeOpt-reconstructed eccentricity model in panel "d"; dashed red line is the 1:1 line.

2004 solution). This differs from the approach used in prior work (Meyers, 2015), which included the precession amplitude modulations periods (eccentricity terms) within the spectral power assessment (Eq. (2)). To accommodate this new approach for obliquity assessment, the option 'fitModPwr' has been incorporated into the function 'timeOpt'.

TimeOpt analysis with a constant *sedimentation template* reveals an optimal average sedimentation rate of 4.49 cm/ka (r^2_{opt} = 0.071; Fig. 19f) that is highly significant (*p*-value = .005; Fig. 19g). The strong concentration of spectral power at the 41 ka cycle is apparent (Fig. 19b), and the Time-Opt derived obliquity modulation model (black line in Fig. 19d) generally shows good agreement with the observed 41 ka amplitude modulation (red line in Fig. 19d); the most obvious exception is a short interval centered on ~500 ka (or ~1.92 Ma on the LR04 chronology; Lisiecki and Raymo, 2005; Fig. 19d), which is suggestive of hiatus (compare with Fig. 12). Explicit hiatus reconstruction is possible, as well as an evaluation of potential differential accumulation across glacial cycles, using more complex sedimentation templates (Fig. 7). For the sake of this initial study, however, the critical observation from the analysis of the Site 607 $\delta^{18}O$ data is that the TimeOpt approach provides a reliable means for evaluating obliquity-forced records; we leave exploration of more elaborate sedimentation templates (Fig. 7) to the reader.

4.3. The Miocene: Mediterranean paleoclimate change

The rhythmic Miocene strata of the Mediterranean have been the focus of cyclostratigraphic inquiry for over two decades (Hilgen et al., 1995), and have contributed to the modern geologic timescale in two capacities. First, these sedimentary rhythms have been utilized to develop a high-resolution astronomical time scale for much of the

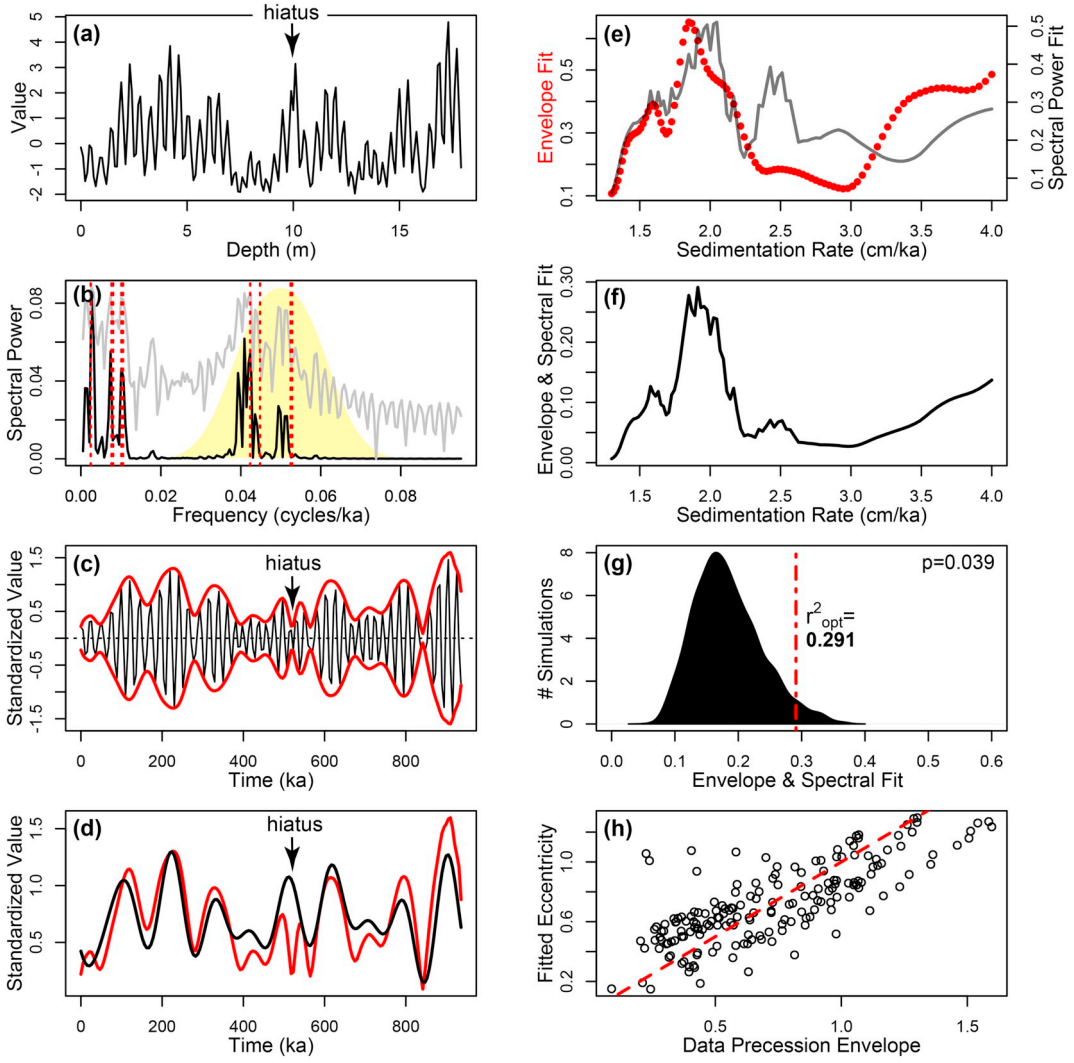

Fig. 12. TimeOpt analysis of the EP model of example 1 (Fig. 5), but with a 100 ka long hiatus at 10 meters depth. This analysis uses the nominal constant *sedimentation template*. (a) The synthetic EP series that is analyzed. (b) Periodogram for the EP model, given the TimeOpt derived average sedimentation rate of 1.91 cm/ka (black line = linear spectrum; gray line = log spectrum). Yellow shaded region illustrates the bandpass filter for evaluation of the precession amplitude envelope. Vertical dashed red lines indicate the eccentricity and precession target periods. (c) Comparison of the band-passed precession signal (black line), and the data amplitude envelope (red line) determined via Hilbert transform. (d) Comparison of the data amplitude envelope (red line) and the TimeOpt-reconstructed eccentricity model (black line; derived using Eq. (1)). (e) Squared Pearson correlation coefficient for the amplitude envelope fit ($r^2_{envelope}$; red dots) and the spectral power fit ($r^2_{spectral}$; dark gray line) at each evaluated sedimentation rate. (f) Combined envelope and spectral power fit (r^2_{opt}) at each evaluated sedimentation rate. (g) Summary of 2000 Monte Carlo simulations with AR1 surrogates (ρ_{AR1} = 0.564), used to evaluate the significance of the maximum observed r^2_{opt} of 0.291 (*p*-value = .039). (h) Cross plot of the data amplitude envelope and the TimeOpt-reconstructed eccentricity model in panel "d"; dashed red line is the 1:1 line.

Miocene, allowing calibration of all biostratigraphic and magnetostratigraphic datums at the precession-scale (Hilgen et al., 2012). Second, the interpreted astronomical record has also been utilized to calibrate one of the key monitor minerals used in Ar/Ar geochronology (Fish Canyon Sanidine), removing bias and reducing its uncertainty by an order of magnitude (Kuiper et al., 2008). The resulting improvements in our knowledge of the Ar/Ar monitor mineral age – due to its astronomical calibration – propagate throughout much of the geologic timescale, to any rocks that have been dated using Fish Canyon Sanidine as a reference (Meyers et al., 2012; Gradstein et al., 2012; Sageman et al., 2014).

These two landmark achievements rely upon accurate identification of astronomical rhythms in the Mediterranean strata. The abundance of evidence from integrated stratigraphy (basinwide evaluation of these deposits; magnetostratigraphic and biostratigraphic constraints; paleoclimate simulations) supports the proposed astronomical interpretations (Hilgen et al., 2014), yet a rigorous statistical assessment that overcomes the problems noted in Section 2, has yet to be conducted. Here, we apply the TimeOpt method to a high-resolution planktic foraminiferal $\delta^{18}O$ record from Ain el Beida, Morocco (AEB; van der Laan et al., 2012;Fig. 15c). The planktonic $\delta^{18}O$ data is specifically selected because it has the potential to preserve monsoonal climate forcing dominated by precession, as well as an ice volume signal that includes high latitude obliquity forcing (Section 4.2).

Power spectral analysis of the planktonic $\delta^{18}O$ data does not reveal spatial bedding cycles that exceed the 95% multiple testing confidence level, relative to an AR1 null model (Fig. 16c), although two spectral peaks are just shy of this threshold. The excellent magnetostratigraphic constraints for the strata indicate plausible sedimentation rates from ~7–9 cm/ka. To begin the TimeOpt assessment, a constant *sedimentation template* (Fig. 7a) is utilized to evaluate this record using an astronomical target that contains the dominant obliquity and precession terms, as derived from an analysis of the theoretical solution (Laskar et al., 2004). Based on a preliminary assessment, we explore sedimentation rates that slightly exceed the magnetostratigraphically-constrained bounds, to clearly define the maximum in r^2_{opt} (Fig. 20f). The

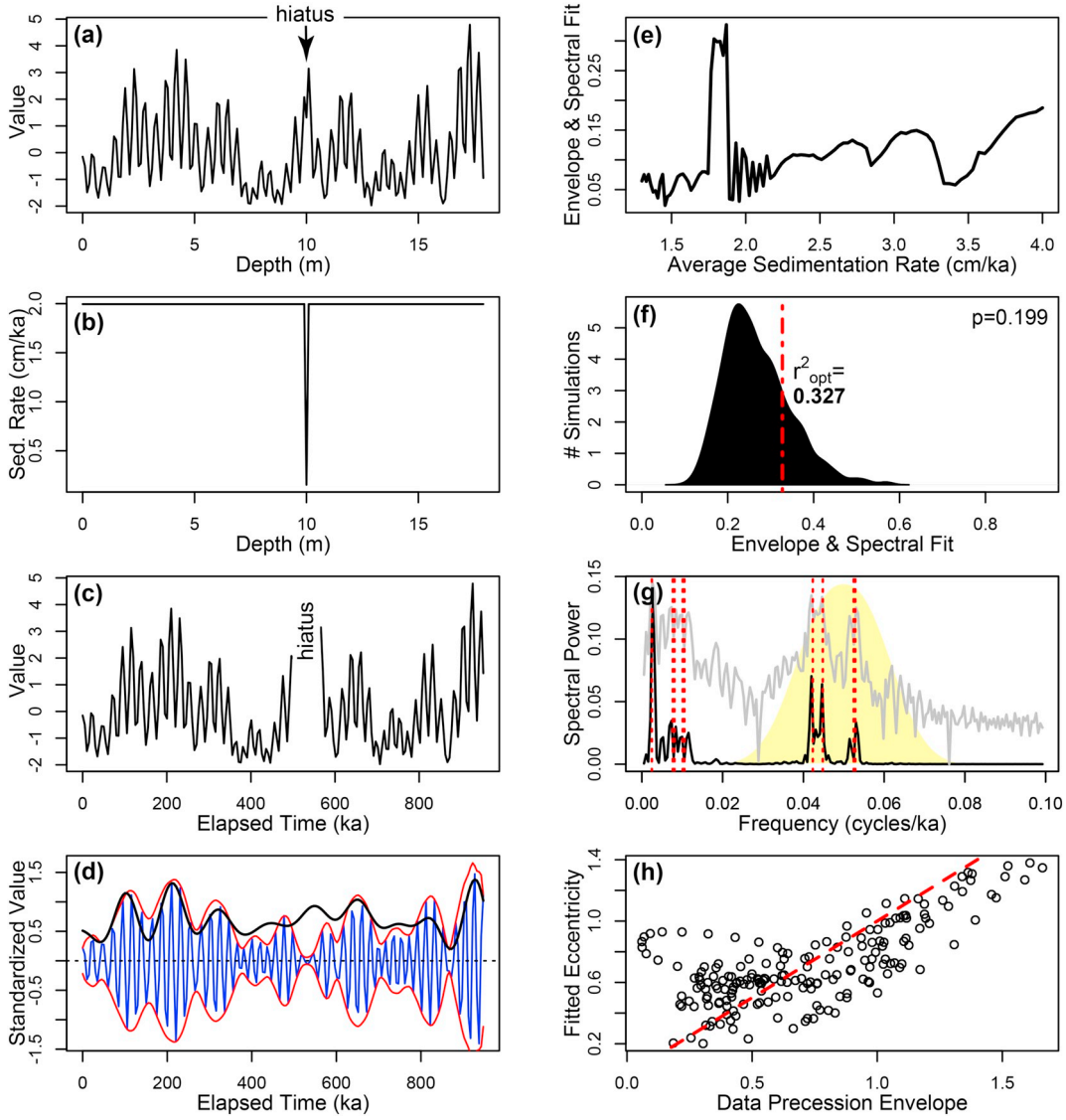

Fig. 13. TimeOpt analysis of the EP model of example 1 (Fig. 5), but with a 100 ka long hiatus at 10 meters depth. This analysis uses a hiatus *sedimentation template*. (a) The synthetic EP series that is analyzed. (b) TimeOpt-reconstructed sedimentation rate history. (c) Astronomically-tuned stratigraphic series using the sedimentation rate history in (b). (d) Comparison of the band-passed precession signal (blue line), the data amplitude envelope (red line) determined via Hilbert transform, and the TimeOpt-reconstructed eccentricity model (black line; derived using Eq. (1)). (e) Combined envelope and spectral power fit (r^2_{opt}) at each evaluated average sedimentation rate. (f) Summary of 2000 Monte Carlo simulations with AR1 surrogates (ρ_{AR1} = 0.564), used to evaluate the significance of the maximum observed r^2_{opt} of 0.327 (p-value = .199). (g) Periodogram for the EP model, given the TimeOpt derived sedimentation history in (b) (black line = linear spectrum; gray line = log spectrum). Yellow shaded region illustrates the bandpass filter for evaluation of the precession amplitude envelope. Vertical dashed red lines indicate the eccentricity and precession target periods. (h) Cross plot of the data amplitude envelope and the TimeOpt-reconstructed eccentricity model in panel "d"; dashed red line is the 1:1 line.

analysis indicates an optimal sedimentation rate of 8.93 cm/ka (r^2_{opt} = 0.149), significant at a *p*-value of 0.0685. Distortions observed in the spectrum (Fig. 20b) and envelope fit (Fig. 20d), however, are consistent with sedimentation instability.

Previous astronomical tuning of the AEB section suggests an average sedimentation rate of 7.6 cm/ka, although the interpreted sedimentation rate history is highly variable throughout the study interval (van der Laan et al., 2012). A progressive increase in the thickness of the individual beds up section suggests an overall increase in sedimentation rate (van der Laan et al., 2012) (Fig. 15c). Based on this stratigraphic observation, and the initial TimeOpt results presented in Fig. 20, we perform an analysis using an increasing ramp template (Fig. 7b). In conducting this analysis, we include one additional minor obliquity term in the astronomical target (29.7 ka; based on Laskar et al., 2004), which upon initial inspection, serves to improve the fit.

The optimization resolves a linear sedimentation rate increase of 7.4 cm/ka to 8.5 cm/ka through the stratigraphic interval (Fig. 21b), with an average sedimentation rate of 7.95 cm/ka (r^2_{opt} = 0.195, *p*-value = .1035; Fig. 21f). Application of an increasing ramp *sedimentation template* yields a substantial improvement in both the spectral fit (Fig. 21g), and the envelope fit (Fig. 21d; note the greatly improved eccentricity model).

An important source of misfit in these results is a slight misalignment of the predicted and observed obliquity term (~40.8 ka), which also appears to be bifurcated in the AEB spectrum (Fig. 21g). This bifurcation may be due to the presence of a hiatus (see Meyers and Sageman, 2004), sedimentation rate changes that are unresolved by the increasing ramp *sedimentation template*, or may be due to *contamination* of the spectrum by stochastic variability. The observed misalignment may also be attributable to inaccuracy in the theoretical obliquity

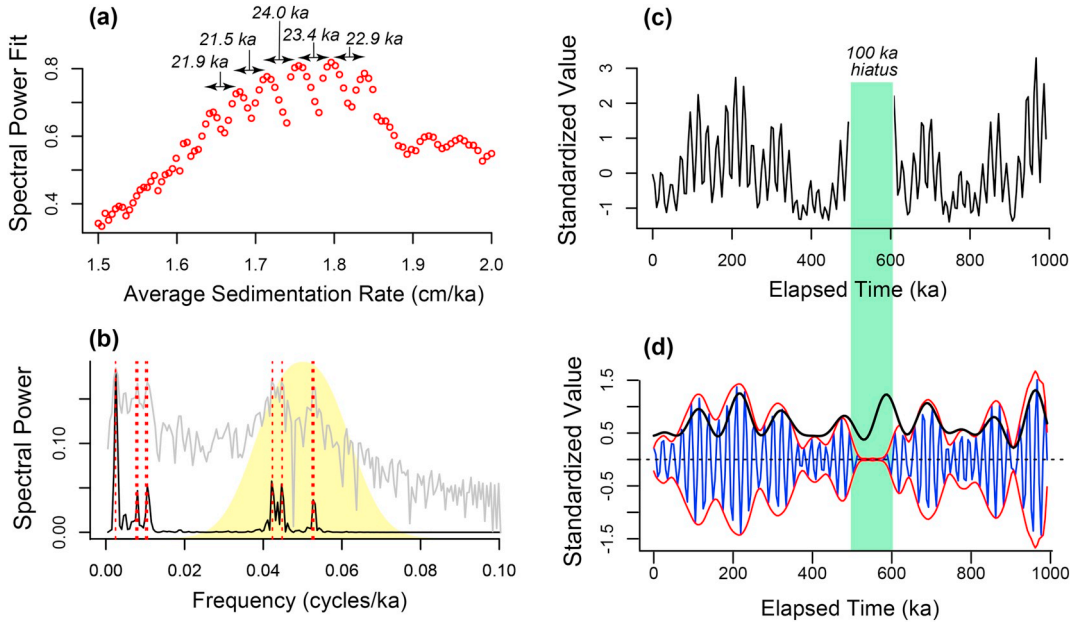

Fig. 14. TimeOpt analysis of the EP model of example 1 (Fig. 5), but with a 100 ka long hiatus at 10 meters depth. This analysis uses a hiatus *sedimentation template*, and only considers spectral power assessment (Eq. (2)). (a) Spectral power fit ($r^2_{spectral}$) at each evaluated average sedimentation rate. (b) Periodogram for the EP model, given the TimeOpt derived sedimentation history (black line = linear spectrum; gray line = log spectrum). Yellow shaded region illustrates the bandpass filter for evaluation of the precession amplitude envelope. Vertical dashed red lines indicate the eccentricity and precession target periods. (c) Astronomically-tuned stratigraphic series using the TimeOpt derived sedimentation rate history. (d) Comparison of the band-passed precession signal (blue line), the data amplitude envelope (red line) determined via Hilbert transform, and the TimeOpt-reconstructed eccentricity model (black line).

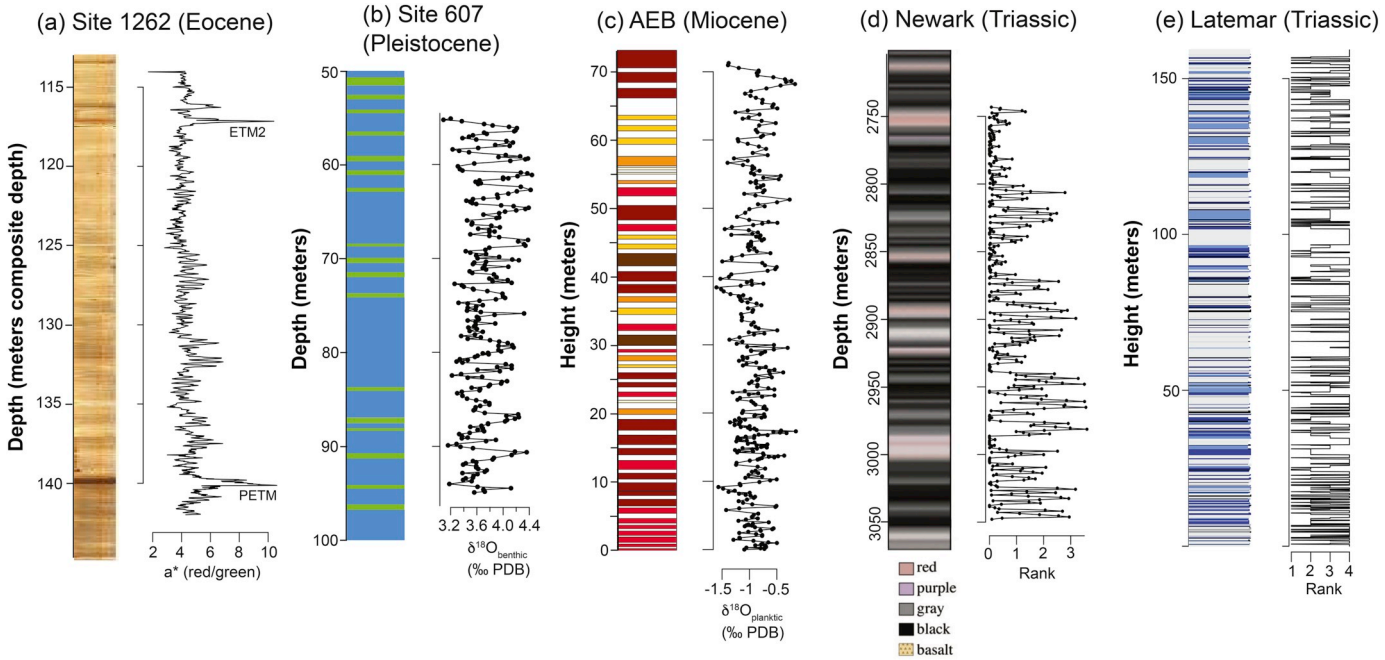

Fig. 15. Stratigraphic sections/core photos and the stratigraphic series that are analyzed in the five case studies. (a) Core photo and a* (red/green) data from Site 1262 (Zachos et al., 2004), spanning the latest Paleocene to earliest Eocene (PETM = Paleocene-Eocene Thermal Maximum; ETM2 = Eocene Thermal Maximum 2). The sediments consist of nannofossil ooze with some interbedded chert layers, while the PETM and ETM2 intervals are distinctive deep red clay layers. (b) Pleistocene Site 607 $\delta^{18}O_{benthic}$ data (Lisiecki and Raymo, 2005, stratigraphic column based on Raymo et al., 1989 and Ruddiman et al., 1989). The sediments consist of marly foraminiferal-nannofossil ooze (shown as green), and foraminiferal-nannofossil ooze (shown as blue) (Ruddiman et al., 1987). (c) Miocene $\delta^{18}O_{planktic}$ data from AEB (van der Laan et al., 2012; stratigraphic column reproduced from van der Laan et al., 2012). The section consists of marly sediments that alternate from yellow-beige to reddish in colour (van der Laan et al., 2012). (d) Triassic Newark Basin depth rank data (Olsen and Kent, 1999; stratigraphic column reproduced from Olsen et al., 2011). (e) Triassic Latemar Limestone CDL depth rank data (Preto et al., 2001). Black (rank 1) indicates caliches and soils, blue (rank 2) indicates supratidal flat, light blue (rank 3) indicates restricted, subtidal lagoon, and gray (rank 4) indicates open, subtidal lagoon. See Preto et al. (2001) for details on the lithofacies through this section.

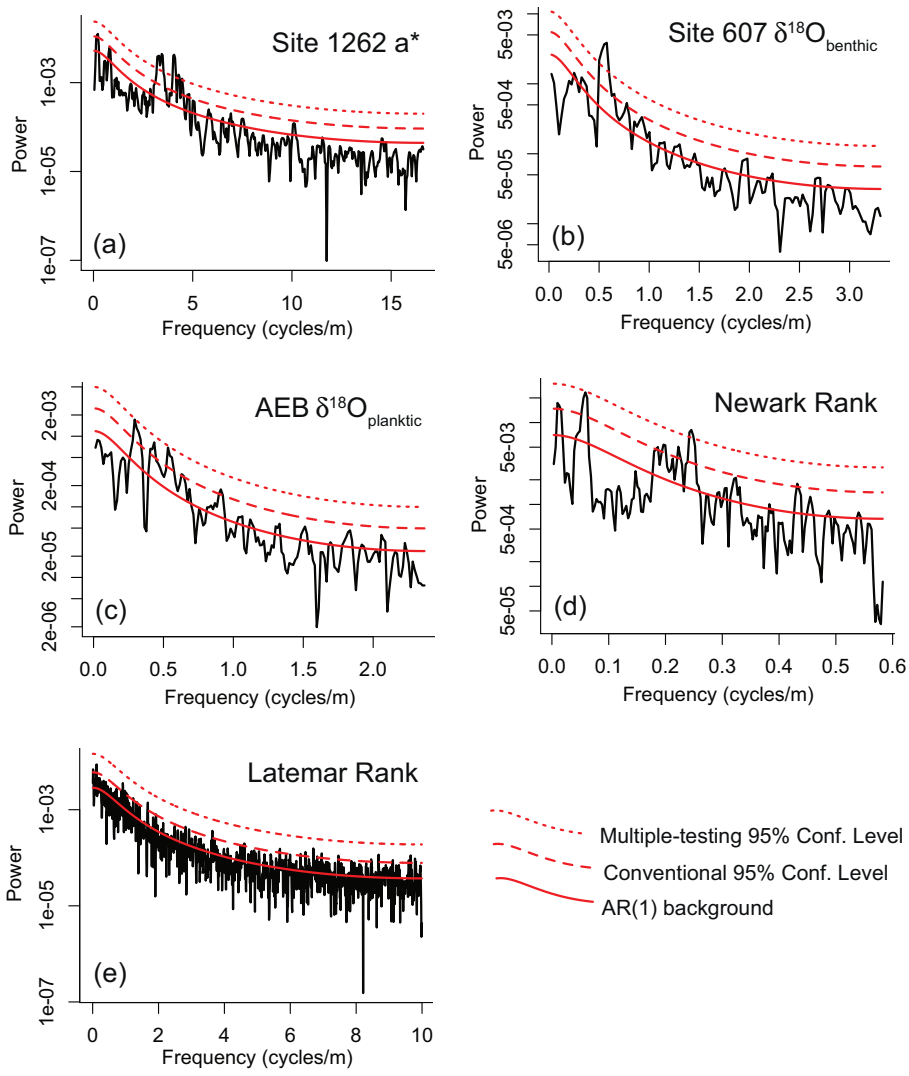

Fig. 16. Standard power spectrum assessment of the stratigraphic series evaluated in the five case studies. All spectral analysis are conducted with the multi-taper method, using three 2π prolate tapers. The AR1 red noise background is identified with a solid red line, the dashed red line is the standard 95% confidence level, and the dotted line indicates the 95% confidence level corrected for multiple testing (Bonferroni correction). (a) Power spectrum for the Eocene Site 1262 a* (red/green) data (Zachos et al., 2004). (b) Power spectrum for the Pleistocene Site 607 $\delta^{18}O_{benthic}$ data (Lisiecki and Raymo, 2005). (c) Power spectrum for the Miocene $\delta^{18}O_{planktic}$ data (van der Laan et al., 2012). (d) Power spectrum for the Triassic Newark Basin depth rank data (Olsen and Kent, 1999). (e) Power spectrum for the Triassic Latemar Limestone CDL depth rank data (Preto et al., 2001).

period (Laskar et al., 2004). These hypotheses are directly motivated by the results of the TimeOpt analyses, and deserve further study.

4.4. The Triassic: the Newark Supergroup cycles

For the next case study, we turn to the classic rhythmic strata of the Triassic Newark Basin of North America (Van Houten, 1962; Olsen, 1986; Olsen and Kent, 1999; Kent et al., 2018), which preserves a 40 million year long record of lacustrine deposition within an ancient continental rift. The composite depth rank series of Olsen and Kent (1999) – a measure of relative water depth – has served as a primary data set for astronomical interpretation in prior work, and it is the focus of evaluation in this case study (Fig. 22a).

To provide an initial assessment of this exceptionally long stratigraphic series, we apply an evolutive implementation of the TimeOpt method ('eTimeOpt'), using a constant *sedimentation template*. For this analysis, a 300-meter long window is sequentially shifted through the series, allowing evaluation of secular changes in sedimentation rate throughout the stratigraphy. We focus on eccentricity scale variance, including evaluation of the amplitude modulation of the short eccentricity signal, which is expected to preserve a long eccentricity rhythm. Our focus on eccentricity-scale variability is motivated by the fact that its spectral signature should be less strongly distorted by shorter-term (e.g., precession-scale) sedimentation instability that may occur within the 300 meter window. This greater stability is attributable to two phenomena: (1) higher precession-scale sedimentation rates are potentially compensated for by lower precession-scale sedimentation rates across an eccentricity cycle, and (2) Fourier spectra are characterized by a non-linear scaling of periods, where spectral peaks associated with shorter periods are more strongly smeared by subtle sedimentation rate changes (Herbert, 1994; Meyers et al., 2001; Weedon, 2003).

The results of the evolutive TimeOpt analysis (Fig. 22) suggest long-term changes in average sedimentation rate (Fig. 23). The sedimentation history is most unambiguously resolved in the spectral power fit ($r^2_{spectral}$), and the combined envelope and spectral power fit (r^2_{opt}), identifying three sedimentation rate regimes (Figs. 22–23): (1) a region of relatively stable sedimentation down to 2025 m depth (average sedimentation rate = 14.1 cm/ka), (2) a high sedimentation interval from 2025 m to 2213 m (average sedimentation rate = 23.8 cm/ka), and (3) an overall decline in sedimentation rates to 3405 meters depth (average sedimentation rate = 19.7 cm/ka). In addition to these secular changes in sedimentation rates, the eTimeOpt results reveal that the quality of the astronomical signal (signal-noise ratio) is generally higher in the deeper/older portion of the record (Fig. 23b,d). The eTimeOpt results show some volatility at the very base of the section and the very top of the section, and from 2025 to 2213 m depth (red symbols in Fig. 23a,c). These portions of the eTimeOpt record should be interpreted with extra caution, as the results reveal ambiguity in the astronomical calibration.

To provide a more detailed statistical evaluation that includes both the precession and eccentricity signals, we focus the interval from

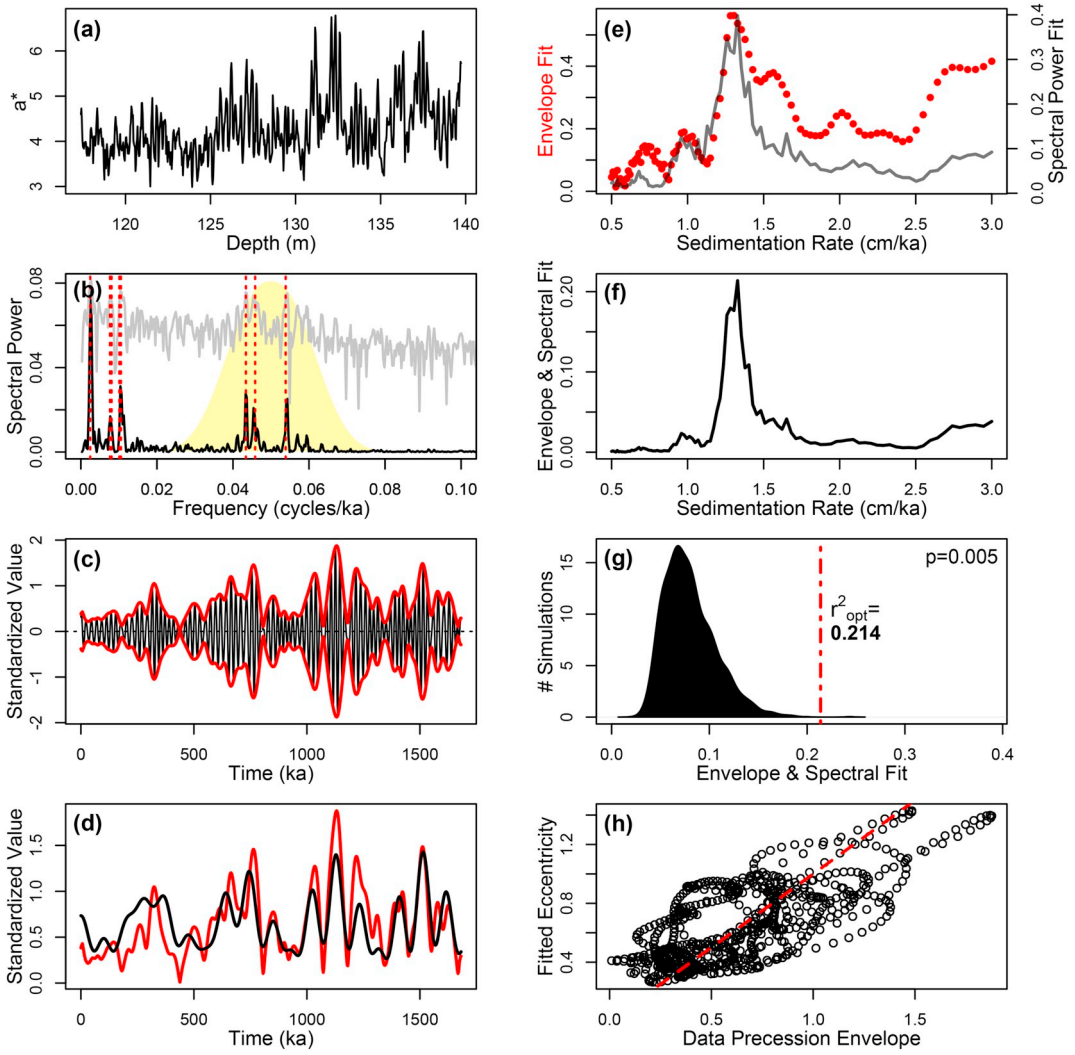

Fig. 17. TimeOpt analysis of the Eocene ODP Site 1262 a* colour data (red/green ratio), evaluated with a constant *sedimentation template*. (a) The ODP Site 1262 a* colour data that is analyzed. (b) Periodogram for the ODP Site 1262 a* colour data, given the TimeOpt derived average sedimentation rate of 1.33 cm/ka (black line = linear spectrum; gray line = log spectrum). Yellow shaded region illustrates the bandpass filter for evaluation of the precession amplitude envelope. Vertical dashed red lines indicate the eccentricity and precession target periods. (c) Comparison of the band-passed precession signal (black line), and the data amplitude envelope (red line) determined via Hilbert transform. (d) Comparison of the data amplitude envelope (red line) and the TimeOpt-reconstructed eccentricity model (black line; derived using Eq. (1)). (e) Squared Pearson correlation coefficient for the amplitude envelope fit ($r^2_{envelope}$; red dots) and the spectral power fit ($r^2_{spectral}$; dark gray line) at each evaluated sedimentation rate. (f) Combined envelope and spectral power fit (r^2_{opt}) at each evaluated sedimentation rate. (g) Summary of 2000 Monte Carlo simulations with AR1 surrogates (ρ_{AR1} = 0.832), used to evaluate the significance of the maximum observed r^2_{opt} of 0.214 (*p*-value = .005). (h) Cross plot of the data amplitude envelope and the TimeOpt-reconstructed eccentricity model in panel "d"; dashed red line is the 1:1 line.

2743.2 to 3048 m depth (Fig. 15d), which illustrates high signal-noise (Fig. 23b,d). Power spectral analysis of the rank data reveals one spatial bedding cycle that exceeds the 95% multiple testing confidence level, relative to an AR1 null model (Fig. 16d). TimeOpt evaluation with a constant *sedimentation template* (Fig. 24), using an astronomical target composed of precession and eccentricity (based on Laskar et al., 2004 and Waltham, 2015), indicates a sedimentation rate of 18.34 cm/ka (r^2_{opt} = 0.135; *p*-value = .005). Strong short and long eccentricity cycles are again observed, although precession scale variance is poorly fit; instead a number of distinct spectral peaks are resolved that are shifted to the left of the predicted precession target frequencies, occurring at periods spanning 22 ka to 31 ka (Fig. 24b). One hypothesis to explain this mismatch is an inaccuracy in the model for secular evolution of the precession constant, which is more poorly constrained with age, due to lack of knowledge about the history of the Earth-Moon system (Waltham, 2015). Alternatively, the mismatch between observed and predicted spectral peaks could be the consequence of distortion of the astronomical signal by variable sedimentation, for example, more rapid accumulation during a particular phase of eccentricity-driven lake development.

To help address this issue, we consider a proxy-specific *sedimentation template* (Fig. 7f, Fig. 25), where sediments deposited at deeper relative water depths accumulate at a faster rate. This approach is consistent with prior paleoenvironmental interpretation (Olsen and Kent, 1999), and initial experiments reveal that it yields a superior fit to the alternative (faster accumulation at shallower depths). Furthermore, inclusion of a linear increase in minimum precession-related sedimentation rates throughout the study interval further improves the fit. A progressive increase in minimum sedimentation rates can be understood as a consequence of longer term lake basin dynamics, perhaps driven by an 1750 ka eccentricity modulation related to interactions between the Earth and Mars (Olsen and Kent, 1999). An average sedimentation rate of 17.97 cm/ka (r^2_{opt} = 0.240; p-value = .005) is resolved (Fig. 25e,f).

The results reveal a strengthening of variance in the shortest eccentricity term (~95 ka; Fig. 25g), and an improvement in the

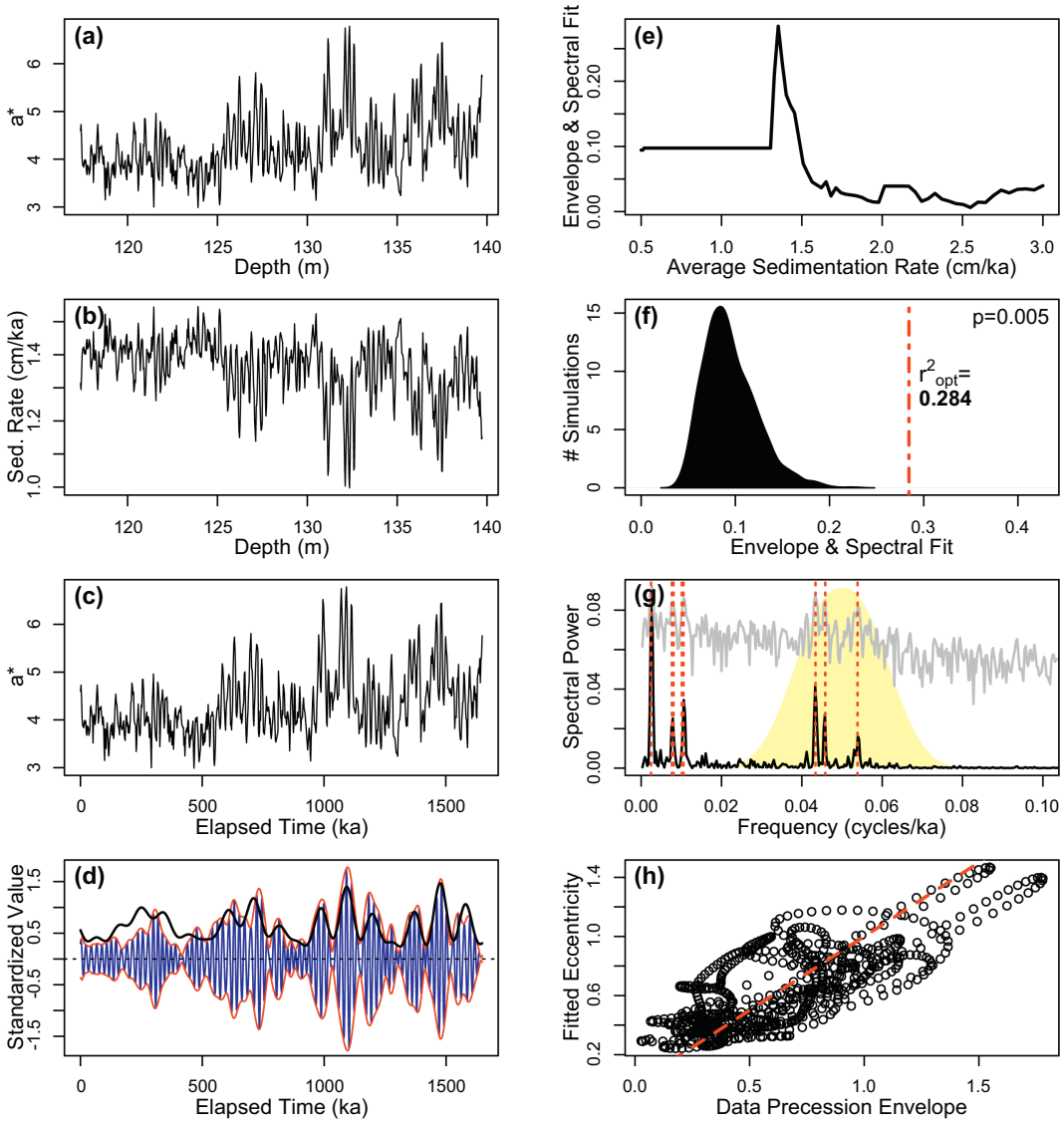

Fig. 18. TimeOpt analysis of the Eocene ODP Site 1262 a* colour data (red/green ratio), evaluated with a proxy/lithology-specific *sedimentation template*. (a) The ODP Site 1262 a* colour data that is analyzed. (b) TimeOpt-reconstructed sedimentation rate history. (c) Astronomically-tuned ODP Site 1262 a* colour data using the sedimentation rate history in (b). (d) Comparison of the band-passed precession signal (blue line), the data amplitude envelope (red line) determined via Hilbert transform, and the TimeOpt-reconstructed eccentricity model (black line; derived using Eq. (1)). (e) Combined envelope and spectral power fit (r^2_{opt}) at each evaluated average sedimentation rate. (f) Summary of 2000 Monte Carlo simulations with AR1 surrogates (ρ_{AR1} = 0.832), used to evaluate the significance of the maximum observed r^2_{opt} of 0.284 (p-value = .005). (g) Periodogram for the EP model, given the TimeOpt derived sedimentation history in (b) (black line = linear spectrum; gray line = log spectrum). Yellow shaded region illustrates the bandpass filter for evaluation of the precession amplitude envelope. Vertical dashed red lines indicate the eccentricity and precession target periods. (h) Cross plot of the data amplitude envelope and the TimeOpt-reconstructed eccentricity model in panel "d"; dashed red line is the 1:1 line.

alignment between the observed precession-band peaks and the predicted target periods (Fig. 25g). We note the improvement in the eccentricity model fit, which is derived from the precession envelope (compare Fig. 24d and Fig. 25d), but also note the mismatch between the precession envelope and eccentricity model in the youngest interval (< 250 ka elapsed time; Fig. 25d), which begs further investigation.

4.5. The Triassic: the Latemar Platform

Carbonate platforms have been the focus of much cyclostratigraphic inquiry and debate, rooted in the seminal work of Schwarzacher (1947) and Fischer (1964). The sensitivity of platform development to sea level variations makes them an appealing target for cyclostratigraphic study, but they are also challenging sedimentary systems for the evaluation of astronomical forcing/pacing (Kemp et al., 2016), due to numerous problems that are intrinsic to the depositional environment (Strasser, 2018). Well known complications include the potential for highly variable sedimentation rates, the expectation of temporal gaps due to emergence ("missed beats"; Goldhammer et al., 1990), the potential for strong autocyclicity (Burgess et al., 2001), and non-uniqueness of facies-depth relations (Purkis et al., 2015). For this reason, it is advisable to approach carbonate platforms – and dynamic shallow marine systems in general – with an extra degree of caution. Given these numerous challenges, it is illustrative to complete our case studies with a classic and highly debated cyclostratigraphic example from the Latemar Limestone, located in the Dolomites, Italy (Fig. 15e).

The Latemar Limestone is a carbonate platform deposit that formed during the Middle Triassic in the western tropical Tethys Ocean (Goldhammer et al., 1987). The ~5 km diameter platform is composed of meter-scale lithologic cycles that are generally characterized by

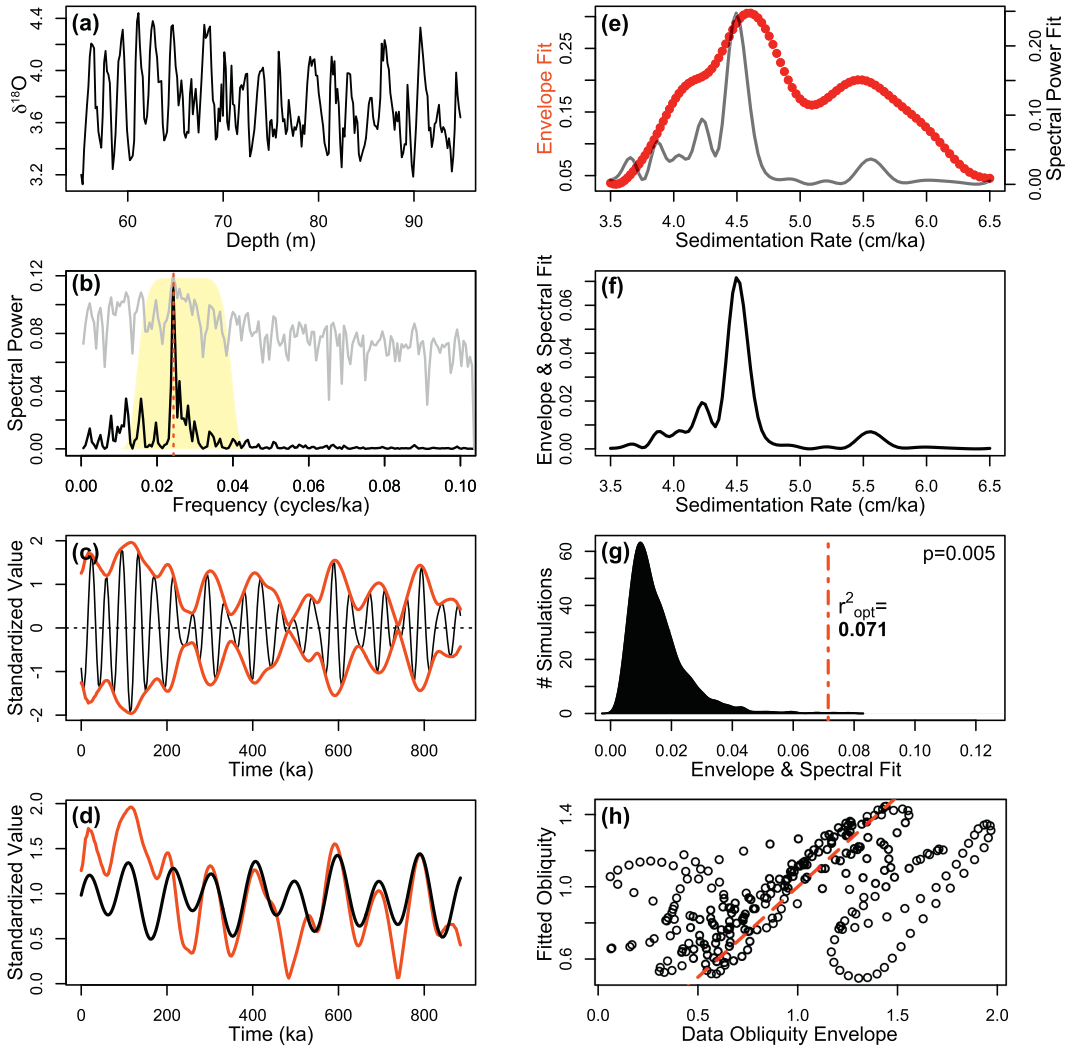

Fig. 19. TimeOpt analysis of the DSDP Site 607 benthic foraminifera $\delta^{18}O$ data, evaluated a constant *sedimentation template*. (a) The DSDP Site 607 benthic foraminifera $\delta^{18}O$ data that is analyzed. (b) Periodogram for the DSDP Site 607 benthic foraminifera $\delta^{18}O$ data, given the TimeOpt derived average sedimentation rate of 4.49 cm/ka (black line = linear spectrum; gray line = log spectrum). Yellow shaded region illustrates the bandpass filter for evaluation of the obliquity amplitude envelope. Vertical dashed red line indicates the obliquity target period. (c) Comparison of the band-passed obliquity signal (black line), and the data amplitude envelope (red line) determined via Hilbert transform. (d) Comparison of the data amplitude envelope (red line) and the TimeOpt-reconstructed obliquity amplitude modulation model (black line; derived using Eq. (1)). (e) Squared Pearson correlation coefficient for the amplitude envelope fit ($r^2_{envelope}$; red dots) and the spectral power fit ($r^2_{spectral}$; dark gray line) at each evaluated sedimentation rate. (f) Combined envelope and spectral power fit (r^2_{opt}) at each evaluated sedimentation rate. (g) Summary of 2000 Monte Carlo simulations with AR1 surrogates (ρ_{AR1} = 0.792), used to evaluate the significance of the maximum observed r^2_{opt} of 0.071 (p-value = .005). (h) Cross plot of the data amplitude envelope and the TimeOpt-reconstructed obliquity amplitude modulation model in panel "d"; dashed red line is the 1:1 line.

lower limestone units (weakly laminated limestones, wackestones, packstones, and grainstones) that alternate with diagenetic dolomitic caps, interpreted as reflecting submergence and emergence cycles (Goldhammer et al., 1987; Preto et al., 2001). A stacking pattern similar to that observed in the "Latemar cycles" has been identified in correlative strata from a carbonate buildup at Mendola Pass, 30 km away from the Latemar platform, which has been taken to support an hypothesized allocyclic origin (Forkner et al., 2009). Yet numerous incompatible astronomical and non-astronomical interpretations have been proposed for these Latemar cycles (Goldhammer et al., 1987; Hinnov and Goldhammer, 1991; Satterley, 1996; Preto et al., 2001, 2004; Zühlke et al., 2003; Mundil et al., 2003; Zühlke, 2004; Kent et al., 2004; Forkner et al., 2009).

The present analysis evaluates a lithofacies rank series developed by Preto et al. (2001), spanning the Upper Cyclic Facies of the Latemar platform (Fig. 15e). The Cimon del Latemar (CDL) series is constructed from field observations of four basic lithofacies, and changes in lithofacies are interpreted to reflect changes in relative water depth (Preto et al., 2001). According to past astronomical interpretations, the entire interval covered by the CDL rank series could represent as much as 3.1 million years (Preto et al., 2001), or as little as 320 thousand years (Kent et al., 2004), in total duration.

Power spectral analysis of the CDL rank series does not reveals any spatial bedding cycles that exceed the 95% multiple testing confidence level, relative to an AR1 null model (Fig. 16e). TimeOpt analysis of the CDL rank series with a constant *sedimentation template* identifies an optimal average sedimentation rate of 48.49 cm/ka (r^2_{opt} = 0.100; Fig. 26f) that is highly significant (p-value = .0085; Fig. 26g). This result is consistent with the proposed timescale and astronomical interpretation of Kent et al. (2004), which is also in agreement with available magnetostratigraphy (Kent et al., 2004; Spahn et al., 2013) and U/Pb radioisotope geochronology (Mundil et al., 1996, 2003; Brack et al., 1996). A strong concentration of spectral power at the ~18 ka precession cycle is apparent (Fig. 26b), and the TimeOpt-reconstructed

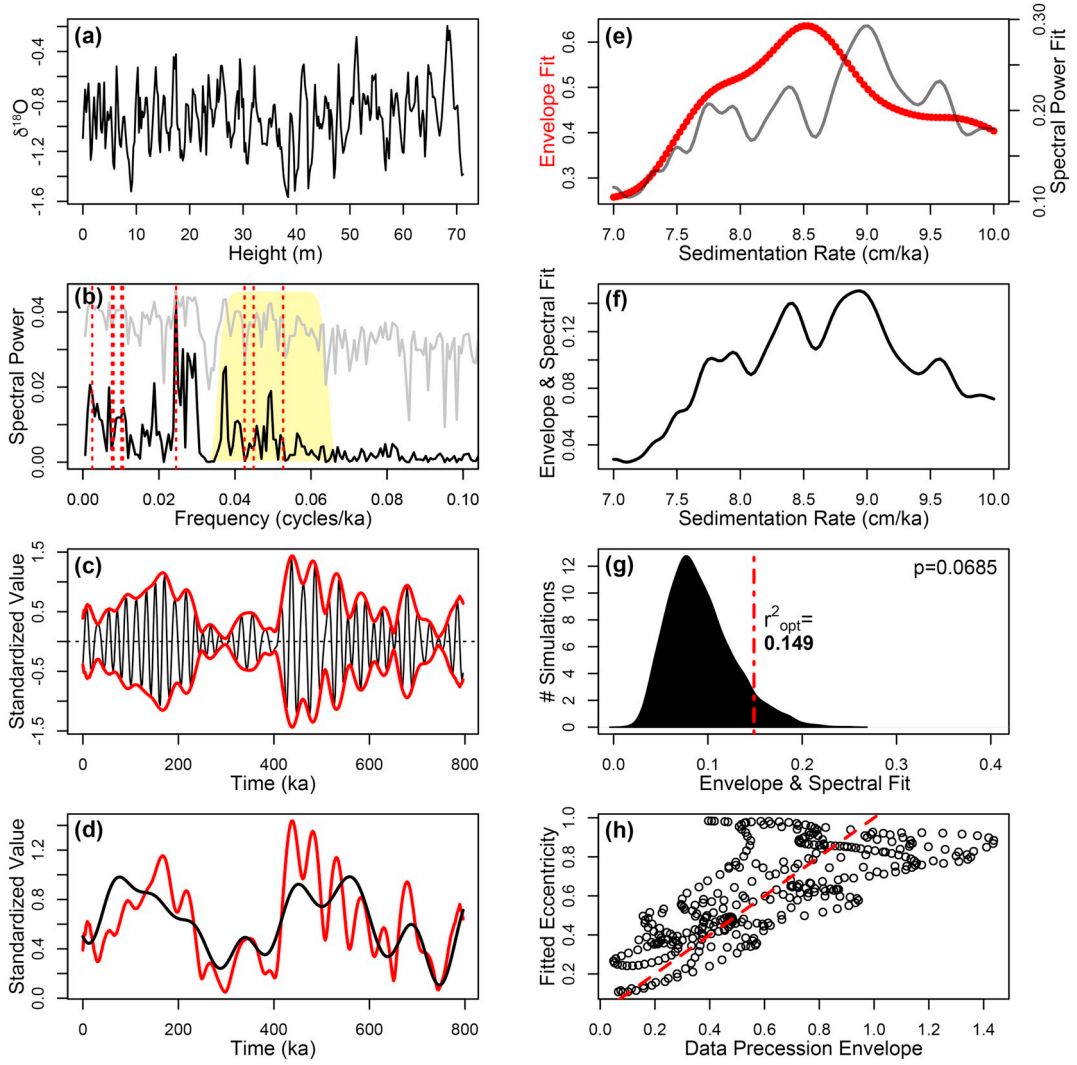

Fig. 20. TimeOpt analysis of the Ain el Beida planktic foraminifera $\delta^{18}O$ data (van der Laan et al., 2012), evaluated with a constant *sedimentation template*. (a) The Ain el Beida planktic foraminifera $\delta^{18}O$ data that is analyzed. (b) Periodogram for the Ain el Beida planktic foraminifera $\delta^{18}O$ data, given the TimeOpt derived average sedimentation rate of 8.93 cm/ka (black line = linear spectrum; gray line = log spectrum). Yellow shaded region illustrates the bandpass filter for evaluation of the precession amplitude envelope. Vertical dashed red lines indicate the precession, obliquity and eccentricity target periods. (c) Comparison of the band-passed precession signal (black line), and the data amplitude envelope (red line) determined via Hilbert transform. (d) Comparison of the data amplitude envelope (red line) and the TimeOpt-reconstructed eccentricity model (black line; derived using Eq. (1)). (e) Squared Pearson correlation coefficient for the amplitude envelope fit ($r^2_{envelope}$; red dots) and the spectral power fit ($r^2_{spectral}$; dark gray line) at each evaluated sedimentation rate. (f) Combined envelope and spectral power fit (r^2_{opt}) at each evaluated sedimentation rate. (g) Summary of 2000 Monte Carlo simulations with AR1 surrogates (ρ_{AR1} = 0.753), used to evaluate the significance of the maximum observed r^2_{opt} of 0.149 (p-value = .0685). (h) Cross plot of the data amplitude envelope and the TimeOpt-reconstructed eccentricity model in panel "d"; dashed red line is the 1:1 line.

eccentricity model (black line in Fig. 26d) shows good agreement with the observed precession amplitude modulation (red line in Fig. 26d). However, it should be noted that the optimal temporal calibration yields a very short record (328 ka long), which prohibits a reliable assessment of long eccentricity. Nonetheless, the statistically significant result (at the 99.15% confidence level) reveals a spectral signature (Fig. 26b) and amplitude modulation structure (Fig. 26c) that is consistent with predicted precession and eccentricity influence on deposition.

The significance of this result for understanding platform deposition in the Triassic is multifold. First, it suggests that the well studied one meter-scale Latemar sedimentary packages (Goldhammer et al., 1987) – previously interpreted as representing Milankovitch cycles – record a much shorter millennial tempo, the ultimate source of which remains uncertain. Second, the extremely high sedimentation rate (48.49 cm/ka) that is reconstructed with TimeOpt suggests fundamental limitations in the use of comparative sedimentology for constraining rates of platform deposition during the Middle Triassic (see Forkner et al., 2009 for a more detailed discussion).

5. Discussion: current status and future directions

5.1. Duplication and triangulation

This study presents a comprehensive approach to astrochronologic testing that considers the inherent challenges of cyclostratigraphic analysis. While much effort has been placed on developing a reliable test that combines multiple lines of inquiry (radioisotopic time control, concentration of spectral power in astronomical bands, amplitude modulation assessment, sedimentation templates), it is prudent to consider the TimeOpt results as supporting evidence within the broader context of the expert knowledge from a sedimentary basin. The TimeOpt fits ($r^2_{spectral}$, $r^2_{envelope}$, r^2_{opt}) and *p*-values provide a useful measure of the statistical evidence for a hypothesis, which should be

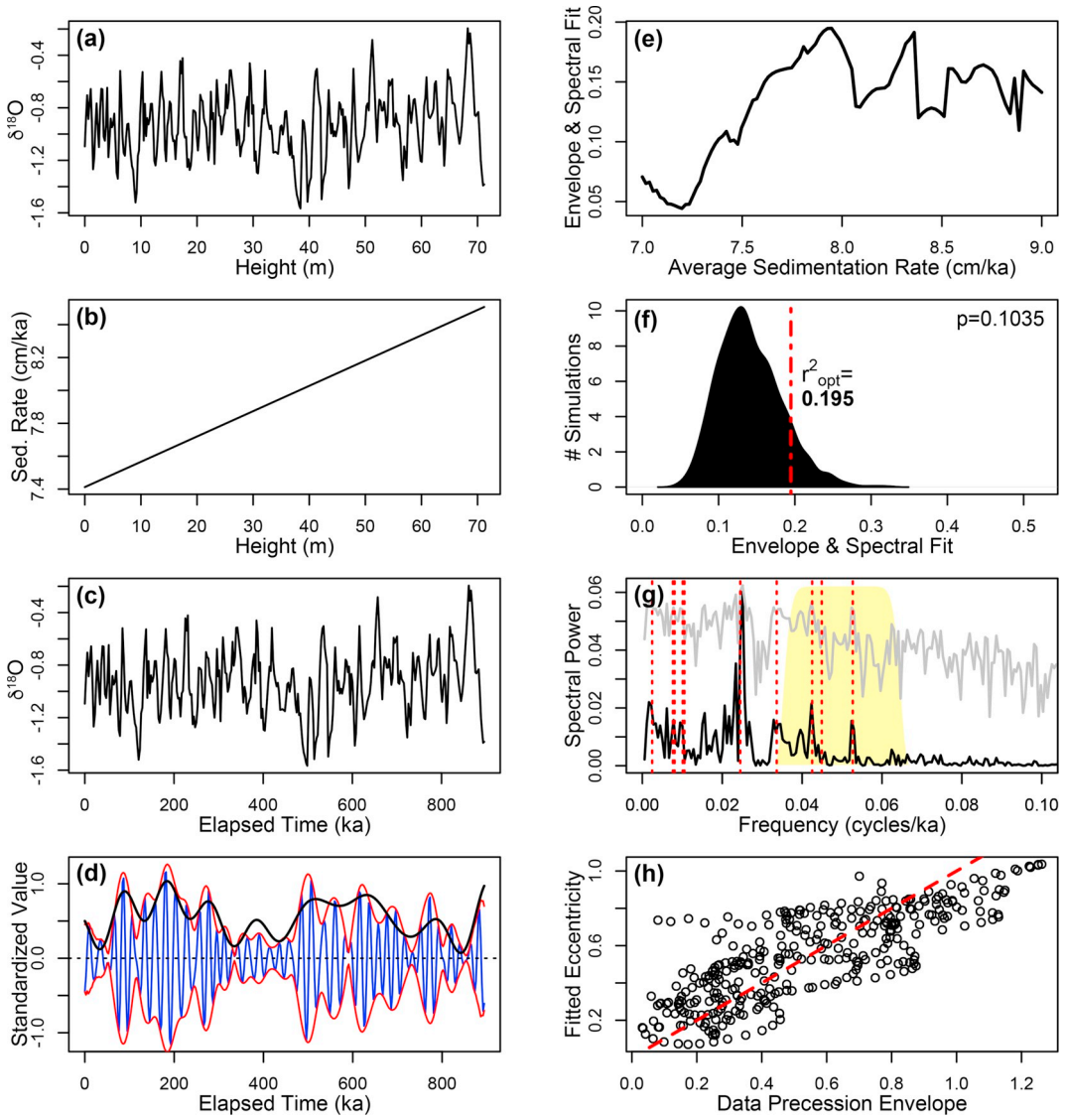

Fig. 21. TimeOpt analysis of the Ain el Beida planktic foraminifera $\delta^{18}O$ data (van der Laan et al., 2012), evaluated with an increasing ramp *sedimentation template*. (a) The Ain el Beida planktic foraminifera $\delta^{18}O$ data that is analyzed. (b) TimeOpt-reconstructed sedimentation rate history. (c) Astronomically-tuned Ain el Beida planktic foraminifera $\delta^{18}O$ data using the sedimentation rate history in (b). (d) Comparison of the band-passed precession signal (blue line), the data amplitude envelope (red line) determined via Hilbert transform, and the TimeOpt-reconstructed eccentricity model (black line; derived using Eq. (1)). (e) Combined envelope and spectral power fit (r^2_{opt}) at each evaluated average sedimentation rate. (f) Summary of 2000 Monte Carlo simulations with AR1 surrogates (ρ_{AR1} = 0.753), used to evaluate the significance of the maximum observed r^2_{opt} of 0.195 (p-value = .1035). (g) Periodogram for the Ain el Beida planktic foraminifera $\delta^{18}O$ data, given the TimeOpt derived sedimentation history in (b) (black line = linear spectrum; gray line = log spectrum). Yellow shaded region illustrates the bandpass filter for evaluation of the precession amplitude envelope. Vertical dashed red lines indicate the eccentricity, obliquity and precession target periods. (h) Cross plot of the data amplitude envelope and the TimeOpt-reconstructed eccentricity model in panel "d"; dashed red line is the 1:1 line.

considered in combination with other statistical and non-statistical criteria. Duplication of results in coeval strata, for example, would provide additional supporting evidence. The Astrochron software (Meyers, 2014) and the supplied R-scripts (supplement) are designed to facilitate such duplication.

While duplication of scientific results is essential, "triangulation" presents another important means for verifying results and increasing scientific certainty, helping to protect against flawed ideas or methodologies (Lawlor et al., 2016; Munafò and Smith, 2018). The underlying premise of "triangulation" is to use multiple approaches – distinct lines of evidence – each with unrelated assumptions, strengths and weaknesses, to evaluate a question (Box 1). An example of the success of "triangulation" is the theory of plate tectonics, which involved the assemblage of a wide array of independent geologic and geophysical evidence (Munafò and Smith, 2018). In the case of astrochronology development, independent time control derived from radioisotopic dating, magnetostratigraphy, chemostratigraphy and biostratigraphy, provide important lines of evidence, as does comparative sedimentology, and paleoceanographic/paleoclimatologic constraints from proxy data and models. Integrated stratigraphy is, by its very nature, poised to utilize triangulation for hypothesis testing. Realizing this potential, however, depends upon the availability of accurate and precise data. In this regard, advancements in instrumentation and analytical approaches in radioisotopic geochronology (e.g., Mattinson, 2005; Schmitz and Kuiper, 2013; Jicha et al., 2016), show great promise for improving astrochronologic testing.

The TimeOpt approach adopts the philosophy of triangulation, through its independent evaluation of spectral power and amplitude modulation assessment, within the constraints of available time control. There are additional aspects of triangulation that can be readily

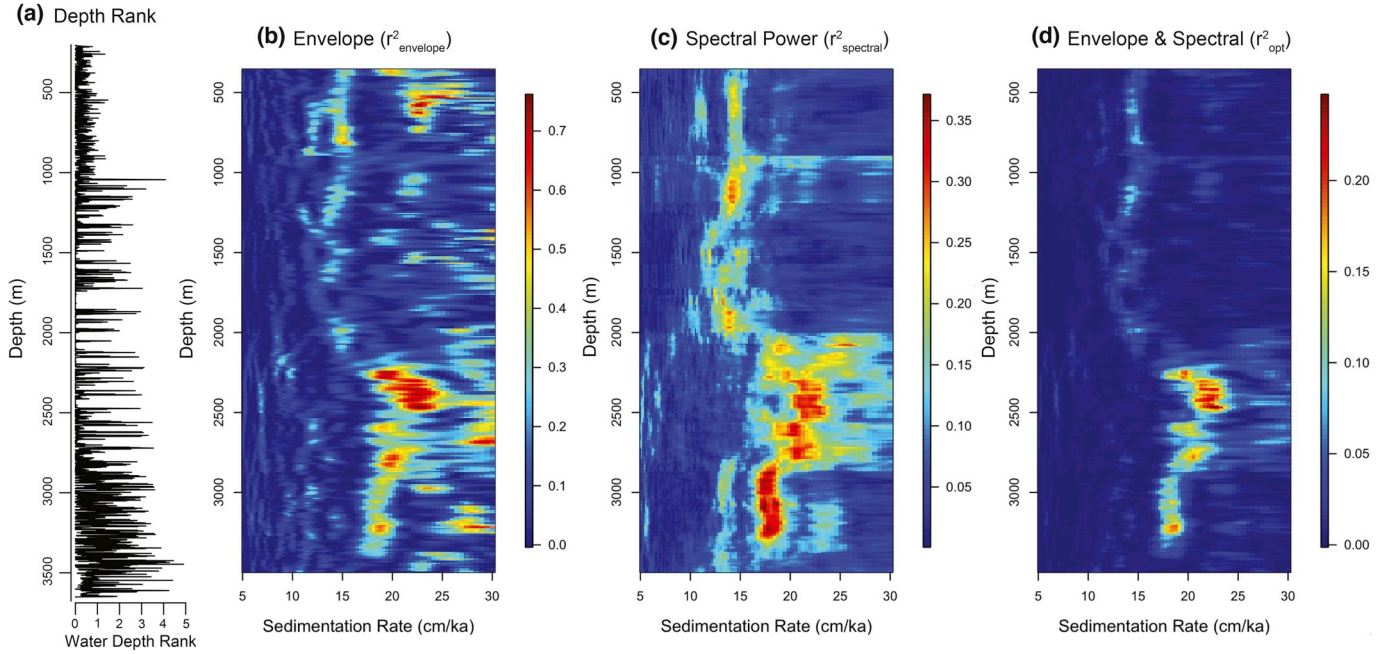

Fig. 22. Evolutive TimeOpt (function 'eTimeOpt') of Newark Basin Rank data (Olsen and Kent, 1999), using a moving window of 300 m. (a) Newark Basin Rank data (Olsen and Kent, *1999*) (b) Squared Pearson correlation coefficient for the amplitude envelope fit ($r^2_{envelope}$). (c) Squared Pearson correlation coefficient for the spectral power fit ($r^2_{spectral}$). (d) Results from the combined envelope and spectral fit (r^2_{opt}).

implemented using the TimeOpt framework. These include an evaluation of the internal consistency of the TimeOpt-reconstructed eccentricity model (which is based on the amplitude modulation of precession), and the eccentricity-scale variability that is directly preserved within a stratigraphic series. Likewise, consistency of the amplitude modulation of short eccentricity with the observed long eccentricity is predicted based on astronomical theory (Laskar et al., 2004). However, disagreements in phase are also plausible under some circumstances, due to the climate and/or depositional system transfer functions (e.g., Laurin et al., 2005; Laurin et al., 2017; see Appendix A.5 for additional discussion).

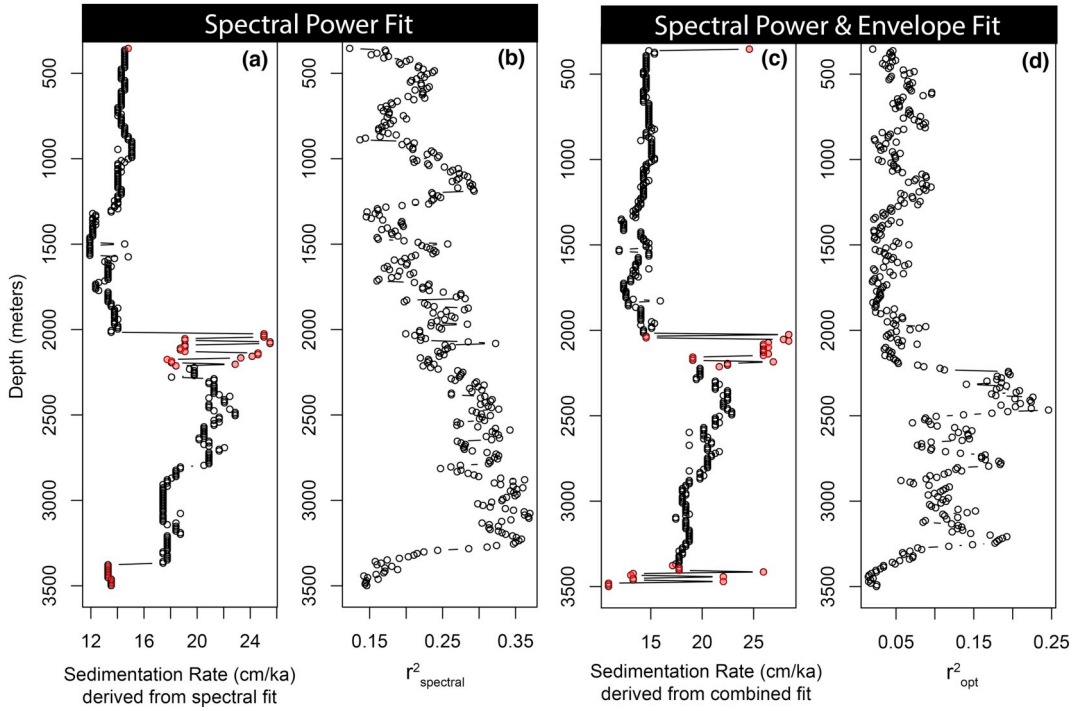

Fig. 23. Sedimentation rate history derived from eTimeOpt analysis of the Newark Basin Rank data (Olsen and Kent, 1999). Optimal sedimentation rates derived for each 300 m window are illustrated, along with the observed fit, which gives a measure of the signal-noise ratio. (a) Sedimentation rates derived from the spectral power fit. (b) $r^2_{spectral}$ results for each sedimentation rate in panel "a". (c) Sedimentation rates derived from the combined envelope and spectral power fit. (d) r^2_{opt} results for each sedimentation rate in panel "c". Red symbols identify results that demonstrate volatility, and should be treated with caution.

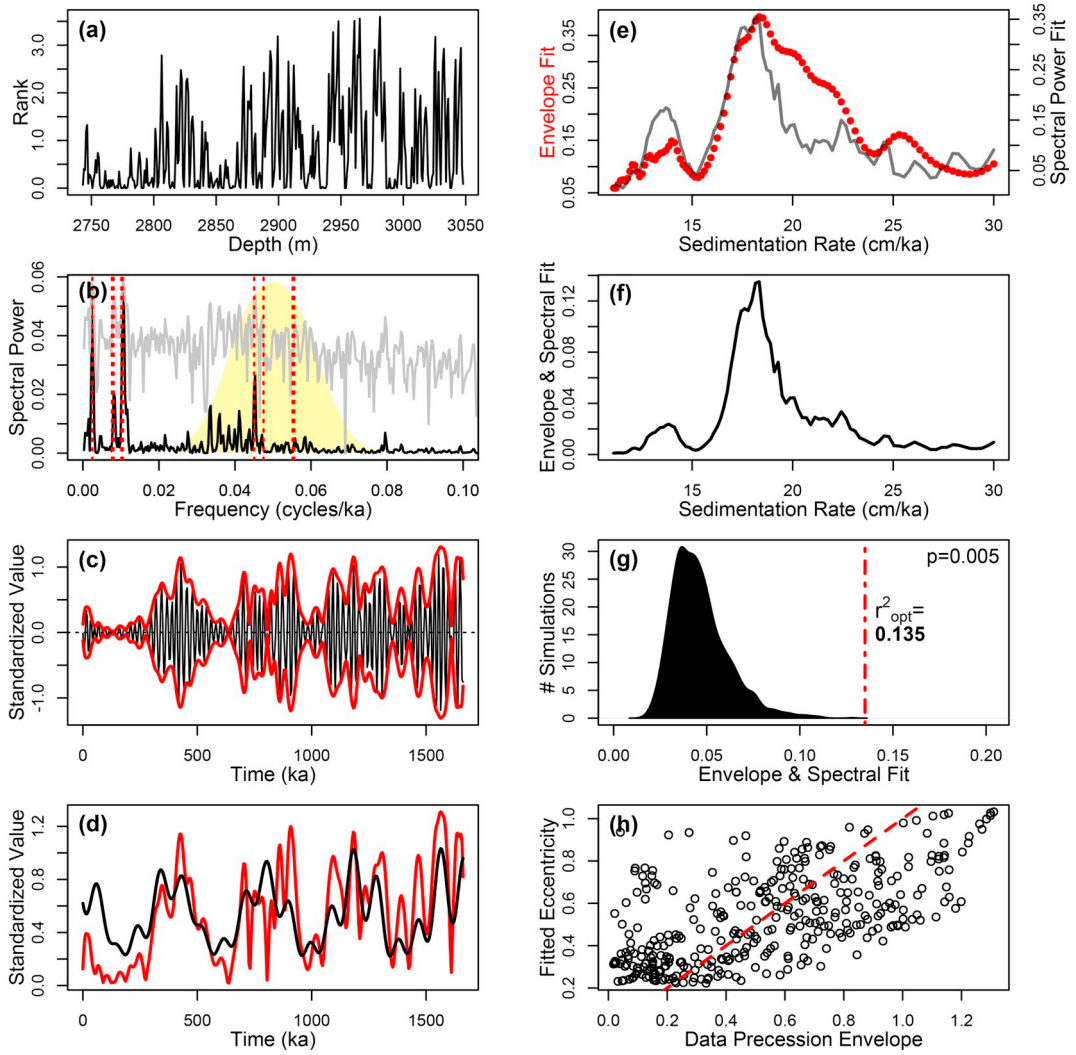

Fig. 24. TimeOpt analysis of the Newark Basin composite depth rank series (Olsen and Kent, 1999), evaluated with a constant *sedimentation template*. (a) The Newark Basin composite depth rank series that is analyzed, spanning 2743.2 to 3048 meters depth. (b) Periodogram for the Newark Basin composite depth rank series, given the TimeOpt derived average sedimentation rate of 18.34 cm/ka (black line = linear spectrum; gray line = log spectrum). Yellow shaded region illustrates the bandpass filter for evaluation of the precession amplitude envelope. Vertical dashed red lines indicate the precession and eccentricity target periods. (c) Comparison of the band-passed precession signal (black line), and the data amplitude envelope (red line) determined via Hilbert transform. (d) Comparison of the data amplitude envelope (red line) and the TimeOpt-reconstructed eccentricity model (black line; derived using Eq. (1)). (e) Squared Pearson correlation coefficient for the amplitude envelope fit ($r^2_{envelope}$; red dots) and the spectral power fit ($r^2_{spectral}$; dark gray line) at each evaluated sedimentation rate. (f) Combined envelope and spectral power fit (r^2_{opt}) at each evaluated sedimentation rate. (g) Summary of 2000 Monte Carlo simulations with AR1 surrogates (ρ_{AR1} = 0.529), used to evaluate the significance of the maximum observed r^2_{opt} of 0.135 (p-value = .005). (h) Cross plot of the data amplitude envelope and the TimeOpt-reconstructed eccentricity model in panel "d"; dashed red line is the 1:1 line.

5.2. Parametric null models, nonparametric null models, and process-based null models

Statistical hypothesis testing requires the formulation of a null model, against which the significance of an observed result may be evaluated. In cyclostratigraphy, it is common to use a first-order autoregressive (AR1) model (Gilman et al., 1963) as the null hypothesis (Weedon, 2003). This is motivated by the fact that the AR1 model represents a simple stochastic process that derives from climate dynamics (Hasselmann, 1976) and depositional system dynamics (Thakur and Scheidegger, 1970; Sadler and Strauss, 1990). The oscillatory stochastic variability embodied by the AR1 model arises when a white noise source (e.g., weather) is integrated by an Earth System component with a slower response time (e.g., the oceans; Hasselmann, 1976). The "redness" is a consequence of the dynamic interaction of fast and slow responding system components, of which there are many in the climate and depositional system.

The AR1 noise model provides a reasonable fit to the spectral background for the case studies investigated here (Fig. 16), which suggests that it is an appropriate null model against which to determine the statistical significance of the observed TimeOpt r^2_{opt} values. While much effort has been made to provide a reliable test of significance given a specified null model, the utility of any p-value is fundamentally dependent upon the use of an appropriate null model. In cases where an AR1 null model is not appropriate (e.g., see Vaughan et al., 2011; Crampton et al., 2018), the TimeOpt framework is easily adapted to a wide range of other parametric noise models, such as power law noise (Wunsch, 1972), bending power law noise (Vaughan et al., 2011), or higher order autoregressive models.

In some cases, parametric models may not provide a reliable null hypothesis. One possibility is to directly utilize the spectral background observed in the stratigraphic data, or some smoothed version of it (Hays et al., 1976; Weedon, 2003) as an estimate of the null model. To facilitate this nonparametric approach, noise surrogates of any given

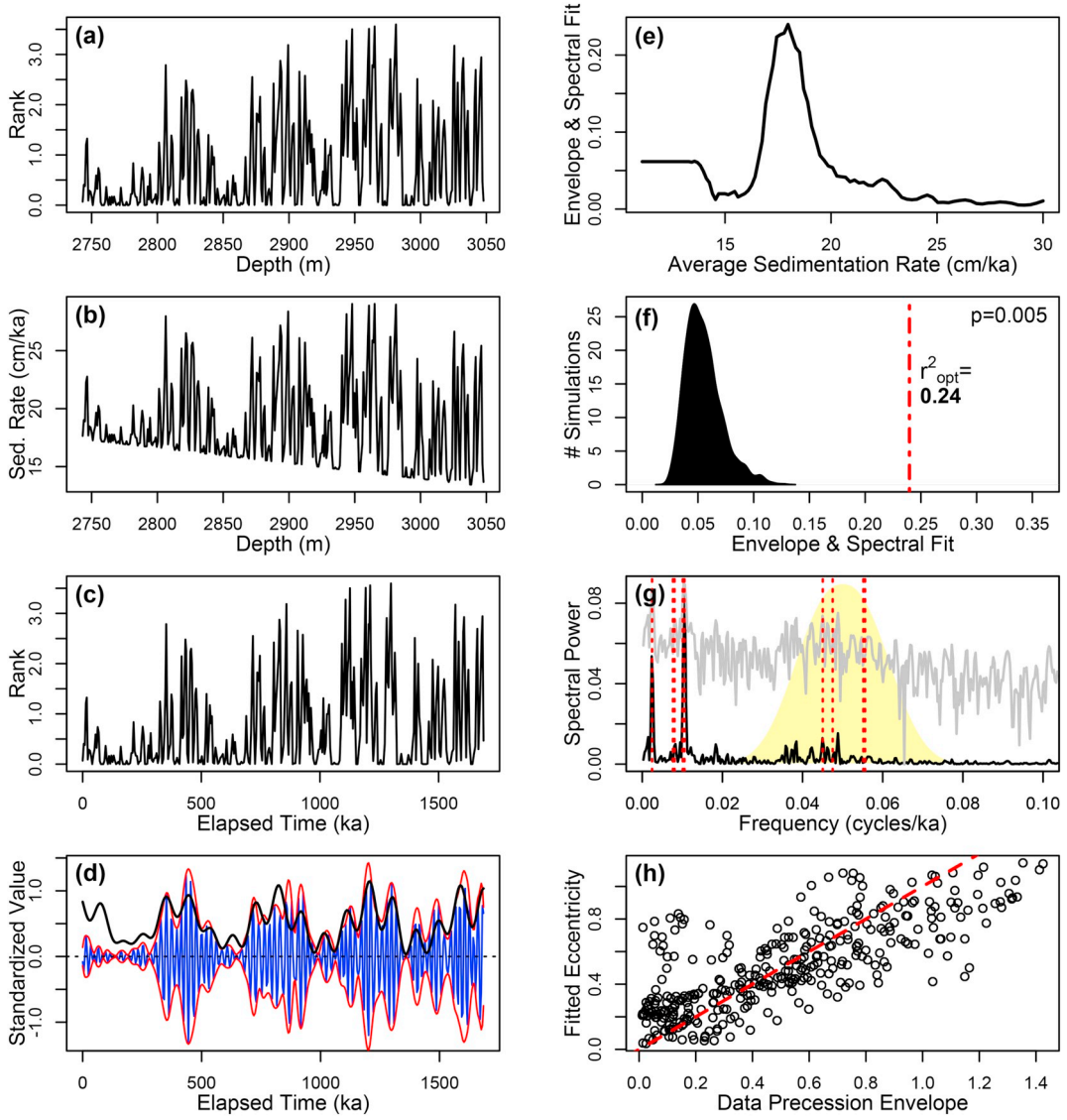

Fig. 25. TimeOpt analysis of the Newark Basin composite depth rank series (Olsen and Kent, 1999), evaluated with a proxy/lithology-specific *sedimentation template*. (a) The Newark Basin composite depth rank series that is analyzed, spanning 2743.2 to 3048 meters depth. (b) TimeOpt-reconstructed sedimentation rate history. (c) Astronomically-tuned Newark Basin composite depth rank series using the sedimentation rate history in (b). (d) Comparison of the band-passed precession signal (blue line), the data amplitude envelope (red line) determined via Hilbert transform, and the TimeOpt-reconstructed eccentricity model (black line; derived using Eq. (1)). (e) Combined envelope and spectral power fit (r^2_{opt}) at each evaluated average sedimentation rate. (f) Summary of 2000 Monte Carlo simulations with AR1 surrogates (ρ_{AR1} = 0.529), used to evaluate the significance of the maximum observed r^2_{opt} of 0.240 (p-value = .005). (g) Periodogram for the EP model, given the TimeOpt derived sedimentation history in (b) (black line = linear spectrum; gray line = log spectrum). Yellow shaded region illustrates the bandpass filter for evaluation of the precession amplitude envelope. Vertical dashed red lines indicate the eccentricity and precession target periods. (h) Cross plot of the data amplitude envelope and the TimeOpt-reconstructed eccentricity model in panel "d"; dashed red line is the 1:1 line.

spectral character can be generated with Astrochron function 'makeNoise'.

An alternative approach that is largely unexplored in cyclostratigraphy is to develop process-based null models for specific depositional systems. This may be especially important for shallow marine systems and fluvial systems where autogenic processes have a strong imprint (Jerolmack and Paola, 2010; Wang et al., 2011; Straub et al., 2015; Hajek and Straub, 2017). For example, physical experiments demonstrate that shallow marine siliciclastic systems can yield strong autogenic variability with peak spectral power at the 'compensation timescale' of the system. The compensation timescale identifies the timescale at which the controls on sedimentation transition from fully autogenic to fully allogenic in the physical model (Hajek and Straub, 2017). Importantly, these process-based models can differ substantially from an AR1 or power law model, which may result in the erroneous attribution of autogenic variability to astronomical influence in analog sedimentary systems (see Fig. 8 of Hajek and Straub, 2017). Similarly, the application of an AR1 or power law model under such scenarios may mask an astrononomical signal that is actually present, especially for Milankovitch cycles that exceed the compensation timescale of the system.

One could envision utilizing simulated cores from physical tank experiments as realizations of the null model (cores randomly selected, with replacement), for astrochronologic significance testing. Likewise, computational stratigraphic models (Pelletier and Turcotte, 1997; Burgess et al., 2001; Burgess and Wright, 2003; Burgess, 2006; Dexter et al., 2009) could be deployed in a similar fashion. In principle, it should be possible to develop a suite of process-based null models that are appropriate for different depositional regimes and environments, beyond the parametric (AR1 & power law) models that often apply to

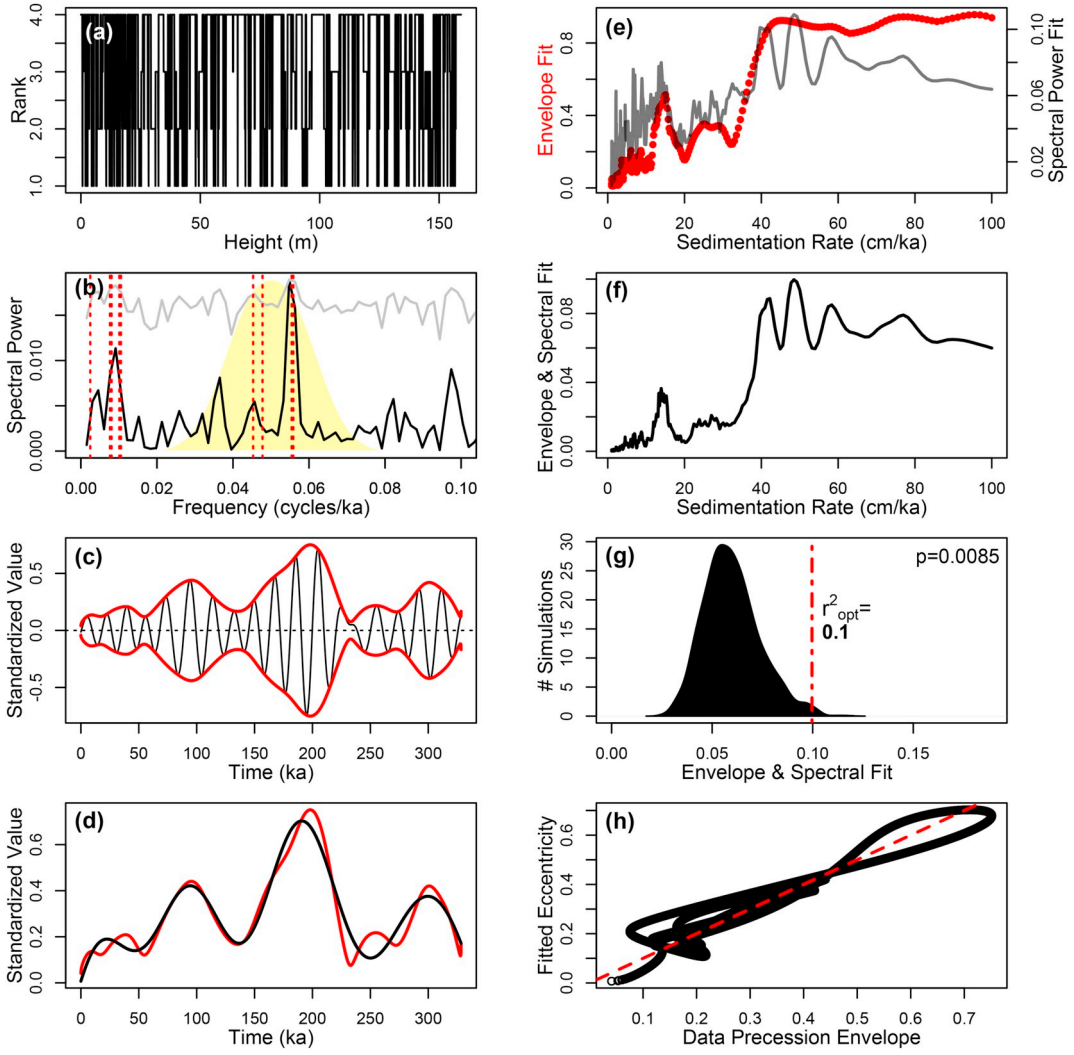

Fig. 26. TimeOpt analysis of the Latemar Limestone CDL depth rank series (Preto et al., 2001), evaluated with a constant *sedimentation template*. (a) The CDL depth rank series that is analyzed. (b) Periodogram for the CDL depth rank series, given the TimeOpt derived average sedimentation rate of 48.49 cm/ka (black line = linear spectrum; gray line = log spectrum). Yellow shaded region illustrates the bandpass filter for evaluation of the precession amplitude envelope. Vertical dashed red lines indicate the precession and eccentricity target periods. (c) Comparison of the band-passed precession signal (black line), and the data amplitude envelope (red line) determined via Hilbert transform. (d) Comparison of the data amplitude envelope (red line) and the TimeOpt-reconstructed eccentricity model (black line; derived using Eq. (1)). (e) Squared Pearson correlation coefficient for the amplitude envelope fit ($r^2_{envelope}$; red dots) and the spectral power fit ($r^2_{spectral}$; dark gray line) at each evaluated sedimentation rate. (f) Combined envelope and spectral power fit (r^2_{opt}) at each evaluated sedimentation rate. (g) Summary of 2000 Monte Carlo simulations with AR1 surrogates (ρ_{AR1} = 0.795), used to evaluate the significance of the maximum observed r^2_{opt} of 0.100 (p-value = .0085). (h) Cross plot of the data amplitude envelope and the TimeOpt-reconstructed eccentricity model in panel "d"; dashed red line is the 1:1 line.

deep-sea hemi-pelagic and pelagic systems. In addition to their utility in significance testing, such process-based null models can provide useful transfer functions for reconstructing depositional system response and deconvolving primary climate forcings (Section 5.3).

5.3. The reconstruction of Earth System transfer functions

When an astronomical rhythm is preserved within a stratigraphic record there exists an extraordinary opportunity to use the preserved signal and its distortion as a means to reconstruct the climate and depositional system transfer functions. The introduction of *sedimentation templates* in the present work constitutes an example of such transfer function reconstruction. In addition, the probabilistic regression model approach used to fit astronomical cycles in TimeOpt, which allows for variable phase and amplitude (e.g., due to non-linear responses), constitutes another example of transfer function reconstruction; this approach is most powerful when reliable constraints on insolation forcing are available for comparison (e.g., over the past 50 million years; Laskar et al., 2004; Laskar et al., 2011a). If bounds on the amplitude and phase responses are known a priori, such constraints can also be included in the optimization.

In principle, the TimeOpt framework can be adapted to include more complex "modules" that represent the physics of the climate and depositional system (Fig. 2), while also seeking to recover an undistorted astronomical-insolation signal. For example, one could envision implementing aspects of the modeling approach of Ripepe and Fischer (1991) or the modeling approach of Zeebe et al. (2017), within the TimeOpt framework. The key principle embodied in this approach is that time is a central component of paleoenvironmental reconstruction, and a simultaneous optimization on the time scale and transfer functions (Brüggemann, 1992) provides a means for more accurate reconstruction of the ancient Earth System. The implementation of such approaches within a Bayesian framework (Section 5.4) provides a rigorous means to simultaneously evaluate uncertainties in the time scale, the astronomical parameters, and the transfer functions. Relevant approaches that may facilitate this endeavor include stratigraphic

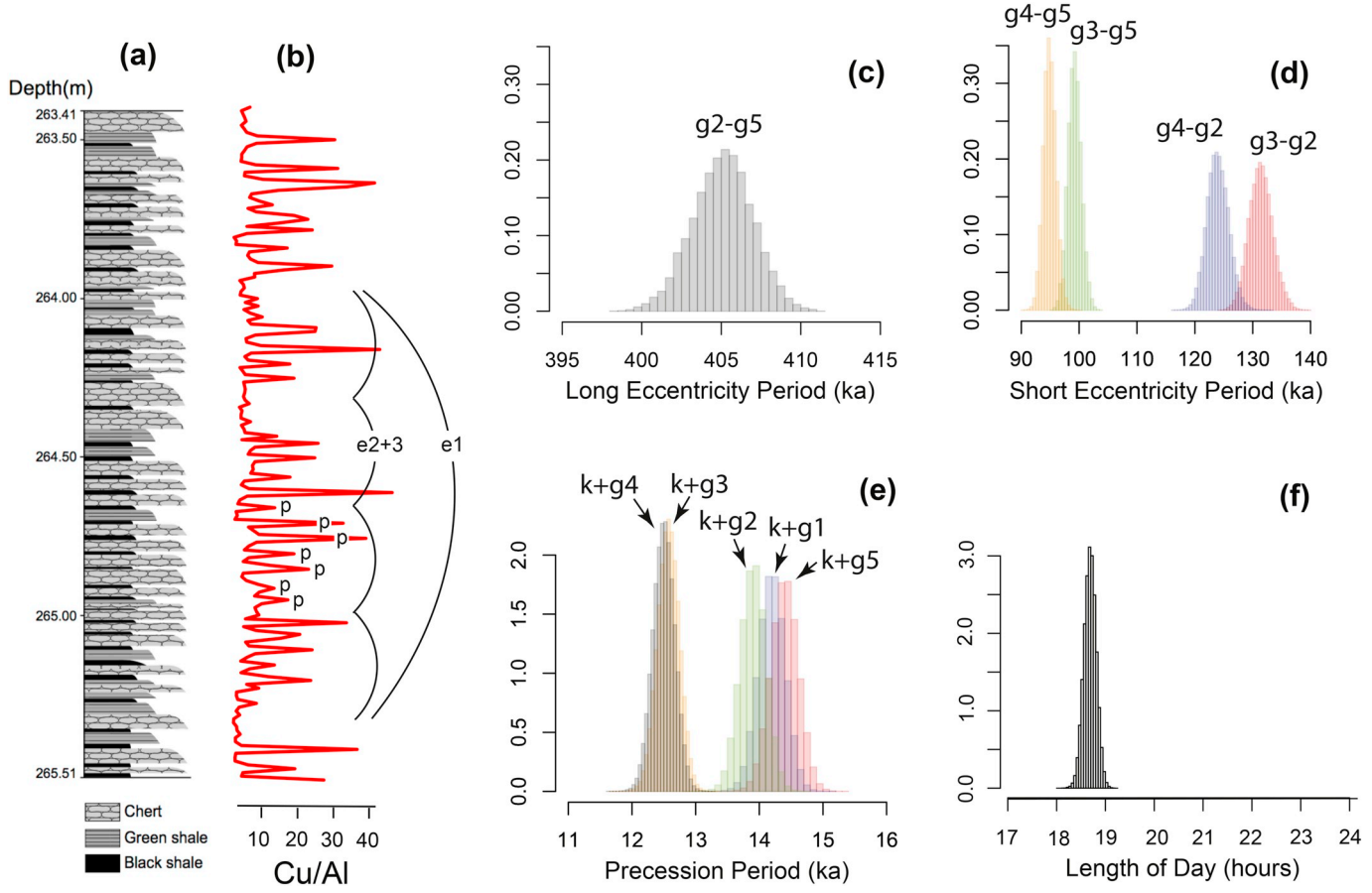

Fig. 27. Summary of results from a Bayesian TimeOptMCMC analysis (Meyers and Malinverno, 2018) of the 1.4 billion year old Xiamaling Formation Cu/Al data (Zhang et al., 2015), which has been interpreted to reflect changes in surface water paleoproductivity and/or redox state within water column/sediments. (a) Stratigraphy of the analyzed interval, reproduced from Zhang et al. (2015), (b) Cu/Al data evaluated with TimeOptMCMC, (c) Posterior statistical distribution of the long eccentricity period at 1.4 Ga, (d) Posterior statistical distributions of the short eccentricity periods at 1.4 Ga, (e) Posterior statistical distributions for the precession periods at 1.4 Ga, (f) Posterior statistical distribution of the length of a day at 1.4 Ga. For details about the TimeOptMCMC method and these results, see *Meyers and Malinverno (2018)*. "g_1" to "g_5" identify fundamental frequencies of the solar system for Mercury (g_1), Venus (g_2), Earth (g_3), Mars (g_4) and Jupiter (g_5). "k" identifies the precession constant. See Laskar et al. (2004) and Meyers and Malinverno (2018) for additional information.

modeling (Schiffelbein and Dorman, 1986; Herbert, 1994; Meyers et al., 2001; Ripepe and Fischer, 1991; Laurin et al., 2005), spectral deconvolution (Wigley, 1976; Goreau, 1980), diagenetic models (Berner, 1980), carbon cycle and Earth System modeling (e.g., Pälike et al., 2006; Ridgwell, 2007; Kirtland Turner and Ridgwell, 2013; Zeebe et al., 2017), and sediment transport experiments (Jerolmack and Paola, 2010; Hajek and Straub, 2017).

5.4. Mapping out ancient Solar System behavior and Earth-Moon history using the geologic archive of Milankovitch cycles

In applying the TimeOpt approach to evaluate Propositions 1–3 (Box 2) it is necessary to specify the periods of the astronomical target, which define the alternative hypothesis. A number of modeling studies have been conducted to estimate the evolution of the astronomical periods over different intervals of Earth History (e.g., Berger et al., 1992; Laskar et al., 2004; Waltham, 2015), which can be employed to construct the astronomical target. It should be emphasized that the amplitudes and phases of these periods are not included in the TimeOpt target, but emerge during the optimization process. This facet is crucial, as amplitudes and phases of the astronomical cycles are poorly constrained for time intervals > 50 Ma. Furthermore the ESTF (Fig. 2; Section 5.3) are expected to modify the astronomical-insolation amplitudes and phases. In the present study, the Laskar et al. (2004) solution has been utilized to define the precession and obliquity periods for the Cenozoic, while the estimates of Waltham (2015) have been utilized for older intervals. Based on the 500 million year long simulations of Laskar et al. (2004), the eccentricity periods are expected to be much more stable than those of precession and obliquity; the eccentricity periods from that study are used in all TimeOpt analyses (see Appendix A.3 for further discussion).

Uncertainty in the astronomical solutions primarily derives from Solar System chaos (Laskar, 1989; Ma et al., 2017), changes in Earth's rotation rate (Berger et al., 1992), and changes in Earth's dynamical ellipticity (related to its moment of inertia terms; Berger et al., 1992). For an excellent review on this topic see Hinnov (2013). Numerous studies have utilized the geologic record to help overcome these uncertainties (Pälike and Shackleton, 2000; Lourens et al., 2001; Pälike et al., 2004; Hinnov, 2013; Zeeden et al., 2014b; Ma et al., 2017). Recently, an implementation of TimeOpt (Meyers and Malinverno, 2018) was introduced that uses a Bayesian model-data integration approach (TimeOptMCMC) to simultaneously constrain the uncertainties on the astronomical time scale, the astronomical periods, and the Earth-Moon history. This new Bayesian approach can rigorously evaluate Propositions 2 and 3 (Box 2), and their uncertainties.

Some of the key results from Meyers and Malinverno (2018) are summarized in Fig. 27, which utilizes the new Bayesian TimeOptMCMC approach to analyze a Cu/Al record from the 1.4 billion year old Xiamaling formation (Zhang et al., 2015). These deposits consist of interbedded cherts, green shales and black shales (Fig. 27a), and Cu/Al has

been interpreted to reflect changes in surface water paleoproductivity and/or redox state with the water column/sediments (Zhang et al., 2015; Meyers and Malinverno, 2018).

The TimeOptMCMC approach resolves the main eccentricity terms and precession terms at 1.4 Ga, and constrains their uncertainties. These periodicities can now be used to develop reliable floating astrochronologies in the Proterozoic. In addition, the length of day and Earth-Moon distance are reconstructed as 18.68 ± 0.25 h (2σ) and 340,900 ± 2600 km (2σ), respectively. The new results provide important constraints on Earth-Moon history (see Fig. 3 and S12 of Meyers and Malinverno, 2018).

In principle, Earth System transfer function reconstruction (Fig. 2 and Section 5.3) can also be conducted within this Bayesian framework, providing explicit uncertainties on each step of the pathway of the astronomical signal.

5.5. Development of anchored astrochronologies

There are two fundamental categories of anchored astrochonologies that are common in cyclostratigraphy: (1) those that are developed by anchoring to a theoretical astronomical solution (Laskar et al., 2004), and (2) floating astrochronologies that are anchored to 'absolute' numerical time using radioisotopic geochronology (either directly or indirectly through stratigraphic correlation). The first class is constructed by maximizing the match between a given stratigraphic series and a theoretical astronomical model (Laskar et al., 2004; Laskar et al., 2011a,b), or alternatively, to an astronomical-climate model (e.g., Imbrie and Imbrie, 1980). Such anchored astrochronologies are often constructed by visual wiggle matching of the stratigraphic series to a tuning target, using the expression of bundling, precession-obliquity interference, and/or long term (~2.4 Myr) eccentricity nodes as diagnostic fingerprints to justify a given anchoring. This approach envisions the theoretical astronomical signal as a stratigraphic section or parameter (either implicitly, or explicitly through modeling; see the function 'synthStrat' in Astrochron), which one may stratigraphically correlate to. As with all stratigraphic correlation, it presents a hypothesis that should be tested by independent means (see Box 2). A superb example of this approach comes from the Mediterranean sapropel sequences of the Miocene, which illustrate striking similarity to the patterns observed in astronomical-insolation (Hilgen et al., 1995, 2014).

A range of computational algorithms have also been introduced to develop such anchored astrochronologies using different fitting criteria (Martinson et al., 1982; Brüggemann, 1992; Lisiecki and Raymo, 2005), including recent advances that provide the ability to explicitly evaluate uncertainties associated with stratigraphic correlation to astronomically-tuned $\delta^{18}O$ stacks (Ahn et al., 2017). It is important to note that quantification of the underlying uncertainties in the astronomical tuning (allowing for uncertainty in the climate system response time, hiatus, etc.) remains an important issue of inquiry that is typically subjectively evaluated (however, see Martinson et al., 1987). Given the uncertainties in the theoretical astronomical solutions (Section 5.4), a direct anchoring to them is generally restricted to the past 50 million years. However, it is expected that the 405 ka long eccentricity cycle is stable enough for direct anchoring through at least the Mesozoic (Laskar et al., 2004, 2011a,2011b; Kent et al., 2018).

The five case studies evaluated in the present article constitute floating astrochronologies. Anchoring of floating astrochronologies requires an explicit integration with independent time control, and should include the uncertainty associated with the anchoring process. A number of statistical anchoring approaches that explicitly incorporate uncertainties associated with radioisotopic geochronology and bio/lithostratigraphic correlation have been proposed (Meyers et al., 2012b; De Vleeschouwer and Parnell, 2014; Sageman et al., 2014; Ma et al., 2017). The Bayesian approach of Meyers and Malinverno (2018) provides a means to more reliably estimate the uncertainties in the astronomical cycle durations, so they can be accurately included in the total uncertainty estimate for a geologic timescale.

The anchoring of floating astrochronologies and their integration with other geochronologic/stratigraphic information remains an important avenue of research, with an opportunity to leverage existing Bayesian frameworks (e.g., "Bchron" of Haslett and Parnell, 2008; "Bacon" of Blaauw and Christen, 2011). Astrochronology demonstrates much potential to resolve ambiguities in radioisotopic data (e.g., Kuiper et al., 2008; Meyers et al., 2012a; De Vleeschouwer and Parnell, 2014; Wotzlaw et al., 2014). Integration of astrochronologic constraints with Bayesian modeling of magmatic processes and mineral crystallization history (e.g., Keller et al., 2018), for example, is a promising endeavor. Once floating astrochronologies are anchored, they also provide a means to test, and potentially improve upon, the theoretical astronomical models. Much like the geologic timescale, the theoretical astronomical solutions should be considered a working hypothesis, perpetually under revision.

6. Conclusions

A key objective of this study has been to articulate a conceptual framework for understanding and evaluating the three challenges to astrochronology – *contamination*, *stratigraphic distortion*, and *temporal calibration*. Guided by the pathway of the astronomical signal (Fig. 2) and the three "fundamental propositions" of astrochronology (Box 2), TimeOpt (Meyers, 2015) is formulated as a solution, providing an approach for astrochronologic testing that evaluates time scale uncertainty while simultaneously identifying the optimal model for climate and depositional system response to astronomical forcing. Several new extensions to the technique have been introduced to allow explicit reconstruction of distortions to the primary forcing that are known to be omnipresent in the stratigraphic record. The concept of a *sedimentation template* is presented as a means to evaluate variable sedimentation, allowing consideration of expert knowledge from integrated stratigraphy, and improved reconstruction of Earth System transfer functions (ESTF) associated with climate and depositional system responses to astronomical forcing.

Application of the TimeOpt methodology to numerous synthetic astronomical series and to five well-studied stratigraphic series throughout the Phanerozoic demonstrates its utility as a cyclostratigraphic approach. Analysis of records from the Pleistocene (Site 607 North Atlantic), Miocene (Mediterranean), Eocene (South Atlantic Walvis Ridge), and the Triassic (Newark Basin and Latemar Platform) supports their astronomical origin with high statistical confidence, and yields new constraints on the evolution of the Earth System and the astronomical solutions themselves.

TimeOpt provides a generalized solution to the problem of astrochronologic testing that encompasses more specialized cases. For example, if amplitudes and phases of the astronomical signals are known a priori, and one is concerned with testing for eccentricity-related amplitude modulation of precession in a tuned record, the TimeOpt approach draws similarities to the methodology of Zeeden et al. (2015). If one is exclusively concerned with evaluating spectral power, the evolutive TimeOpt approach is similar to the methodology of Malinverno et al. (2010). Finally, if an age model for a stratigraphic record is developed independent of astrochronology (e.g., radioisotopic dating, magnetostratigraphy), application of the TimeOpt method using that single time model provides a reliable means for statistical testing of the astronomical hypothesis (*p*-value estimation), if not optimization of the time scale. More generally, the TimeOpt approach recognizes the complexities and ambiguities of the stratigraphic record, providing a quantitative means by which to test and compare multiple astronomical hypotheses. In this regard, it provides an explicit quantification of the signal/noise (r^2_{opt}, $r^2_{spectral}$, $r^2_{envelope}$) within and across individual records and interpretations, providing benchmarks for progressive improvement of astrochronology.

The flexibility of the TimeOpt framework provides the potential to

develop additional/alternative ESTF (Fig. 2) components that can be evaluated during the optimization process. In this way, astrochronologic testing and time scale evaluation are conducted in tandem with the reconstruction of the Earth System response (Schiffelbein and Dorman, 1986; Brüggemann, 1992; Meyers, 2017). This approach recognizes that time and its uncertainty represent fundamental parameters in our evaluation of paleoclimate, which should be explicitly considered. In future work, ESTF reconstruction/optimization can be integrated with more complex diagenetic models (e.g., reactive-transport models; Berner, 1980), carbon cycle models (Zeebe et al., 2017; Meyers, 2017) or even Earth System Models that include astronomical forcing (Ridgwell, 2007; Kirtland Turner and Ridgwell, 2013).

In addition to the approaches noted above, the TimeOpt method has recently been reformulated within a Bayesian framework to simultaneously evaluate uncertainty in the geologic timescale and uncertainty in the astronomical periods, while also reconstructing the Earth-Moon history and the fundamental frequencies of the Solar System (Meyers and Malinverno, 2018). This approach is particularly important to apply when considering pre-Cambrian astrochronology. Integration of the Bayesian methodology with aforementioned ESTF reconstruction approaches (e.g., sedimentation templates, carbon cycle models) shows promise to better constrain our understanding of the ancient Earth System, and the sources of uncertainty in our knowledge as well, through the recognition of astronomy, geochronology, paleoclimatology and depositional system reconstruction as a unified geoscientific inverse problem.

Acknowledgements

This work has benefitted from very helpful critique and advice from numerous colleagues. In particular, I would like to thank Frits Hilgen, Linda Hinnov, Alberto Malinverno, Brad Sageman, Graham Weedon, and Bruce Wilkinson. I thank John Hartigan and Jay Emerson for their advice on the use of linear model optimization for astrochronologic testing. Finally, Mike Meyers is heartily thanked for designing and helping to maintain my computational servers over the past decade, which facilitated this work. This study was made possible by funding from National Science Foundation award EAR-1151438: “CAREER: Deciphering the Beat of a Timeless Rhythm – The Future of Astrochronology”.

Appendix A. Guidance on application of the TimeOpt approach for cyclostratigraphic analysis

A.1. The development of stratigraphic series for TimeOpt analysis

The pathway of the astronomical signal (Fig. 2) provides insight into criteria that should be considered when conducting astrochronologic analysis. Foremost, climate and depositional system response to astronomical-insolation (steps 1 & 3 in Fig. 2) is a hypothesis that one seeks to test. Any of the transfer functions in Fig. 2 could corrupt the preservation of an astronomical signal (reduce the signal-noise ratio) in a given stratigraphic characteristic or paleoclimate proxy. Some transfer functions may even generate cyclic variability, which here serves as noise that can obscure an astronomical signal. Examples of this include autocyclic depositional processes (Step 3 in Fig. 2; Hajek and Straub, 2017), and diagenetic “unmixing” of sediments (Step 5 in Fig. 2; Westphal et al., 2008).

The cyclostratigrapher occupies an essential role in the pathway of the astronomical signal, through their selection of stratigraphic characteristics or paleoclimate proxies for evaluation, and their subsequent development of the stratigraphic series (steps 6 and 7 in Fig. 2). The ensuing decisions ultimately influence the signal-noise ratio of preserved astronomical signals, and one's ability to accurately calibrate them. Primary concerns include: (1) signal aliasing, (2) the development of sufficiently long records to reliably assesses the hypothesized astronomical cycles, and (3) careful consideration of the link between the proxy/stratigraphic observations and primary climate/oceanic parameters (sea level, ice volume, temperature, etc.).

The minimum spatial wavelength (in meters) that one can evaluate in a TimeOpt analysis is two times the sampling interval. The “Nyquist frequency”, expressed in units of cycles/m, is the reciprocal of this minimum wavelength. Spectral power at frequencies greater than the Nyquist frequency will be aliased to lower frequencies, potentially yielding artificial spectral peaks and corrupting the assessment of amplitude modulation (see Fig. 11). To avoid aliasing of precession signals in cyclostratigraphic series, it is necessary to sample at least two times per a hypothesized precession cycle, given the lowest plausible sedimentation rate for a given succession. While this constitutes the minimum required sampling resolution, it is preferable to sample 4–5 times (or greater) per hypothesized precession cycle (see Weedon, 2003 and Mathieu et al., 2016 for additional recommendations).

At the opposite extreme, in order to fully assess both long and short eccentricity-scale variability using the TimeOpt method, one must evaluate a stratigraphic series that is at least 405 ka long, given the highest plausible sedimentation rate. TimeOpt analysis of the Latemar Limestone (Fig. 26) illustrates that this requirement can be relaxed, but the statistical power of the method is necessarily reduced. It is advisable to evaluate records that contain multiple long eccentricity cycles, given the highest plausible sedimentation rate, to increase the statistical power. In some instances, this may require the application of a more complex sedimentation template (Fig. 7). When very long stratigraphic series are evaluated, changes in sedimentation can ultimately limit the size of the analysis interval, and application of the eTimeOpt approach is warranted (e.g., the Newark Basin, Figs. 22–23).

Under ideal conditions, the investigated stratigraphic succession preserves evidence for primary compositional/sedimentologic/paleobiologic variability at the scale of the hypothesized astronomical cycles. However, there are also situations where early diagenesis (Fig. 2, Step 5) is very likely driven by astronomical variability (Chen et al., 2017), and thus proxies for early diagentic processes (redox sensitive trace elements like molybdenum; Meyers et al., 2005) can record astronomical cycles. Theoretical modeling studies have also suggested that diagenesis can, under some circumstances, amplify primary compositional differences (Einsele and Ricken, 1991; however see Westphal et al., 2004; Westphal et al., 2008). Finally, primary compositional variability may also serve to distort the astronomical signal, as in the case of turbidites or volcanic ashes interspersed within a stratigraphic succession; such sediments should generally be excluded (excised) when developing cyclostratigraphic series.

A.2. Significance testing

The recommendations discussed above are intended to increase the potential for accurate identification of Milankovitch cycles, by maximizing the signal-noise ratio of the analyzed stratigraphic series. With regards to the “Three Propositions” noted in Box 2, statistical hypothesis testing with Monte Carlo surrogates provides a safeguard against erroneous detection of astronomical cycles (Proposition 1: Existence), at the stated confidence level. To ensure correct estimation of significance, however, the Monte Carlo surrogates should be preprocessed in an identical fashion as the stratigraphic series, e.g., via linear detrending, and an identical sedimentation template must be employed (yielding the same degrees of freedom). If more complex detrending is used (e.g., polynomials), the Monte Carlo surrogate algorithm should be modified to account for this.

A.3. Selection of the null model (the null hypothesis) and development of the astronomical target (the alternative hypothesis)

The suitability of a given null model is typically judged based on its fit to the observed spectral background. The most common null model

used in cyclostratigraphy is the AR1 model (Gilman et al., 1963; Weedon, 2003), which has two degrees of freedom (average power, and lag-1 autocorrelation coefficient). The AR1 model is the default null hypothesis for TimeOpt. However, a wide array of other null models can be implemented within the TimeOpt framework, including bending power law (Vaughan et al., 2011) and higher order autoregressive models. In developing these more elaborate parametric models one must be cognizant to the fact that the greater degrees of freedom increases the risk of 'over-fitting' the spectrum. For example, a bending power law with two segments has twice the degrees of freedom as a simpler power law model or AR1 model. With this increase in the degrees of freedom of the null model, there comes an increase in the likelihood that it will erroneously fit astronomical cycles if they are present. The problem of over-fitting with parametric models is well known, and Thomson et al. (2001) provide some useful guidance. See Section 5.2 for additional discussion of parametric, non-parametric and process-based null models.

In order to establish an alternative hypothesis for the TimeOpt analysis, the astronomical periods must be specified. When prospecting for precession or obliquity scale variability, this requires some knowledge of the age of the strata, because the duration of the periods are known to shorten with age due to tidal friction and changes in Earth's rotation rate. Laskar et al. (2004) implements an Earth-Moon model that can be used for this purpose. More recently, Waltham (2015) conducted a comprehensive evaluation of the evolution of the main precession and obliquity periods and their uncertainty.

While is it possible to modify the eccentricity target periods that are implemented in TimeOpt, this is generally not advisable for the significance testing. The default eccentricity target utilizes the five dominant eccentricity periods (405.7 ka, 130.7 ka, 123.8 ka, 98.9 ka, 94.9 ka), which combine through variable phase and amplitude to approximate the complex eccentricity patterns observed in the orbital signal (e.g., Astrochron function call 'timeOpt(etp (tmin = 2000,tmax = 3000,oWt = 0),sedmin = 100,sedmax = 100)'). Furthermore, the eccentricity periods are expected to vary by < 2%, and in no clear systematic manner (Berger et al., 1992; Laskar et al., 2004).

Following the initial significance testing (Proposition 1), full uncertainties in the Laskar et al. (2004) and/or Waltham (2015) models can be explicitly evaluated within the Bayesian inversion framework of Meyers and Malinverno (2018; TimeOptMCMC). This allows full quantification of uncertainties in the astronomical time scale, the astronomical periods, the fundamental frequencies of the Solar System, and the Earth-Moon history.

A.4. Selection of a sedimentation template

To develop a reliable floating astrochronology with well-constrained uncertainties (Proposition 3), it is necessary to account for variable sedimentation and hiatus (*sedimentation templates*; Fig. 7), and to estimate uncertainties in the astronomical periods. A myriad of options exist for potential *sedimentation templates* (Fig. 7), and one may ask which template is most appropriate. The answer depends upon the specific question at hand (Box 2).

For the sake of Proposition 1, it is ideal to begin with a constant *sedimentation template*, as it is the simplest a priori model (depth as a proxy for time) with the fewest degrees of freedom. As additional degrees of freedom are added to the *sedimentation template*, both the data and noise surrogates are given a greater flexibility to adjust to fit the proposed astronomical rhythms. As a consequence, if sedimentation is indeed relatively constant throughout the stratigraphic series, an increase in the degrees of freedom will reduce the statistical significance (increase the *p*-value) of the TimeOpt result. However, when sedimentation is indeed variable (Figs. 8–11), an increase in the degrees of freedom of the *sedimentation template* can more dramatically improve the fit of the data than the surrogates, yielding a significant result. Regardless of the template employed to evaluate Proposition 1, if the null model has been rejected, and the general calibration has been identified (Proposition 2), it is then reasonable to increase the complexity of the *sedimentation template* to further improve the floating astrochronology fit, or to use other approaches for astronomical tuning (e.g., Martinson et al., 1987; Hilgen et al., 1995; Lisiecki and Raymo, 2005).

A.5. Evaluation of the TimeOpt results

In addition to reporting multiple measures of fit (r^2_{opt}, $r^2_{spectral}$, $r^2_{envelope}$) and a formal p-value, the TimeOpt approach provides a range of criteria with which to evaluate Propositions 1 and 2, including the following:

(1) Good evidence to support a correct temporal calibration exists when the r^2_{opt} maximum aligns (approximately) with maxima in both $r^2_{spectra}$ and $r^2_{envelope}$. The differential accumulation model in Fig. 8, illustrates a scenario where this is not the case (see also Fig. 10). In particular, if r^2_{opt} is associated with low $r^2_{spectra}$ and high $r^2_{envelope}$, the temporal calibration should be avoided.
(2) A source of supporting evidence for a TimeOpt calibration is the internal consistency of the TimeOpt-reconstructed eccentricity model, and the eccentricity-scale variability that is directly preserved within the stratigraphic series (if present). Likewise, a consistency of the amplitude modulation of short eccentricity with the observed long eccentricity would be expected based on astronomical theory (Laskar et al., 2004). However, disagreements in phase are plausible under some circumstances, due to the climate and/or depositional system transfer functions (e.g., Laurin et al., 2005; Laurin et al., 2017).
(3) A TimeOpt analysis can be conducted exclusively on eccentricity, when it is preserved within a stratigraphic series. Such an assessment considers the spectral power of the eccentricity cycles, and amplitude modulation of short eccentricity, which should preserve a 405 ka signal. The results of this assessment should ideally yield a similar sedimentation rate as the precession-based model.
(4) When a strong obliquity signal emerges from a TimeOpt analysis that implements precession and/or eccentricity target periods, this provides additional independent evidence to support the astronomical interpretation and sedimentation rate (and vice versa).

A range of other non-statistical criteria should also be considered when evaluating the TimeOpt results, including basin architecture, biochemo-magneto-lithostratigraphic constraints, radioisotopic constraints, comparative sedimentology, and paleoceanographic/paleoclimatologic constraints. Irrespective of the reported p-value and fit, one should ask whether the cyclostratigraphic interpretation makes practical sense. False positives and false negatives (Box 1) are an inherent component of the statistical hypothesis test, and interpretation of the results, without due regard for their stratigraphic and geologic context, is a risky enterprise. Ultimately, verification of an astronomical interpretation is strengthened by both duplication and triangulation (Box 1).

Appendix B. Supplementary data

Supplementary data to this article can be found online at https://doi.org/10.1016/j.earscirev.2018.11.015.

References

Ahn, S., Khider, D., Lisiecki, L.E., Lawrence, C.E., 2017. A probabilistic Pliocene–Pleistocene stack of benthic $\delta^{18}O$ using a profile hidden Markov model. Dyn. Stat. Clim. System 1–16. https://doi.org/10.1093/climsys/dzx002.

Aswasereelert, W., Meyers, S.R., Carroll, A.R., Peters, S.E., Smith, M.E., Feigl, K.L., 2013. Basin-scale cyclostratigraphy of the Green River Formation, Wyoming. GSA Bull. 125, 216–228.
Bailey, R.J., Smith, D.G., 2008. Quantitative tests for stratigraphic cyclicity. Geol. J. 43. https://doi.org/10.1002/gj.1115.
Berger, A., Loutre, M.F., Dehant, V., 1989. Astronomical frequencies for pre-quaternary palaeoclimate studies. Terra Nova 1, 474–479.
Berger, A., Loutre, M.F., Laskar, J., 1992. Stability of the astronomical frequencies over the Earth's history for paleoclimate studies. Science 255, 560–566.
Berner, R.A., 1980. Early Diagenesis: A Theoretical Approach. Princeton Univ. Press, Princeton, N. J., pp. 256.
Blaauw, M., Christen, J.A., 2011. Flexible paleoclimate age-depth models using an autoregressive gamma process. Bayesian Anal. 6, 457–474.
Brack, P., Mundil, R., Oberli, F., Meier, M., Rieber, H., 1996. Biostratigraphic and radiometric age data question the Milankovitch characteristics of the Latemar cycles (Southern Alps, Italy). Geology 24, 371–375. https://doi.org/10.1130/0091–7613(1996)024<0371:BARADQ>2.3.CO;2.
Brüggemann, W., 1992. A minimal cost function method for optimizing the age-depth relation of deep-sea sediment cores. Paleoceanography 7, 467–487.
Burgess, P.M., 2006. The signal and the noise: forward modeling of allocyclic and autocyclic processes influencing peritidal carbonate stacking patterns. J. Sed. Res. 76, 962–977.
Burgess, P.M., Wright, V.P., 2003. Numerical forward modeling of carbonate platform dynamics: an evaluation of complexity and completeness in carbonate strata. J. Sed. Res. 73, 637–652.
Burgess, P.M., Wright, V.P., Emery, D., 2001. Numerical forward modelling of peritidal carbonate parasequence development: implications for outcrop interpretation. Basin Res. 13, 1–16.
Chen, M., Kim, Ji-Hoon, Choi, J., Lee, Y.K., Hur, J., 2017. Biological early diagenesis and insolation-paced paleoproductivity signified in deep core sediment organic matter. Scient. Rep. 7, 1581. https://doi.org/10.1038/s41598-017-01759-4.
Crampton, J.S., Meyers, S.R., Cooper, R.A., Sadler, P.M., Foote, M., Harte, D., 2018. Pacing of Paleozoic macroevolutionary rates by Milankovitch grand cycles. PNAS 115, 5686–5691. https://doi.org/10.1073/pnas.1714342115.
De Vleeschouwer, D., Parnell, A.C., 2014. Reducing time-scale uncertainty for the Devonian by integrating astrochronology and Bayesian statistics. Geology 42, 491–494.
Dexter, T.A., Kowalewski, M., Read, J.F., 2009. Distinguishing Milankovitch-driven processes in the rock record from stochasticity using computer-simulated stratigraphy. J. Geol. 117, 349–361.
Einsele, G., Ricken, W., 1991. Limestone-marl alternation — an overview. In: Einsele, G., Ricken, W., Seilacher, A. (Eds.), Cycles and Events in Stratigraphy. Springer, Heidelberg, pp. 23–47.
Evans, D.L., Freeland, H.J., 1977. Variations in the Earth's orbit: pacemaker of the ice ages? Science 198, 528–529.
Fischer, A.G., 1964. Lofer cyclothems of the alpine Trias. Kans. Geol. Surv. Bull. 169, 107–148.
Fisher, R.A., 1929. Tests of Significance in Harmonic Analysis, Proceedings of the Royal Society A, 54–59.
Forkner, R.M., Hinnov, L.A., Goldhammer, R.K., Hardie, L.A., 2009. The allocyclic interpretation of the 'Latemar Cycles' (Middle Triassic, the Dolomites, Italy) and implications for high-frequency cyclostratigraphic forcing. Int. Assoc. Sedimentol. Spec. Publ. 41, 215–238.
Gilman, D.L., Fuglister, F.J., Mitchell Jr., J.M., 1963. On the power spectrum of 'red noise'. J. Atmos. Sci. 20, 182–184. https://doi.org/10.1175/1520-0469(1963)020<0182:OTPSON>2.0.CO;2.
Goldhammer, R.K., Dunn, P.A., Hardie, L.A., 1987. High frequency glacio-eustatic sea-level oscillations with Milankovitch characteristics recorded in middle Triassic platform carbonates in northern Italy. Am. J. Sci. 287, 853–892.
Goldhammer, R.K., Dunn, P.A., Hardie, L.A., 1990. Depositional cycles, composite sea-level changes, cycle stacking patterns, and the hierarchy of stratigraphic forcing: examples from Alpine Triassic platform carbonates. Bull. Geol. Soc. Am. 102, 535–562.
Goreau, T.J., 1980. Frequency sensitivity of the deep-sea climatic record. Nature 287, 620–622.
Gradstein, F.M., Ogg, J.G., Smith, A.G., 2012. A Geologic Time Scale 2012. Cambridge University Press, New York.
Hajek, E.A., Straub, K.M., 2017. Autogenic sedimentation in clastic stratigraphy. Annu. Rev. Earth Planet. Sci. 45, 681–709.
Hallam, A., 1986. Origin of minor limestone-shale cycles: Climatically induced or diagenetic? Geology 14, 609–612.
Haslett, J., Parnell, A., 2008. A simple monotone process with application to radiocarbon-dated depth chronologies. Appl. Statist. 57, 399–418.
Hasselmann, K., 1976. Stochastic climate models: Part I. Theory. Tellus 6, 473–485.
Hays, J.D., Imbrie, J., Shackleton, N.J., 1976. Variations in the Earth's orbit: pacemaker of the ice ages. Science 194, 1121–1132. https://doi.org/10.1126/science.194.4270.1121.
Herbert, T.D., 1992. Paleomagnetic calibration of Milankovitch cyclicity in Lower Cretaceous sediments. Earth Planet. Sci. Lett. 112, 15–28.
Herbert, T.D., 1994. Reading orbital signals distorted by sedimentation: Models and examples. In: de Boer, P.L., Smith, D.G. (Eds.), Orbital Forcing and Cyclic Sequences: International Association of Sedimentologists. Vol. 19. pp. 483–507 Special Publication.
Hilgen, F.J., Krijgsman, W., Langereis, C.G., Lourens, L.J., Santarelli, A., Zachariasse, W.J., 1995. Extending the astronomical (polarity) time scale into the Miocene. Earth Planet. Sci. Lett. 136, 495–510.
Hilgen, F. J., Schwarzacher, W., Strasser A., 2004. Concepts and definitions in cyclostratigraphy (second report of the cyclostratigraphy working group). – SEPM. Spec. Publ. 81, 303–305, Tulsa.
Hilgen, F.J., Lourens, L.J., Van Dam, J.A., 2012. The Neogene Period. In: Gradstein, F.M., Ogg, J.G., Smith, A.G. (Eds.), A Geologic Time Scale 2012. Cambridge University Press, New York, pp. 923–978.
Hilgen, F.J., Hinnov, L.A., Abdul Aziz, H., Abels, H.A., Batenburg, S., Bosmans, J.H.C., De Boer, B., Husing, S.K., Kuiper, K.F., Lourens, L.J., Rivera, T., Tuenter, E., van de Wal, R.S.W., Wotzlaw, J-F, Zeeden, C., 2014. Stratigraphic continuity and fragmentary sedimentation: the success of cyclostratigraphy as a part of integrated stratigraphy. From: Smith, D. G., Bailey, R. J., Burgess, P. M., Fraser, A. J. (eds) Strata and Time: Probing the Gaps in Our Understanding. Geological Society, London, Special Publications, 404, https://doi.org/10.1144/SP404.12
Hinnov, L.A., 2013. Cyclostratigraphy and its revolutionizing applications in the Earth and planetary sciences. Geol. Soc. Am. Bull. 125, 1703–1734.
Hinnov, L.A., Goldhammer, R.K., 1991. Spectral analysis of the middle Triassic Latemar limestone. J. Sediment. Petrol. 61, 1173–1193.
Hinnov, L.A., Park, J., 1998. Detection of astronomical cycles in the stratigraphic record by frequency modulation (FM) analysis. J. Sediment. Res. 68, 524–539.
Huybers, P., 2007. Glacial variability over the last 2 Ma: an extended depth-derived agemodel, continuous obliquity pacing, and the Pleistocene progression. Quat. Sci. Rev. 26, 37–55.
Huybers, P., 2011. Combined obliquity and precession pacing of the late Pleistocene glacial cycles. Nature 480, 229–232.
Huybers, P., Wunsch, C., 2004. A depth-derived Pleistocene age model: uncertainty estimates, sedimentation variability, and non-linear climate change. Paleoceanography 19, PA1028. https://doi.org/10.1029/2002PA000857.
Huybers, P., Wunsch, C., 2005. Obliquity pacing of the late Pleistocene glacial terminations. Nature 434, 491–494.
Imbrie, J., Imbrie, J.Z., 1980. Modeling the climatic response to orbital variations. Science 207, 943–953.
Jerolmack, D.J., Paola, C., 2010. Shredding of environmental signals by sediment transport. Geophys. Res. Lett. 37, L19401. https://doi.org/10.1029/2010GL044638.
Jicha, B.R., Singer, B.S., Sobol, P., 2016. Re-evaluation of the ages of $^{40}Ar/^{39}Ar$ sanidine standards and supereruptions in the western U.S. using a Noblesse multi-collector mass spectrometer. Chem. Geol. 431, 54–66.
Keller, C.B., Schoene, B., Samperton, K.M., 2018. A stochastic sampling approach to zircon eruption age interpretation. Geochem. Perspect. Lett. 8, 31–35.
Kelly, D.C., Zachos, J.C., Bralower, T.J., Schellenberg, S.A., 2005. Enhanced terrestrial weathering/runoff and surface ocean carbonate production during the recovery stages of the Paleocene-Eocene thermal maximum. Paleoceanography 20, PA4023. https://doi.org/10.1029/2005PA001163.
Kemp, D.B., 2016. Optimizing significance testing of astronomical forcing in cyclostratigraphy. Paleoceanography 31, 1516–1531. https://doi.org/10.1002/2016PA002963.
Kemp, D.B., Van Manen, S.M., Pollitt, D.A., Burgess, P.M., 2016. Investigating the preservation of orbital forcing in peritidal carbonates. Sedimentology 63, 1701–1718.
Kennett, J.P., Stott, L.D., 1991. Abrupt deep-sea warming, palaeoceanographic changes and benthic extinctions at the end of the Palaeocene. Nature 353, 225–229.
Kent, D.V., Muttoni, G., Brack, P., 2004. Magnetostratigraphic confirmation of a much faster tempo for sea-level change for the Middle Triassic Latemar platform carbonates. Earth Planet. Sci. Lett. 228, 369–377. https://doi.org/10.1016/j.epsl.2004.10.017.
Kent, D.V., Olsen, P.E., Rasmussen, C., Lepre, C., Mundil, R., Irmis, R.B., Gehrels, G.E., Giesler, D., Geissman, J.W., Parker, W.G., 2018. Empirical evidence for stability of the 405-kiloyear Jupiter-Venus eccentricity cycle over hundreds of millions of years. Proc. Natl. Acad. Sci. https://doi.org/10.1073/pnas.1800891115.
Kirtland Turner, S., Ridgwell, A., 2013. Recovering the true size of an Eocene hyperthermal from the marine sedimentary record. Paleoceanography 28, 700–712.
Kirtland Turner, S., Sexton, P.F., Charles, C.D., Norris, R.D., 2014. Persistence of carbon release events through the peak of early Eocene global warmth. Nat. Geosci. 7, 748–751.
Kominz, M.A., Bond, G.C., 1990. A new method of testing periodicity in cyclic sediments: application to the Newark Supergroup. Earth Planet. Sci. Lett. 98, 233–244.
Kuiper, K.F., Deino, A., Hilgen, F.J., Krijgsman, W., Renne, P.R., Wijbrans, J.R., 2008. Synchronizing rock clocks of Earth history. Science 320, 500–504. https://doi.org/10.1126/science.1154339.
Laskar, J., 1989. A numerical experiment on the chaotic behavior of the solar system. Nature 338, 237–238.
Laskar, J., Robutel, P., Joutel, F., Gastineau, M., Correia, A.C.M., Levard, B., 2004. A long-term numerical solution for the insolation quantities of the Earth. Astron. Astrophys. 428, 261–285. https://doi.org/10.1051/0004-6361:20041335.
Laskar, J., Fienga, A., Gastineau, M., Manche, H., 2011a. La2010: a new orbital solution for the long-term motion of the Earth. Astron. Astrophys. A89. https://doi.org/10.1051/0004-6361/201116836.
Laskar, J., Gastineau, M., Delisle, J.-B., Farres, A., Fienga, A., 2011b. Strong chaos induced by close encounters with Ceres and Vesta. Astron. Astrophys. 532, L4.
Laurin, J., Meyers, S.R., Sageman, B.B., Waltham, D.A., 2005. Phase lag in amplitude modulation of hemipelagic cycles: a new tool for recognition of relative sea level change. Geology 33, 569–572.
Laurin, J., Růžek, B., Giorgioni, M., 2017. Orbital signals in carbon isotopes: phase distortion as a signature of the carbon cycle. Paleoceanography 32 (11), 1236–1255.
Lawlor, D.A., Tilling, K., Davey Smith, G., 2016. Triangulation in aetiological epidemiology. Int. J. Epidemiol. 45, 1866–1886.
Leek, Jeff, McShane, Blakeley B., Gelman, Andrew, Colquhoun, David, Nuijten, Michèle B., Goodman, Steven N., 2017. Five ways to fix statistics. Nature 551, 557–559.

Li, M., Kump, L.R., Hinnov, L.A., Mann, M.E., 2018. Tracking variable sedimentation rates and astronomical forcing in Phanerozoic paleoclimate proxy series with evolutionary correlation coefficients and hypothesis testing. Earth Planet. Sci. Lett. 501, 165–179.
Lisiecki, L.E., 2010. Links between eccentricity forcing and the 100,000-year glacial cycle. Nat. Geosci. 3, 349–352.
Lisiecki, L.E., Raymo, M.E., 2005. A Pliocene-Pleistocene stack of 57 globally distributed benthic $\delta^{18}O$ records. Paleoceanography 20, PA1003. https://doi.org/10.1029/2004PA001071.
Lourens, L.J., Wehausen, R., Brumsack, H.J., 2001. Geological constraints on tidal dissipation and dynamical ellipticity of the Earth over the past three million years. Nature 409, 1029–1033.
Lourens, L.J., Sluijs, A., Kroon, D., Zachos, J.C., Thomas, E., Röhl, U., Bowles, J., Raffi, I., 2005. Astronomical pacing of late Palaeocene to early Eocene global warming events. Nature 435, 1083–1087.
Ma, C., Meyers, S.R., Sageman, B.B., 2017. Theory of chaotic orbital variations confirmed by cretaceous geological evidence. Nature 542, 468–470.
Malinverno, A., Erba, E., Herbert, T.D., 2010. Orbital tuning as an inverse problem: chronology of the early Aptian oceanic anoxic event 1a (Selli Level) in the Cismon APTICORE. Paleoceanography 25, PA2203. https://doi.org/10.1029/2009PA001769.
Mann, M.E., Lees, J.M., 1996. Robust estimation of background noise and signal detection in climatic time series, Clim. Change 33, 409–445. https://doi.org/10.1007/BF00142586.
Martinson, D.G., Menke, W., Stoffa, P., 1982. An inverse approach to signal correlation. J. Geophys. Res. 87, 4807–4818.
Martinson, D.G., Pisias, N.G., Hays, J.D., Imbrie, J., Moore, T.C., Shackleton, N.J., 1987. Age dating and the orbital theory of the ice ages: development of a high-resolution 0 to 300,000-year chronostratigraphy. Quat. Res. 27, 1–29.
Mathieu, M., Kotov, S., De Vleeschouwer, Pas, Pälike, H., 2016. Testing the impact of stratigraphic uncertainty on spectral analyses of sedimentary series. Clim. Pastoralism 12, 1765–1783. https://doi.org/10.5194/cp-12-1765-2016.
Mattinson, J.M., 2005. Zircon U/Pb chemical abrasion (CA-TIMS) method: combined annealing and multi-step partial dissolution analysis for improved precision and accuracy of zircon ages. Chem. Geol. 220, 47–66. https://doi.org/10.1016/j.chemgeo.2005.03.011.
Meyers, S.R., 2008. Resolving Milankovitchian controversies: the Triassic Latemar limestone and eocene green river formation. Geology 36, 319–322.
Meyers, S.R., 2012. Seeing red in cyclic stratigraphy: spectral noise estimation for astrochronology. Paleoceanography 27, PA3228. https://doi.org/10.1029/2012PA002307.
Meyers, S. R., 2014. Astrochron: An R package for astrochronology. [Available at http://cran.r-project.org/package=astrochron.]
Meyers, S.R., 2015. The evaluation of eccentricity-related amplitude modulation and bundling in paleoclimate data: an inverse approach for astrochronologic testing and time scale optimization. Paleoceanography 30 (12), 1625–1640.
Meyers, S.R., 2017. Cracking the paleoclimate code. Nature 546, 219–220. https://doi.org/10.1038/nature22501.
Meyers, S.R., Malinverno, A., 2018. Proterozoic Milankovitch cycles and the history of the solar system. Proc. Natl. Acad. Sci. https://doi.org/10.1073/pnas.1717689115.
Meyers, S.R., Sageman, B.B., 2007. Quantification of deep-time orbital forcing by average spectral misfit. Am. J. Sci. 307 (5), 773–792.
Meyers, S.R., Sageman, B., Hinnov, L., 2001. Integrated quantitative stratigraphy of the Cenomanian-Turonian bridge creek limestone member using evolutive harmonic analysis and stratigraphic modeling. J. Sediment. Res. 71, 627–643.
Meyers, S.R., Sageman, B.B., Lyons, T., 2005. Organic carbon burial rate and the molybdenum proxy: theoretical framework and application to Cenomanian-Turonian OAE II. Paleoceanography, PA2002. https://doi.org/10.1029/2004PA001068.
Meyers, S.R., Sageman, B.B., Pagani, M., 2008. Resolving Milankovitch: consideration of signal and noise. Am. J. Sci. 308, 770–786.
Meyers, S.R., Sageman, B.B., Arthur, M.A., 2012a. Obliquity forcing of organic matter accumulation during Oceanic Anoxic Event 2. Paleoceanography 27, PA3212. https://doi.org/10.1029/2012PA002286.
Meyers, S.R., Siewert, S.E., Singer, B.S., Sageman, B.B., Condon, D.J., Obradovich, J.D., Jicha, B.R., Sawyer, D.A., 2012b. Intercalibration of radioisotopic and astrochonologic time scales for the Cenomanian-Turonian boundary interval, Western Interior Basin, USA. Geology 40, 7–10.
Miall, A.D., 1995. Wither Stratigraphy. Sediment. Geol. 100, 5–20.
Miall, A.D., Miall, C.E., 2004. Empiricism and model-building in stratigraphy: around the hermeneutic circle in the pursuit of stratigraphic correlation. Stratigraphy 1, 27–46.
Munafò, M.R., Smith, G.D., 2018. Repeating experiments is not enough. Nature 553, 399–401.
Mundil, R., Brack, P., Meier, M., Reiber, H., Oberli, F., 1996. High resolution U-Pb dating of Middle Triassic volcaniclastics: Time-scale calibration and verification of tuning parameters for carbonate sedimentation. Earth Planet. Sci. Lett. 141, 137–151. https://doi.org/10.1016/0012–821X (96)00057-X.
Mundil, R., Zühlke, R., Bechstädt, T., Peterhansel, A., Egenhoff, S.O., Oberli, F., Meier, M., Brack, P., Rieber, H., 2003. Cyclicities in Triassic platform carbonates: Synchronizing radio-isotopic and orbital clocks. Terra Nova 15, 81–87. https://doi.org/10.1046/j.1365–3121.2003.00475.x.
Olsen, P.E., 1986. A 40-million-year lake record of early mesozoic orbital climate forcing. Science 234, 842–848.
Olsen, P.E., Kent, D.V., 1999. Long-period milankovitch cycles from the late triassic and early jurassic of eastern north America and their implications for the calibration of the early mesozoic time-scale and the long-term behavior of the planets. Phil. Trans. 357, 1761–1786.
Olsen, P.E., Kent, D.V., Whiteside, J.H., 2011. Implications of the Newark Supergroup-based astrochronology and geomagnetic polarity time scale (Newark-APTS) for the tempo and mode of the early diversification of the Dinosauria. Earth Environ. Sci. Trans. Royal Soc. Edinburgh 101, 201–229.
Pälike, H., Shackleton, N.J., 2000. Constraints on astronomical parameters from the geological record for the last 25 Myr. Earth Planet. Sci. Lett. 182, 1–14.
Pälike, H., Laskar, J., Shackleton, N.J., 2004. Geologic constraints on the chaotic diffusion of the solar system. Geology 32, 929–932.
Pälike, H., Norris, R., Herrle, J.O., Wilson, P., Coxall, H.K., Lear, C.H., Shackleton, N.J., Tripati, A.K., Wade, B.S., 2006. The heartbeat of the Oligocene climate system. Science 314, 1894–1898.
Pelletier, J.D., Turcotte, D.L., 1997. Synthetic stratigraphy with a stochastic diffusion model of fluvial sedimentation. J. Sed. Res. 67, 1060–1067.
Peper, T., Cloetingh, S., 1995. Autocyclic perturbations of orbitally forced signals in the sedimentary record. Geology 23, 937–940.
Preto, N., Hinnov, L.A., De Zanche, V., Mietto, P., Hardie, L.A., 2004. The Milankovitch interpretation of the Latemar Platform cycles (Dolomites, Italy): Implications for geochronology, biostratigraphy, and Middle Triassic carbonate accumulation. 81. SEPM Special Publication, pp. 167–182.
Preto, N., Hinnov, L.A., Hardie, L.A., De Zanche, V., 2001. Middle Triassic orbital signature recorded in the shallow-marine Latemar carbonate buildup (Dolomites, Italy). Geology 29, 1123–1126. https://doi.org/10.1130/0091–7613(2001)029<1123:MTOSRI>2.0.CO;2.
Proistosescu, C., Huybers, P., Maloof, A., 2012. To tune or not to tune: Detecting orbital variability in Oligo-Miocene climate records. Earth Planet. Sci. Lett. 325–326. https://doi.org/10.1016/j.epsl.2012.01.022.
Purkis, S.J., Rowlands, G.P., Kerr, J.M., 2015. Unravelling the influence of water depth and wave energy on the facies diversity of shelf carbonates. Sedimentology 62, 541–565.
R Core Team, 2017. R: A Language and Environment for Statistical Computing. R Foundation for Statistical Computing, Vienna.
Raymo, M.E., Ruddiman, W.F., Backman, J., Clement, B.M., Martinson, D.G., 1989. Late pliocene variation in northern hemisphere ice sheets and north Atlantic deep water circulation. Paleoceanography 4, 413–446.
Raymo, M.E., Hodell, D., Jansen, E., 1992. Response of deep ocean circulation to initiation of Northern Hemisphere glaciation (3–2 MA). Paleoceanography 7, 645–672.
Ridgwell, A., 2007. Interpreting transient carbonate compensation depth changes by marine sediment core modeling. Paleoceanography 22, PA4102. https://doi.org/10.1029/2006PA001372.
Ripepe, M., Fischer, A.G., 1991. Stratigraphic rhythms synthesized from orbital variations. In: Franseen, E.K., Watney, W.L., Kendall, C.G.St.C., Ross, W. (Eds.), Sedimentary Modeling. Computer Simulations and Methods for Improved Parameter Definition: Kansas State Geological Survey, Bulletin Vol. 233. pp. 335–344.
Rivera, T.A., Storey, M., Zeeden, C., Hilgen, F.J., Kuiper, K., 2011. A refined astronomically calibrated $^{40}Ar/^{39}Ar$ age for fish Canyon sanidine. Earth Planet. Sci. Lett. 311, 420–426.
Ruddiman et al., 1987. Site 607, Initial Rep. Deep Sea Drill. Proj. 94, 75–147.
Ruddiman, W.F., Raymo, M.E., Martinson, D.G., Clement, B.M., Backman, J., 1989. Pleistocene evolution of Northern Hemisphere climate. Paleoceanography 4, 353–412.
Sadler, P.M., Strauss, D., 1990. Estimation of completeness of stratigraphical sections using empirical data and theoretical models. J. Geol. Soc. Lond. 147, 471–485.
Sageman, B.B., Singer, B.S., Meyers, S.R., Siewert, S.E., Condon, D., Jicha, B.R., Obradovich, J.D., Sawyer, D.A., 2014. Integrating $^{40}Ar/^{39}Ar$, U-Pb, and astronomical clocks in the Cretaceous Niobrara Formation, Western Interior Basin, USA. Geol. Soc. Am. Bull. 126, 956–973.
Satterley, A.K., 1996. The interpretation of cyclic successions of the middle and Upper Triassic of the northern and southern Alps. Earth-Sci. Rev. 40, 181–207.
Schiffelbein, P., Dorman, L., 1986. Spectral effects of time–depth nonlinearities in deep sea sediment records: a demodulation technique for realigning time and depth scales. J. Geophys. Res. 91, 3821–3835.
Schmitz, M.D., Kuiper, K., 2013. High-Precision Geochronology. Elements 9, 25–30.
Schwarzacher, W., 1947. Uber die sediment€are Rhytmik der Dachsteinkalkes von Lofer. Verh. Geol. Bundesanstalt H10-12, 175–188.
Shackleton, N.J., 2000. The 100,000-year ice-age cycle identified and found to lag temperature, carbon dioxide, and orbital eccentricity. Science 289, 1897–1902.
Shackleton, N., Hagelberg, T., Crowhurst, S., 1995. Evaluating the success of astronomical tuning: pitfalls of using coherence as a criterion for assessing pre-Pleistocene timescales. Paleoceanography 10, 693–697. https://doi.org/10.1029/95PA01454.
Spahn, Z.P., Kodama, K.P., Preto, N., 2013. High-resolution estimate for the depositional duration of the Triassic Latemar Platform: a new magnetostratigraphy and magnetic susceptibility cyclostratigraphy from basinal sediments at Rio Sacuz. Italy. Geochem. Geophys. Geosyst. 14, 1–14.
Strasser, A., 2018. Cyclostratigraphy of shallow-marine carbonates – limitations and opportunities. Stratigr. Timescales 3, 151–187.
Strasser, A., Hilgen, F.J., Heckel, P.H., 2006. Cyclostratigraphy – concepts, definitions, and applications. Newsl. Stratigr. 42 (2), 75–114.
Straub, K.M., Li, Q., Benson, W.M., 2015. Influence of sediment cohesion on deltaic shoreline dynamics and bulk sediment retention: a laboratory study. Geophys. Res. Lett. 42, 9808–9815.
Taner, M.T., Koehler, F., Sheriff, R.E., 1979. Complex trace analysis. Geophysics 44, 1041–1063.
Thakur, T.R., Scheidegger, A.E., 1970. Chain model of river meanders. Water Resour. Res. 12, 25–47.
Thomson, D.J., 1982. Spectrum estimation and harmonic analysis, Proc. IEEE 70, 1055–1096. https://doi.org/10.1109/PROC.1982.12433.
Thomson, D.J., Lanzerotti, L.J., Maclennan, C.G., 2001. The interplanetary magnetic

field: Statistical properties and discrete modes. J. Geophys.Res. 106, 15941–15962.
Thomson, D.J., 1990. Quadratic-inverse spectrum estimates: applications to palaeoclimatology. Philos. Trans. R Soc. Lond. A Phys. Eng. Sci. 332, 539–597.
van Dam, J.A., Abdul Aziz, H., Ángeles Álvarez Sierra, M., Hilgen, F.J., van den Hoek Ostende, L.W., Lourens, L.J., Mein, P., van der Meulen, A.J., Pelaez-Campomanes, P., 2006. Long-period astronomical forcing of mammal turnover. Nature 443, 687–691.
van der Laan, E., Hilgen, F.J., Lourens, L.J., de Kaenel, E., Gaboardi, S., Iaccarino, S., 2012. Astronomical forcing of Northwest African climate and glacial history during the late Messinian (6.5–5.5 Ma). Palaeogeogr. Palaeoclimatol. Palaeoecol. 313-314, 107–126.
Van Houten, F.B., 1962. Cyclic sedimentation and the origin of analcime-rich Upper Triassic Lockatong formation, West-central New Jersey and adjacent Pennsylvania. Am. J. Sci. 260, 561–576.
Vaughan, S., Bailey, R.J., Smith, D.G., 2011. Detecting cycles in stratigraphic data: Spectral analysis in the presence of red noise. Paleoceanography 26, PA4211. https://doi.org/10.1029/2011PA002195.
Vaughan S, Bailey RJ, Smith DG, 2014. Cyclostratigraphy: data filtering as a source of spurious spectral peaks, From: Smith, D. G., Bailey, R. J., Burgess, P. M. & Fraser, A. J. (eds) Strata and Time: Probing the Gaps in Our Understanding. Geological Society, London, Special Publications, 404, https://doi.org/10.1144/SP404.11
Waltham, D., 2015. Milankovitch period uncertainties and their impact on cyclostratigraphy. J. Sediment. Res. 85, 990–998.
Wang, Y., Straub, K.M., Hajek, E.A., 2011. Scale-dependent compensational stacking: an estimate of autogenic time scales in channelized sedimentary deposits. Geology 39, 811–814.
Wasserstein, R.L., Lazar, N.A., 2016. The ASA's statement on p-values: Context, process, and purpose. Am. Stat. 70, 129–133.
Weedon, G.P., 2003. Time-Series Analysis and Cyclostratigraphy; Examining Stratigraphic Records of Environmental Cycles. Cambridge University Press, Cambridge, UK, pp. 259.
Westerhold, T., Röhl, U., Laskar, J., Raffi, I., Bowles, J., Lourens, L., Zachos, J., 2007. On the duration of magnetochrons C24r and C25n and the timing of early Eocene global warming events: Implications from the Ocean Drilling Program Leg 208 Walvis Ridge depth transect. Paleoceanography 22, PA2201. https://doi.org/10.1029/2006PA001322.
Westerhold, T., Röhl, U., Frederichs, T., Bohaty, S.M., Zachos, J.C., 2015. Astronomical calibration of the geological timescale: closing the middle Eocene gap, Clim. Pastoralism 11, 1181–1195.
Westphal, H., Bohm, F., Bornholdt, S., 2004. Orbital frequencies in the carbonate sedimentary record: distorted by diagenesis. Facies 50, 3–11.
Westphal, H., Munnecke, A., Böhm, F., Bornholdt, S., 2008. In: Pratt, Holmden (Eds.), Limestone–Marl Alternations in Epeiric Sea Settings— Witnesses of Environmental Changes or Diagenesis? Special Paper 48: Dynamics of Epeiric Seas.
Westphal, H., Lavi, J., Munnecke, A., 2015. Diagenesis makes the impossible come true: intersecting beds in calcareous turbidites. Facies 61. https://doi.org/10.1007/s10347-015-0427-7.
Wigley, T.M.L., 1976. Spectral analysis and the astronomical theory of climatic change. Nature 264, 629–631.
Wilkinson, B.H., Drummond, C.N., 2006. Facies mosaics across the Persian Gulf and around Antigua – Stochastic and deterministic products of shallow-water sediment accumulation. J. Sediment. Res. 74, 513–526.
Wilkinson, B.H., Diedrich, N.W., Drummond, C.N., 1996. Facies successions in peritidal carbonate sequences. J. Sediment. Res. 66, 1065–1078.
Wilkinson, B.H., Diedrich, N.W., Drummond, C.N., Rothman, E.D., 1998. Michigan hockey, meteoric precipitation, and rhythmicity of accumulation on peritidal carbonate platforms. GSA Bull. 110, 1075–1093.
Wotzlaw, J.-F., Hüsing, S.K., Hilgen, F.J., Schaltegger, U., 2014. High-precision zircon U-Pb geochronology of astronomically dated volcanic ash beds from the Mediterranean Miocene. Earth Planet. Sci. Lett. 407, 19–34.
Wunsch, C., 1972. Bermuda sea level in relation to tides, weather, and baroclinic fluctuations. Rev. Geophys. 10, 1–49.
Wunsch, C., 2003. The spectral description of climate change including the 100 ky energy. Clim. Dyn. 20, 353–363. https://doi.org/10.1007/s00382-002-0279-z.
Wunsch, C., 2004. Quantitative estimate of the Milankovitch-forced contribution to observed Quaternary climate change. Quat. Sci. Rev. 23, 1001–1012. https://doi.org/10.1016/j.quascirev.2004.02.014.
Zachos, J., Pagani, M., Sloan, L., Thomas, E., Billups, K., 2001. Trends, rhythms, and aberrations in global climate 65 Ma to present. Science 292, 686–693. https://doi.org/10.1126/science.1059412.
Zachos, J.C., et al., 2004. Proceedings ODP. Init. Repts. Ocean Drilling Program, College Station, Tex. Vol. 208https://doi.org/10.2973/odp.proc.ir.208.2004.
Zachos, J.C., Rohl, U., Schellenberg, S.A., Sluijs, A., Hodell, D.A., Kelly, D.C., Thomas, E., Nicolo, M., Raffi, I., Lourens, L.J., McCarren, H., Kroon, D., 2005. Rapid acidification of the ocean during the Paleocene-Eocene. Science 308, 1611–1615.
Zachos, J.C., McCarren, H., Murphy, B., Rohl, U., Westerhold, T., 2010. Tempo and scale of late Paleocene and early Eocene carbon isotope cycles: Implications for the origin of hyperthermals. Earth Planet. Sci. Lett. 299, 242–249.
Zeebe, R.E., Westerhold, T., Littler, K., Zachos, J.C., 2017. Orbital forcing of the Paleocene and Eocene carbon cycle. Paleoceanography. https://doi.org/10.1002/2016PA003054.
Zeeden, C., Rivera, T.A., Storey, M., 2014a. An astronomical age for the Bishop Tuff and concordance with radioisotopic dates. Geophys. Res. Lett. https://doi.org/10.1002/2014GL059899.
Zeeden, C., Hilgen, F.J., Hüsing, S.K., Lourens, L.J., 2014b. The Miocene astronomical time scale 9–12 Ma: New constraints on tidal dissipation and their implications for paleo-climatic investigations. Paleoceanography 29, 296–307.
Zeeden, C., Meyers, S.R., Lourens, L.J., Hilgen, F.J., 2015. Testing astronomically tuned age models. Paleoceanography 30, 369–383. https://doi.org/10.1002/2014PA002762.
Zhang, S., Wang, X., Hammarlund, E.U., Wang, H., Mafalda Costa, M., Bjerrum, C.J., Connelly, J.N., Zhang, B., Bian, L., Canfield, D.E., 2015. Orbital forcing of climate 1.4 billion years ago. Proc. Natl. Acad. Sci. https://doi.org/10.1073/pnas.1502239112.
Zühlke, R., 2004. Integrated cyclostratigraphy of a model Mesozoic carbonate platform - the Latemar (Middle Triassic, Italy). In: D'Argenio (Ed.), Cyclostratigraphy: Approaches and case histories: SEPM (Society for Sedi- mentary Geology). 81. pp. 183–211 Special Publication.
Zühlke, R., Bechstädt, T., Mundil, R., 2003. Sub-Milankovitch and Milankovitch forcing on a model Mesozoic carbonate platform—the Latemar (Middle Triassic, Italy). Terra Nova 15, 69–80. https://doi.org/10.1046/j.1365–3121.2003.00366.x.